

SYNTHESIS OF  $\text{TiO}_2/\text{SiO}_2/\text{GSs}$  COMPOSITE PHOTOCATALYST FOR  
REMOVAL OF N-NITROSODIETHYLAMINE (NDEA) IN  
CONTAMINATED WATER



MIA LESTARI AYUNINGTYAS

A Thesis Submitted in Partial Fulfillment of the Requirements for  
the Degree of Ph. D. of Engineering in Material Engineering  
Suranaree University of Technology  
Academic Year 2021

การสังเคราะห์วัสดุเชิงประกอบ  $\text{TiO}_2/\text{SiO}_2/\text{GSs}$  โฟโตคาตะลิสต์สำหรับการ  
กำจัดสาร N-NITROSODIETHYLAMINE (NDEA) ที่ปนเปื้อนในน้ำ



นาง เมียร์ เลสตารี आयुNINGเทียส

วิทยานิพนธ์นี้เป็นส่วนหนึ่งของการศึกษาตามหลักสูตรปริญญาวิศวกรรมศาสตรดุษฎีบัณฑิต  
สาขาวิชาวิศวกรรมวัสดุ  
มหาวิทยาลัยเทคโนโลยีสุรนารี  
ปีการศึกษา 2564

SYNTHESIS OF TiO<sub>2</sub>/SiO<sub>2</sub>/GSs COMPOSITE PHOTOCATALYST FOR  
REMOVAL OF N-NITROSODIETHYLAMINE (NDEA) IN  
CONTAMINATED WATER

Suranaree University of Technology has approved this thesis submitted in partial fulfillment of the requirements for the Degree of Doctor Philosophy.

Thesis Examining Committee

Onlamee Kamon-in

(Asst. Prof. Dr. Onlamee Kamon - in)

Chairperson Sukasem W.

(Asst. Prof. Dr. Sukasem Watcharamaisakul)

Member (Thesis Advisor)

SUPUNNEE J.

(Dr. Supunnee Junpirom)

Member (Thesis Co-Advisor)

Siriwan Chokkha

(Asst. Prof. Dr. Siriwan Chokkha)

Member Jir.

(Asst. Prof. Dr. Jiratchaya Ayawana)

Member Sutin

(Assoc. Prof. Dr. Sutin Kuharuangrong)

Member S. Jiansirisomboon

(Assoc. Prof. Dr. Sukanda Jiansirisomboon)

Member Pornsiri

Chatchai Jothityangkoon

(Assoc. Prof. Dr. Chatchai Jothityangkoon) (Assoc. Prof. Dr. Pornsiri Jongkol)

Vice Rector for Academic Affairs and

Dean of Institute of Engineering

Quality Assurance

เมียร์ เลสตาร์/อายุนิ่งเทียส : การสังเคราะห์วัสดุเชิงประกอบ  $\text{TiO}_2/\text{SiO}_2/\text{GSs}$  โฟโตคะตะลิสต์สำหรับการกำจัดสาร N-NITROSODIETHYLAMINE (NDEA) ที่ปนเปื้อนในน้ำ (SYNTHESIS OF  $\text{TiO}_2/\text{SiO}_2/\text{GSs}$  COMPOSITE PHOTOCATALYST FOR REMOVAL OF N-NITROSODIETHYLAMINE (NDEA) IN CONTAMINATED WATER). อาจารย์ที่ปรึกษา : ผู้ช่วยศาสตราจารย์ ดร. สุขเกษม วัชรมัณฑกุล, 125 หน้า

คำสำคัญ :  $\text{TiO}_2/\text{SiO}_2/\text{GSs}$  คอมโพสิต โคลเจล ตัวเร่งปฏิกิริยา NDEA

$\text{TiO}_2$  เป็นวัสดุที่มีแถบพลังงาน (Bandgap energy) ค่อนข้างกว้าง ซึ่งถูกใช้เป็นตัวเร่งปฏิกิริยาโฟโตคะตะลิสต์ในหลายๆ ด้านในขณะที่วัสดุกราฟีนเป็นที่รู้จักกันดีว่าเป็นวัสดุแต่งเติมชนิดหนึ่งที่สามารถช่วยเพิ่มสมบัตินำไฟฟ้าให้กับโฟโตคะตะลิสต์ได้และส่งผลกระทบต่อความสามารถของตัวเร่งปฏิกิริยาด้วยแสง จากงานวิจัยนี้ได้มุ่งเน้นว่าวัสดุกราฟีนมีผลต่อสมบัติอย่างไร โดยเฉพาะอย่างยิ่งการช่วยลดความกว้างของแถบพลังงานของ  $\text{TiO}_2$  เพื่อให้โฟโตคะตะลิสต์สามารถทำงานภายใต้ช่วงแสงปกติที่มองเห็นได้ (Visible light) การเตรียมชิ้นงานจะทำการเคลือบสาร  $\text{TiO}_2/\text{SiO}_2/\text{GSs}$  ที่สังเคราะห์ได้ลงบนวัสดุรองรับ (Substrate) ที่ทำจากฟองน้ำโดยใช้วิธีการจุ่มเคลือบโดยใช้โพลีไวนิลแอลกอฮอล์เป็นสารช่วยในการยึดเกาะ

งานส่วนแรก คือ การสังเคราะห์วัสดุเชิงประกอบ  $\text{TiO}_2/\text{SiO}_2$  และ Graphene Sheets (GSs) โดยใช้วิธีโคลเจล โดยมีการศึกษาอุณหภูมิที่ใช้ในการการเผา (Tcal) และอัตราส่วนผสมของ  $\text{TiO}_2/\text{GSs}$  เพื่อให้ได้สภาวะที่เหมาะสมที่สุดในการสังเคราะห์ พบว่าที่  $2\theta$  ที่มุม  $26^\circ-27^\circ$  ของกราฟ XRD แสดงเฟส Anatase และ Rutile รวมถึงกราฟีน แนวโน้มของปริมาณเฟส Anatase จะขึ้นอยู่กับปริมาณอัตราส่วนของ GSs และอุณหภูมิที่ใช้ในการการเผา (Tcal) และจะมีปริมาณเฟสลดลงเมื่อปริมาณอัตราส่วน GSs และ Tcal เพิ่มขึ้น ผลจากการทดสอบประสิทธิภาพของโฟโตคะตะลิสต์ที่อยู่ภายใต้แสงแดดเมื่อเทียบกับที่อยู่ภายใต้แสงยูวี พบว่าตัวเร่งปฏิกิริยาด้วยแสงที่มีอัตราส่วนผสมที่ 0.07 และ Tcal ที่  $450^\circ\text{C}$  จะมีประสิทธิภาพสูงสุดในการย่อยสลาย Methylene blue (MB) ที่ 97.83 เปอร์เซ็นต์ ภายใน 3 ชั่วโมง ภายใต้แสงแดด ดังนั้นสภาวะที่เหมาะสมที่ได้จากการทดลองนี้จะถูกนำไปใช้กับ วัสดุเชิงประกอบโฟโตคะตะลิสต์ สำหรับงานในส่วนที่สอง

งานส่วนที่สอง นำสาร  $\text{TiO}_2/\text{SiO}_2/\text{GSs}$  ที่สังเคราะห์ได้เคลือบลงบนวัสดุรองรับ (Substrate) ที่ทำจากฟองน้ำโดยใช้วิธีการจุ่มเคลือบโดยใช้โพลีไวนิลแอลกอฮอล์เป็นสารช่วยในการยึดเกาะ โดยเตรียมด้วยความหนาของวัสดุรองรับ (Substrate) ที่แตกต่างกัน จากการวิเคราะห์การสลายตัวของ Methylene blue (MB) ด้วยความหนาของฟองน้ำ จะให้ผลลัพธ์ที่แตกต่างกัน ใน 60 นาทีแรก

พบว่าตัวอย่างที่มีความหนาของวัสดุรองรับ (Substrate) ที่ 1 ซม. จะมีความสามารถในการย่อยสลายสูงสุดถึง 95% อย่างไรก็ตามพบว่าความหนาของฟองน้ำจะไม่มีผลกระทบต่อประสิทธิภาพของโฟโตคะตาไลติกภายใต้แสงแดดที่มีต่อกระบวนการย่อยสลาย Methylene blue (MB)

ผลการทดสอบประสิทธิภาพของวัสดุเชิงประกอบ  $\text{TiO}_2/\text{SiO}_2/\text{GSs}$  โฟโตคะตาลิสต์ ที่มีต่อสารก่อมลพิษในสิ่งแวดล้อม ได้ทำการทดลองกับสารละลาย N-Nitrosodiethylamine (NDEA) เมื่อทำการวิเคราะห์ก่อนและหลังการย่อยสลายภายใต้แสงแดด พบว่าการสลายตัวของ NDEA ทำได้ภายใน 300 นาที โดยใช้วัสดุเชิงประกอบ  $\text{TiO}_2/\text{SiO}_2/\text{GSs}$  โฟโตคะตาลิสต์ ที่มีความหนาของฟองน้ำที่ 0.5 ซม. ซึ่งมีประสิทธิภาพการย่อยสลาย NDEA ถึง 95.52%



สาขาวิชาวิศวกรรมเซรามิก

ปีการศึกษา 2564

ลายมือชื่อนักศึกษา.....

ลายมือชื่ออาจารย์ที่ปรึกษา.....

ลายมือชื่ออาจารย์ที่ปรึกษาร่วม.....

*Supunnee J.*  
*Supunnee J.*  
SUPUNNEE J.



MIA LESTARI/AYUNINGTYAS : SYNTHESIS OF  $\text{TiO}_2/\text{SiO}_2/\text{GSs}$  COMPOSITE PHOTOCATALYST FOR REMOVAL OF N-NITROSODIETHYLAMINE (NDEA) IN CONTAMINATED WATER. THESIS ADVISOR : ASST. PROF. SUKASEM WATCHARAMAISAKUL, Ph. D. 125 PP.

Keyword :  $\text{TiO}_2/\text{SiO}_2/\text{GSs}$  COMPOSITE SOL GEL PHOTOCATALYST NDEA

$\text{TiO}_2$  with large bandgap energy has been used as a photocatalyst in many applications while graphene is known to be one of the doped materials that can enhance electrical conductivity which affects the ability of photocatalyst. This study is focused on how graphene affects the properties especially the bandgap energy of  $\text{TiO}_2$  to be able to work under visible light work range. The composite of  $\text{TiO}_2/\text{SiO}_2/\text{GSs}$  then was coated onto a sponge substrate by using the dipping method with Polyvinyl alcohol as a binder.

The first part is the synthesis of  $\text{TiO}_2/\text{SiO}_2$  composite with Graphene Sheets (GSs) by using the sol-gel method. The calcination temperature (Tcal) and the ratio of  $\text{TiO}_2/\text{GSs}$  have been studied to get the optimum condition of synthesis. At the near point of  $2\theta$  ( $26^\circ$ - $27^\circ$ ), the XRD pattern exhibits anatase and rutile phases, as well as graphene. The propensity of anatase phase according to GSs ratio and Tcal variables decreases as GSs ratio and Tcal increase. The photocatalytic activity obtained under sunlight is comparable to that obtained under UV light. The photocatalyst with a ratio of 0.07 and Tcal at  $450^\circ\text{C}$  demonstrated the highest efficiency of MB degradation under solar light with 97.83 % within 3 hours. This optimum condition is used to get the composite photocatalyst for the second part.

The second part is coating the powder onto the sponge substrate by using the dipping method with Polyvinyl alcohol as a binder prepared with various thicknesses. The degradation of methylene blue was analyzed with the various thickness of the sponge substrate gave different results, on the first 60 min, a sample with a thickness of 1 cm has the highest degradation of 95 %. However, the thickness of the sponge substrate in the degradation

process has no significant effect occurs to photocatalytic activity under solar light.

The effect of  $\text{TiO}_2/\text{SiO}_2/\text{GSs}$  composite photocatalyst on the pollutant in environment, the experiment was conducted to N-Nitrosodiethylamine (NDEA) in contaminated solution. The solution was analyzed before and after photodegradation under solar light. Degradation of NDEA was done in 300 minutes by using  $\text{TiO}_2/\text{SiO}_2/\text{GSs}$  compact with the chosen thickness of 0.5 cm and get the efficiency of 95.52 % degradation.



School of Ceramic Engineering  
Academic Year 2021

Student's Signature.....*[Signature]*.....  
Advisor's Signature.....*[Signature]*.....  
Co-advisor's Signature.....*SUPUNNEE J.*.....

## ACKNOWLEDGEMENT

I would like to express my deepest gratitude to the following people for helping with this dissertation which could not have been performed and completed without the supports of them.

First, I would like to express my sincere acknowledgment to Suranaree University of Technology (SUT) for their SUT-Ph.D. Scholarship Program for ASEAN that give me the precious opportunity to spend thoroughly years doing research at SUT. Secondly, I want to give a special thanks to my advisor, Assistant Professor Dr. Sukasem Watcharamaisakul for providing valuable guidance, support, and encouragement so positively throughout my study at SUT. I would like to thank my co-advisor Dr. Supunnee Junpirom for insight and knowledge through fruitful discussions into the research. Also, I am thankful to the committee members, Associate Professor Dr. Sutin Kuharuangrong, Associate Professor Dr. Sukanda Jiansirisomboon, Assistant Professor Dr. Siriwan Chokkha, and Assistant Professor Dr. Jiratchaya Ayawanna and especially, the external committee member, Assistant Professor Dr. Onlamee Kamon – in, for their advice, comments, and suggestions that useful for this thesis.

Next, my gratitude also goes to Parasitic Disease Research Center staff members, especially to Associate Professor Dr. Natthakapach K. Rattanapitoon and Ms. Phornphitcha Pechdee for their kindly helps and detailed technical advice in plentiful ways during my research in their laboratory. Thanks to all my friends in SUT for helping me, giving me advice, supporting me, sharing good and bad moments during my study. Special thanks go to Windy Metasari, Ratih Dianingtyas, Dea Aulia Kartini, and Istiftakhun Nikmah who generously give their support for my study and life, along with tears and laughs. See you when I see you.

Surely, I could never come this far without the endless love, understanding and supports from my family. I would like to thank and dedicate this Ph.D. thesis to



my late father, Ir. Nana Sumarna, who educated me, also always believe, and encouraged me to study as much as possible. Though it is late, but I can keep my last promise to him to finish this study. And for my mother, Mrs. Ida Farida, who not only give me a life but also raised me with much love and care through my entire life. Lastly, I immensely appreciate to my partner in life, Miki Arian Saputra, for his enduring love, for believing in me long after I'd lost way and belief in myself, and for sharing my wish to reach the goal of completing this study but caring enough to love me even if I never achieved it. He also supported the family during much of my graduate studies. And Arkana Xavier Ryu Adrian, he is the one we have been waiting for and becomes the strength also light, like his name, so that I can go through my study.

MIA LESTARI AYUNINGTYAS

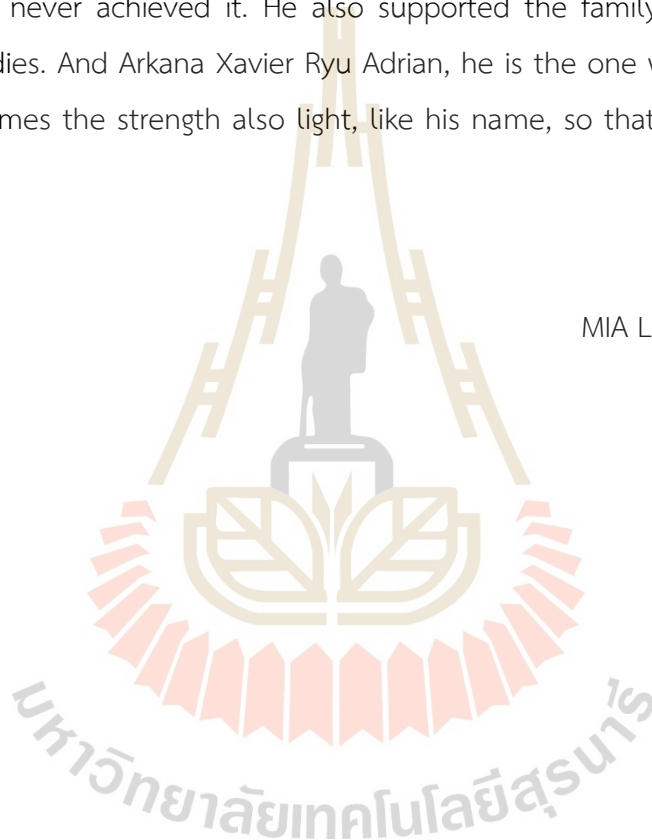


## TABLE OF CONTENTS

	Page
ABSTRACT (THAI).....	I
ABSTRACT (ENGLISH).....	III
ACKNOWLEDGEMENT.....	V
TABLE OF CONTENTS.....	VII
LIST OF TABLES.....	XII
LIST OF FIGURES.....	XIII
LIST OF ABBREVIATIONS.....	XVI
<b>CHAPTER</b>	
<b>I INTRODUCTION.....</b>	<b>1</b>
1.1 Background of Study.....	1
1.2 Research Objectives.....	3
1.3 Scopes and Limitations of Study.....	4
1.4 Hypothesis.....	4
1.5 Research Contribution.....	5
<b>II LITERATURE REVIEW.....</b>	<b>7</b>
2.1 Photocatalyst.....	7
2.1.1 Adsorption Process.....	8
2.1.2 Photocatalytic Activity.....	11
2.1.3 Application of Photocatalyst.....	16
2.1.4 Photocatalyst Research.....	16
2.2 TiO <sub>2</sub> .....	17
2.2.1 Application of TiO <sub>2</sub> .....	20
2.2.2 Related Research of TiO <sub>2</sub> as Photocatalyst.....	20

## TABLE OF CONTENTS (Continued)

	Page
2.3	SiO <sub>2</sub> ..... 21
2.4	Graphene Sheets..... 23
2.5	Preparation of Photocatalyst..... 24
2.5.1	Sol-Gel Method..... 24
2.5.2	Coating of Photocatalyst..... 25
2.6	Monte Carlo Simulation..... 26
2.6.1	Application of Monte Carlo in Photocatalyst..... 27
2.7	N- Nitrosamine..... 28
2.7.1	N-Nitrosodiethylamine (NDEA)..... 29
2.8	Characterization..... 30
2.8.1	X-Ray Diffraction (XRD)..... 30
2.8.2	SEM..... 32
2.8.3	TEM..... 34
2.8.4	Surface Area Analyzer..... 35
2.8.5	UV-Vis spectroscopy..... 37
2.8.6	Gas Chromatography..... 39
<b>III</b>	<b>EFFECTIVE SOLAR LIGHT PHOTOCATALYSIS BY GSs ADDITION ON THE COMPOSITE TiO<sub>2</sub>/SiO<sub>2</sub>..... 41</b>
3.1	Abstract..... 41
3.2	Introduction..... 41
3.3	Experimental Procedure..... 43
3.3.1	Preparation of TiO <sub>2</sub> /SiO <sub>2</sub> /GSs..... 43
3.3.2	Characterizations..... 43
3.3.3	Photocatalytic activity..... 45
3.4	Results and Discussion..... 48

## TABLE OF CONTENTS (Continued)

	Page
3.4.1 XRD Results.....	48
3.4.1.1 Effect of Calcination temperature (Tcal).....	48
3.4.1.2 Effect of GSs ratio .....	50
3.4.2 SEM/EDS and TEM Results.....	51
3.4.3 BET Results.....	55
3.4.3.1 Effect of Calcination temperature (Tcal).....	55
3.4.3.2 Effect of GSs ratio .....	56
3.4.4 Degradation of Methylene Blue (MB) Solution.....	57
3.4.4.1 Optimum Condition.....	57
3.4.4.2 Effect of Tcal.....	60
3.4.4.3 Effect of GSs Ratio .....	61
3.4.4.4 Effect of Reusable/Stability.....	63
3.5 Conclusion .....	64
<b>IV REMOVAL NITROSODIETHYLAMINE (NDEA) BY COATED OF TiO<sub>2</sub>/SiO<sub>2</sub>/GSs COMPOSITE PHOTOCATALYST ONTO SUPPORTING MATERIALS.....</b>	<b>65</b>
4.1 Abstract .....	65
4.2 Introduction.....	65
4.3 Experimental Procedure .....	67
4.3.1 Coating of TiO <sub>2</sub> /SiO <sub>2</sub> /GSs .....	67
4.3.2 Characterization of TiO <sub>2</sub> /SiO <sub>2</sub> /GSs Compact.....	68
4.3.3 Optimum Condition of Photocatalytic Activity .....	68
4.3.4 Removal NDEA in Contaminated Water.....	68
4.4 Results and Discussion .....	69
4.4.1. The Characteristics and Properties of TiO <sub>2</sub> /SiO <sub>2</sub> /GSs.....	69

## TABLE OF CONTENTS (Continued)

	Page
4.4.2. Optimum Condition of Photocatalytic Activity .....	71
4.4.3. Removal NDEA in contaminated water.....	72
4.5 Conclusion.....	73
<b>V SIMULATION OF PHOTOCATALYTIC REACTION ON TiO<sub>2</sub>/SiO<sub>2</sub>/GSs</b>	
<b>PHOTOCATALYST.....</b>	<b>75</b>
5.1 Abstract .....	75
5.2 Introduction.....	75
5.3 Experimental Procedure .....	77
5.4 Results and Discussion .....	78
5.4.1 Structural Model and Mechanism of TiO <sub>2</sub> /SiO <sub>2</sub> /GSs.....	78
5.4.2 Simulation of Photocatalytic Reaction TiO <sub>2</sub> /SiO <sub>2</sub> /GSs...	80
5.5 Conclusion.....	82
<b>VI CONCLUSION AND RECOMMENDATION.....</b>	<b>84</b>
6.1 Conclusion.....	84
6.2 Recommendation.....	85
REFERENCES.....	87
APPENDICES.....	101
RAW DATA OF ANALYSIS OF TiO <sub>2</sub> /SiO <sub>2</sub> /GSs POWDER .....	102
A.1 Data XRD.....	102
A.2 Data EDS .....	103
A.3 Data BET .....	106
A.4 Data MB degradation.....	107
RAW DATA OF ANALYSIS OF TiO <sub>2</sub> /SiO <sub>2</sub> /GSs COMPACT .....	117
B.1 Data MB degradation.....	117
B.2 Experimental procedure of NDEA degradation.....	122



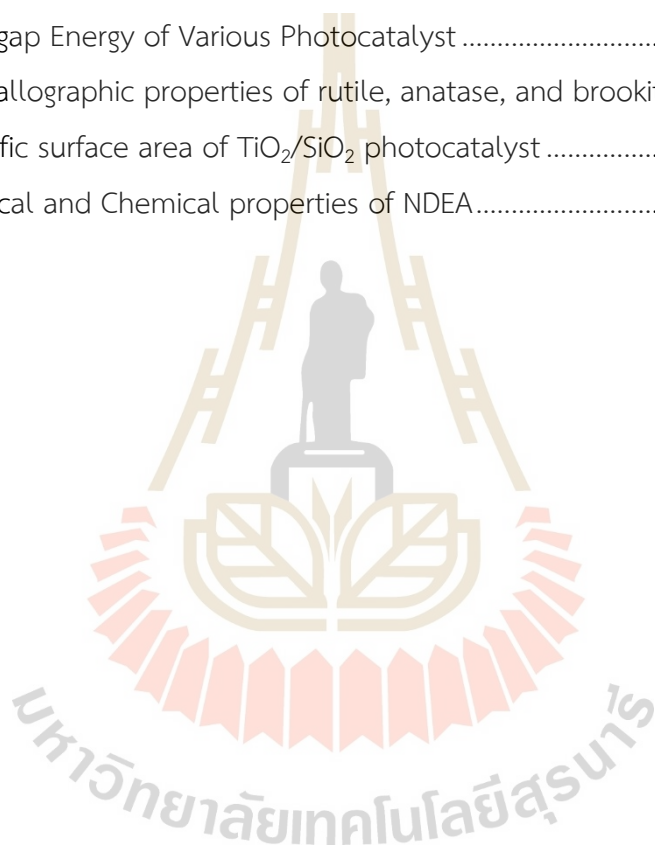
TABLE OF CONTENTS (Continued)

	Page
B.3 Data NDEA degradation .....	123
LIST OF PUBLICATIONS .....	129
VITAE.....	130



## LIST OF TABLES

Table		Page
2.1	Bandgap Energy of Various Photocatalyst .....	12
2.2	Crystallographic properties of rutile, anatase, and brookite.....	17
2.3	Specific surface area of $\text{TiO}_2/\text{SiO}_2$ photocatalyst .....	22
2.4	Physical and Chemical properties of NDEA.....	30



## LIST OF FIGURES

Figure		Page
2.1	The five types of adsorption isotherms .....	9
2.2	Comparison of wavelength, frequency, and energy for the electromagnetic spectrum .....	11
2.3	Mechanism of Photocatalyst .....	13
2.4	Structures of (a) Rutile, (b) Anatase, and (c) Brookite .....	18
2.5	Silicon dioxide .....	22
2.6	Process Flow Chart for the Preparation of TiO <sub>2</sub> based photocatalyst by Sol-Gel methods.....	25
2.7	General structure of nitrosamine.....	28
2.8	Chemical structure of NDEA.....	29
2.9	Bragg's Law of Diffraction.....	31
2.10	The essential parts of a small angle scattering system. T = x-ray source, S = sample, $\theta$ = the scattering angle, the slit used to define the incident and scattered beam, and D = detector .....	32
2.11	Types of interactions between electrons and a sample .....	33
2.12	Mechanism of SEM.....	33
2.13	Transmission electron microscope .....	35
2.14	BET plot and the relation between c and nm to slope and intercept of the y-axis .....	36
2.15	Lambert-Beer Laws .....	38
2.16	The components in gas chromatography.....	40
3.1	Experimental setup for Methylene Blue degradation by TiO <sub>2</sub> photocatalyst in the dark box (left) and with different light sources (left) and an open system under solar light (right).....	46

## LIST OF FIGURES (Continued)

Figure	Page
3.2	XRD pattern of TiO <sub>2</sub> photocatalyst G0.07 with a variation of Tcal ..... 49
3.3	The interpretation data of XRD result (G0.07)..... 49
3.4	XRD pattern of TiO <sub>2</sub> photocatalyst with a variation of GSs ratio (T450 °C) ..... 50
3.5	The interpretation data of the XRD result. .... 51
3.6	EDS result of TiO <sub>2</sub> /SiO <sub>2</sub> /GSs at Tcal 450 °C (left) and G0.07 in different Tcal (right)..... 52
3.7	Ratio of TiO <sub>2</sub> :GSs at Tcal 450 °C (left) and G0.07 in different Tcal (right). (Interpretation of XRD results)..... 52
3.8	SEM images of (a) GSs and TiO <sub>2</sub> /SiO <sub>2</sub> /GSs composite (b) G0, (c) G0.04, (d) G0.07 and (e) G0.14 at Tcal 450 °C..... 54
3.9	TEM images of TiO <sub>2</sub> /SiO <sub>2</sub> /GSs composite (a) G0, (b) G0.04, (c) G0.07 and (d) G0.14 at Tcal 450 °C..... 54
3.10	SEM images of G0.07 TiO <sub>2</sub> /SiO <sub>2</sub> /GSs composite (a) T400, (b) T450, and (c) T500. .... 55
3.11	TEM images of G0.07 TiO <sub>2</sub> /SiO <sub>2</sub> /GSs composite (a) T400, (b) T450, and (c) T500. .... 55
3.12	The effect of the amount of TiO <sub>2</sub> photocatalyst for degradation of MB. .... 57
3.13	The effect of the concentration of MB on the degradation process. .... 58
3.14	The effect of degradation under four conditions; dark, UV lamp (366 nm), solar light, and LED lamp on TiO <sub>2</sub> G0.04T500. .... 58
3.15	Adsorption of TiO <sub>2</sub> /SiO <sub>2</sub> /GSs under the dark condition at the first hour of degradation for each ratio and Tcal. .... 60
3.16	The effect of Tcal on $\eta$ degradation for G0.07 TiO <sub>2</sub> /SiO <sub>2</sub> /GSs..... 61
3.17	The rate constant of G0.07 TiO <sub>2</sub> /SiO <sub>2</sub> /GSs for each Tcal (left) and validity between experiment data and model data (right). .... 61
3.18	The effect of ratio Ti:GSs to $\eta$ degradation (%) for T450..... 62

## LIST OF FIGURES (Continued)

Figure	Page
3.19	The rate constant of $\text{TiO}_2/\text{SiO}_2/\text{GSs}$ for each ratio at T450 (left) and validity between experiment data and model data (right). ..... 63
3.20	Effect of recycled G0.07T450 $\text{TiO}_2$ photocatalyst on $\eta$ degradation..... 64
4.1	SEM images of sponge substrate of $\text{TiO}_2/\text{SiO}_2/\text{GSs}$ sample (a) t0.3, (b) t0.5, (c) t0.8, and (d) t1 (cm)..... 70
4.2	The effect of thickness of $\text{TiO}_2/\text{SiO}_2/\text{GSs}$ compact on the sponge to $\eta$ degradation (%). ..... 71
4.3	Degradation of NDEA by $\text{TiO}_2/\text{SiO}_2/\text{GSs}$ (G0.07T450) compact (t0.5)..... 72
4.4	(a) Rate constant of degradation of NDEA by $\text{TiO}_2/\text{SiO}_2/\text{GSs}$ compact (t0.5) (b) validity between experiment data and model data. .... 73
5.1	The proposed structural model of $\text{TiO}_2/\text{SiO}_2/\text{GSs}$ in a one-unit cell of anatase phase..... 78
5.2	Bonding on $\text{TiO}_2/\text{SiO}_2/\text{GSs}$ photocatalyst..... 79
5.3	Mechanism of photocatalytic degradation of MB by $\text{TiO}_2/\text{SiO}_2/\text{GSs}$ composite. .... 80
5.4	System of $\text{TiO}_2$ -GSs(cube) and pollutants (red dot)..... 81



## LIST OF ABBREVIATIONS

$\lambda$	= Wavelength
$\mu\text{g/l}$	= microgram per liter
$\theta$	= Surface coverage of adsorbent by adsorbate
$\sigma$	= Adsorption cross-section of a gas
$\nu$	= Frequency
BET	= Brunauer–Emmett–Teller
C	= Concentration of adsorbate that was adsorbed
CB	= Conduction band
$C_0$	= Initial concentration of adsorbate
$C_e$	= Concentration of adsorbate solution (mg/L).
$C_m$	= The maximum concentration of adsorbate to make a monolayer
d	= The distance between adjacent planes of atoms (the d-spacings)
$e^-$	= Free electron
E $\gamma$	= Gap energy of the bandgap
EDS	= Energy Dispersive X-ray Spectrometer
eV	= electron volt
GSs	= Graphene Sheets
h	= Planck's constant
$h^+$	= Hole
$H^+$	= Hydrogen ion
$\text{HO}_2^\bullet$	= Hydroperoxyl
$\text{H}_2\text{O}$	= Water
$\text{H}_2\text{O}_2$	= Hydrogen peroxide
J	= Joule
J.s	= Joule second
k	= Rate constant
K	= Equilibrium constant of Langmuir

## LIST OF ABBREVIATIONS (Continued)

$K_L$	= adsorption rate constants of Langmuir
$k_r$	= Reaction rate constant
L/mg	= liter per milligram
m	= meter
m/s	= meter per second
mg/L	= milligram per liter
mg/L.min	= milligram per liter minute
NDEA	= Nitrosodiethylamine
$O_2$	= Oxygen
$O_2^\bullet$	= Oxygen radical
$OH^\bullet$	= Hydroxyl radical
$OH^-$	= Hydroxide ion
p	= Partial pressure or the molar concentration of adsorbate
$p_0$	= Vapor pressure
$q_e$	= Amount of adsorbate that adsorbed by a gram of adsorbent
$q_m$	= Amount of adsorbate to make a complete monolayer
r	= Photocatalytic rate
SEM	= Scanning Electron Microscope
$SiO_2$	= Silicon dioxide
$S_t$	= Total surface area
t	= Time
TEM	= Transmission Electron Microscopy
$TiO_2$	= Titanium dioxide
UV	= Ultraviolet
V	= Volume of adsorbate that adsorbed by a gram of adsorbent
VB	= Valence band
$V_m$	= Volume of adsorbate to make a complete monolayer
XRD	= X-Ray Powder Diffraction

# CHAPTER I

## INTRODUCTION

### 1.1 Background of Study

N-Nitrosamines are one pollutant that can be occurred naturally in the environment. When nitrate sources react with the amine in specific conditions like acidify and temperature, it will form N-nitrosamine (Wainright, 1986). Amines and amines-related compounds are found in surface water, like rivers, lakes, reservoirs, wetlands, and seawater (Bartsch & Montesano, 1984; X. Li et al., 2016). Then nitrates sources, in environments, some of nature is found and can be added from industrial waste and fertilizer. In practice, N-nitrosamines are not the main concern in the water treatment either the wastewater or drinking water treatment yet their presences cannot be separated in water resources (Andrzejewski & Nawrocki, 2018; Breider & Von Gunten, 2017). In some sewage treatment plant effluent in Ontario in 1990, N-nitrosamines were detected in 27 of 39 samples, with the maximum concentration being 0.22 µg/l (WHO, 2008). Most of the individual form of N-nitrosamines currently become interested in research because it has been known as potential mutagens and carcinogens (Andrzejewski & Nawrocki, 2018; Bartsch & Montesano, 1984).

In these areas, rising incomes, coupled with increasing concerns about poor water and air quality and expanding consumer awareness about the types of treatment systems available, will propel demand growth. Globally, 1 billion people do not have access to safe drinking water, and 2.6 billion do not have access to basic sanitation, (Muller et al., 2010). This is especially true for the least developed regions of Asia, Central and South America, and Africa, where innovative water purification systems are desperately needed. Therefore, waste treatment must be a pressing environmental problem caused by industries.

If concerned with effective and efficient methods, there are a few advanced

treatment methods that can be applied in industries. Photocatalyst is one of the advanced oxidation technologies that attract the most attention as waste treatment lately. Photocatalyst is one of the advanced treatment methods to mitigate pollutants in various media. Photocatalytic is related to the development of solar energy use. A photocatalyst is a "catalyst that accelerates the solar photo process," and the following parameters must be met to become a photocatalyst: (i) the photocatalyst should not participate directly in the reaction or be consumed; and (ii) needs to provide other mechanism routes from existing photoreactions and accelerated reaction rate (Castellote & Bengtsson, 2011; Moura & Suyanto, 2004; Turchi & Ollis, 1990). Photocatalyst self is an excellent method especially in water waste and air pollutant treatments which are certainly difficult to process when just using conventional methods. It is because photocatalyst uses an oxidation process thus needs simple pre-treatment and does not need to use in a large area. The solar photocatalysis technique is affordable, environmentally friendly, and universally applicable if it uses sunshine. The equipment required is modest, making it ideal for underdeveloped countries or rural locations without access to electricity.

Photocatalyst requires light to activate catalyst function. The Source of light that can be used is dependent on the bandgap of the materials. All semiconductors in nanomaterials form can be used in photocatalysis. In 2007, the global market for nanotechnological applications in water and wastewater treatment reached \$1.6 billion,  $\text{TiO}_2$  is the most widely used among them (Muller et al., 2010).  $\text{TiO}_2$  has sparked interest due to its favorable physicochemical features, which include thermal and chemical stability, relatively high photocatalytic activity, low toxicity, and low cost (Castellote & Bengtsson, 2011; Dalton et al., 2002; Singh & Dutta, 2018).

However, the bandgap of  $\text{TiO}_2$  is generally a range of 3.0-3.2 eV, which gives a work range as photocatalyst under UV range (380 – 400 nm) (Castellote & Bengtsson, 2011). It almost makes  $\text{TiO}_2$  cannot effectively work under the radiation of sunlight (no more than 4 % yield of the solar spectrum). Meanwhile, visible light adsorption can occur on semiconductors with gap energy less than or equal to 3 eV. To increase photocatalytic of  $\text{TiO}_2$  under visible light, many methods have been introduced in

much research for example impure doping (metal/non-metal), surface modification, hybrid composite (integration with other materials), etc.

Somehow, nonmetal doping was effective to obtain a visible light response. In recent years, carbon in graphene form is popular doping material to decrease the bandgap of semiconductors, especially in photocatalyst application. Its properties such as high thermal and electrical conductivity, high specific surface area, and high charge carrier mobility at room temperature (Au-pree et al., 2021; Najafi et al., 2017; Tang et al., 2018). Therefore, the composite of graphene and semiconductors, especially  $\text{TiO}_2$ , is currently being considered as a potential photocatalyst in air and water purification. The graphene-based  $\text{TiO}_2$  composite exhibits an enhanced photocatalytic activity in comparison with only  $\text{TiO}_2$  (Y. Zhang et al., 2010).

$\text{TiO}_2$  in powder form will give higher photocatalytic activity than in coating of  $\text{TiO}_2$  yet has difficulty in separating the suspended  $\text{TiO}_2$  and need another installation to separate it (Larumbe et al., 2014). To avoid free nanoparticles in water, nano- $\text{TiO}_2$  particles are usually coated on a substrate or integrated into thin films and other materials (Doll & Frimmel, 2004). The Coating of  $\text{TiO}_2$  makes it easy to be installed and recycle but will be reduced photocatalytic activity because of the reduction of the effective surface area. By adding material that has high surface area into  $\text{TiO}_2$  and/or reduced the structure into nanoscale (nanostructured), gives a chance of  $\text{TiO}_2$  to has high photocatalytic activity when in the coated form.

## 1.2 Research Objectives

The objectives of this research are as follows:

- a. To synthesize  $\text{TiO}_2/\text{SiO}_2/\text{GSs}$  photocatalyst by sol-gel method.
- b. To investigate the optimum properties of photocatalyst powder in photodegradation of methylene blue.
- c. To determine the best thickness of  $\text{TiO}_2/\text{SiO}_2/\text{GSs}$  photocatalyst sponge that give the highest photoactivity (by using nitrosamine solution).



d. To arrange the structure and simulate photodegradation by using Monte Carlo Simulation.

### 1.3 Scopes and Limitations of Study

The scopes of this research are as follow:

- a. Preparation of  $\text{TiO}_2/\text{SiO}_2/\text{GSs}$  photocatalyst by using sol-gel method.
- b.  $\text{SiO}_2$  that will be used is synthesized from rice husk by using  $\text{H}_2\text{SO}_4$ .
- c. GSs are synthesized by using the chemical exfoliation method from Graphene Oxide.
- d. The ratio of  $\text{TiO}_2$  : GSs and experimental conditions that give the highest photoactivity.
- e. The size (thickness) of  $\text{TiO}_2/\text{SiO}_2/\text{GSs}$ .
- f. Characterize  $\text{TiO}_2/\text{SiO}_2/\text{GSs}$  photocatalyst with XRD, SEM-EDS, TEM, and BET.
- g. Characterize the photocatalytic activity of  $\text{TiO}_2/\text{SiO}_2/\text{GSs}$  photocatalyst by using methylene blue.
- h. The decomposed activity of photocatalyst by using water contaminated with NDEA.

### 1.4 Hypothesis

Previous studies of photocatalyst only focused on photocatalyst in powder form. Then the removal of NDEA only focused on the photolysis process yet it needs another installation which is UV irradiator. In this thesis, the work will focus on coating photocatalyst. The removal process of NDEA will be conducted by photocatalyst under visible light. The hypothesis of this research can be simplified as:

a. The research will take place in  $\text{TiO}_2$  as a photocatalyst that can work under a visible wavelength range. The powder form of photocatalyst is not effectively used because it needs an advanced separation between the system (water) and the photocatalyst. Because of that, this research will be focused on coated  $\text{TiO}_2$  by a coating method.

b. The coated form has a disadvantage as the photocatalytic activity of  $\text{TiO}_2$  will decrease because of its surface area. Moreover, since the work range of  $\text{TiO}_2$  is around 387 nm (under UV range), the graphene will be doped into  $\text{TiO}_2$  to decrease the bandgap of  $\text{TiO}_2$  and enhance the photocatalytic activity of  $\text{TiO}_2$  before it coated into substrate.

c. The reaction in the photocatalysis process is included the adsorption process and photocatalytic activity. The adsorption of the photocatalyst influence the number of pollutants to be near the surface of the photocatalyst.  $\text{SiO}_2$  presence can increase the adsorption ability of photocatalyst.

## 1.5 Research Contribution

This research offers valuable contribution to research novelty in the following area:

a. This research will enrich a growing number of studies in the photocatalyst area, especially in  $\text{TiO}_2$  development.

b. Doped- $\text{TiO}_2$  has been extensively studied to improve photocatalytic activity in the visible light area but no literature has researched compacted photocatalyst.

c. Finding the optimum condition of preparation of compacted photocatalyst will further help the industries especially the community in water treatment management considering not only can be used with sunlight but also easy in installation.

- d. Finding the alternative solution to solve the problem of nitrosamine in the water reservoir and food in advance.



## CHAPTER II

### LITERATURE REVIEW

Photocatalyst has recently is given attention by researchers because of its performances, both adsorption (explained by Langmuir equation) and photocatalytic activity (Pseudo nth order reaction and Langmuir Hinshelwood equation), in environmental purification. Titanium dioxide ( $\text{TiO}_2$ ) is one of the most promising semiconductor materials used in heterogeneous photocatalysis. Adding silica and graphene sheet in  $\text{TiO}_2$  as composite by using sol-gel method gave bandgap reduction and photocatalytic activity increasing in powder form based on Chen's work (Chen et al., 2015) while in its coated form will be investigated.

#### 2.1 Photocatalyst

When a substance accelerates a chemical process without being consumed as a reactant, it is said to be a catalyst. Then, photocatalysis can be defined as the acceleration of a photoreaction by the presence of a catalyst (Castellote & Bengtsson, 2011). According to the phase of photocatalyst and reactants that exist, there are two types, heterogeneous and homogenous photocatalyst. The former gain interest due to its advantages in the separation process especially from an environmental point of view. In the term of heterogeneous photocatalyst, solid material, usually semiconductor, is used in both the aqueous and the gas phase, furthermore, it is called just photocatalyst. Photocatalyst has two main stages: (i) adsorption of the reactants on to catalyst surface and (ii) photocatalytic activity of catalyst as a reaction with reactants (Jain & Vaya, 2017; Zhu & Wang, 2017). The latter gives a difference from the catalyst by using photonic radiation as an activator.

### 2.1.1 Adsorption Process

Adsorption is a surface phenomenon that occurs when atoms, ions, or molecules from a gas, liquid, or dissolved solid (adsorbate) adhere to an adsorbent's surface, in this case, is a photocatalyst surface. The capability of catalysts to drawn substances depends on the type of adsorbent, explain different surface energy in each material, either physical force, chemical, or both simultaneously.

Adsorption is typically characterized using isotherms, which show the amount of adsorbate on the adsorbent as a function of pressure (if gas) or concentration (if liquid) at a constant temperature. This isotherm behavior could be the result of the combination of surface heterogeneity and interactions between adsorbed molecules. So, by measuring adsorption equilibrium, isosteric heat, and the topography of the surface, as the observed adsorption isotherm, full energy distribution can be determined (Sing, 1985).



According to Le-Chatelier principle, When an equilibrium system is subjected to a change in concentration, temperature, volume, or pressure, the system readjusts itself to (partially) counterbalance the effect of the applied change, and a new equilibrium is formed (*Le Chatelier's Principle Fundamentals*, 2021). If an excess of pressure is applied to the equilibrium system, the equilibrium will move in the direction of a decrease in the number of molecules. Because the quantity of molecules reduces in the forward direction as pressure increases, the forward direction of equilibrium will be preferred.

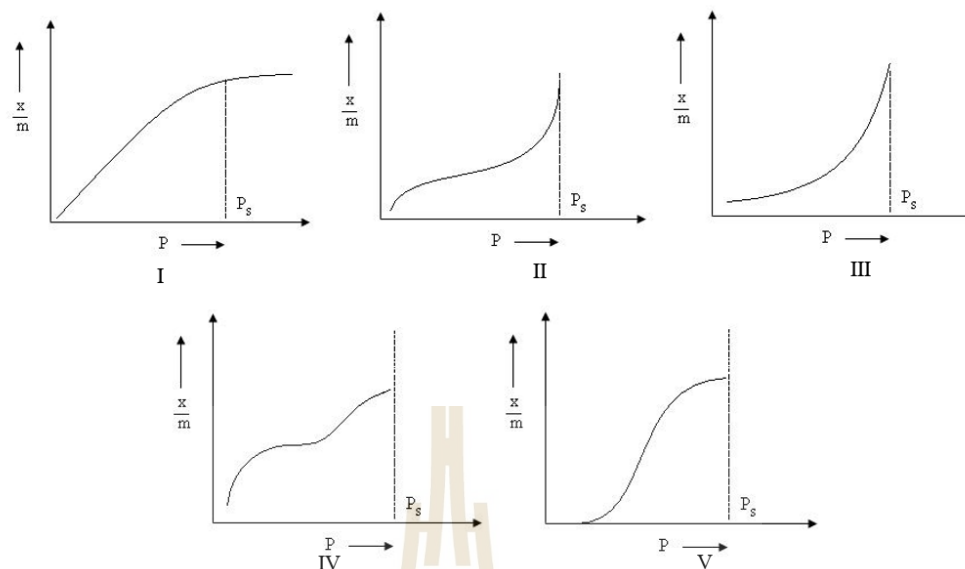


**Figure 2.1** The five types of adsorption isotherms (Brunauer et al., 1940).

There exist five different types of isotherms. Type I is the well-known Langmuir adsorption isotherm, Type II is the S-shaped or sigmoid isotherm, shows a large deviation from the Langmuir model of adsorption. Type III explains the formation of the multilayer. Types II and III are closely related to Types IV and V, only in the former cases does the adsorption increases as the vapor pressure  $p_0$  of the adsorbed gas is approached, whereas in the latter cases the maximum adsorption is attained, or almost attained, at some pressure lower than the vapor pressure of the gas (Brunauer et al., 1940).

The simplest model, which is type I, describing the heterogeneity of solid surface is that of Langmuir (Langmuir, 1916). Langmuir proposed a new Adsorption Isotherm called the Langmuir Adsorption Isotherm. This isotherm is founded on several assumptions, one of which is that dynamic equilibrium exists between adsorbed and free gaseous molecules. It is a semi-empirical isotherm with a kinetic basis that was calculated using statistical thermodynamics. Because of its simplicity and ability to match a wide range of adsorption data, it is the most used isotherm equation. It is predicated on four premises:

- a. Each adsorption site is equivalent, and each site can only hold one molecule.
- b. The surface is energetically homogenous, and the molecules that are adsorbed do not interact.
- c. There are no phase transitions.
- d. Only a monolayer form at maximum adsorption.

From these assumptions, it can show the relationship between adsorbing molecules and adsorbents as the following equation (Do, 1998).

$$\theta = \frac{Kp}{(1+Kp)} \quad (2.3)$$

where  $\theta$  is surface coverage of adsorbent by adsorbate, explained by  $\frac{V}{V_m}$ ,  $V$  is the volume of adsorbate that is adsorbed by a gram of adsorbent,  $V_m$  is the volume of adsorbate to make a complete monolayer,  $K$  is the equilibrium constant of Langmuir, and  $p$  is the partial pressure or the molar concentration of adsorbate by substituting the value  $\theta$  and make in linear equation, will get Langmuir Adsorption Equation.

$$\frac{P}{V} = \frac{P}{V_m} + \frac{1}{KV_m} \quad (2.4)$$

Thus, if the graph was plotted between  $\frac{P}{V}$  versus  $P$ , the graph will be linear with the slope  $\frac{1}{V_m}$  and the intercept  $\frac{1}{KV_m}$ . Those values can be used to calculate the surface coverage of adsorption. Langmuir equation can also be expressed in concentration for absorptivity in a liquid-solid phase like



$$\frac{q_e}{q_m} = \frac{KC_e}{(1+KC_e)} \quad (2.5)$$

where  $q_e$  is the amount of adsorbate that is adsorbed by a gram of adsorbent,  $q_m$  is the amount of adsorbate to make a complete monolayer, and  $C_e$  is the concentration of adsorbate solution (mg/L).

### 2.1.2 Photocatalytic Activity

Photocatalysis is a reaction that occurs when light energy hits the surface of materials. Semiconductors are good photocatalysts because of their electronic structure, which includes an empty vacuum between the top of the full valence band (VB) and the bottom of the empty conduction band (CB), which permits electron-hole pairs to form (S. G. Kumar & Devi, 2011).

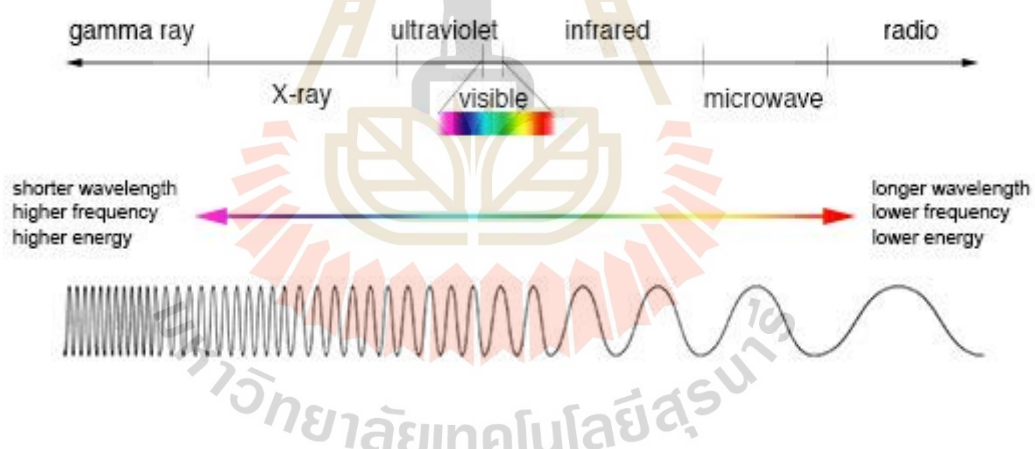


**Figure 2.2** Comparison of wavelength, frequency, and energy for the electromagnetic spectrum (*National Aeronautics and Space Administration Goddard Space Flight Center, 2013*).

The energy required for the electron excitation depends on the characteristics of the semiconductors. The minimum wavelength necessary for the photoexcitation ( $\lambda_{E_{bg}}$ ) depends on the bandgap of the photocatalyst. The low bandgap energy for many of these materials allows them to absorb light from a wide

area inside the visible light spectrum. The bandgap of a solid and the wavelength of light are related via the Planck-Einstein Relation (French & Taylor, 1978),

$$E_{\gamma} = h\nu = \frac{hc}{\lambda} \quad (2.6)$$

where  $E_{\gamma}$  is the gap energy of the bandgap (J),  $h$  is Planck's constant  $6.63 \times 10^{-34}$  (J.s),  $\nu$  the frequency (hertz),  $c$  is the speed of light  $3.0 \times 10^8$  (m/s), and  $\lambda$  is the wavelength (m).

However, as typical for oxide semiconductors with a narrow bandgap, they are photo catalytically inactive due to rapid recombination of the photoinduced electron-hole pair. A good photocatalyst should be (i) photoactive, (ii) able to utilize visible and/or near UV light, (iii) biologically and chemically inert, (iv) photostable (not prone to photo corrosion), (v) inexpensive, and (vi) non-toxic (Bezerra et al., 2017; Bhatkhande et al., 2002; Ota & Maroto-Valer, 2015). Table 2.1 gives the bandgap energies of the photocatalyst.

**Table 2.1** Bandgap Energy of Various Photocatalyst (Bhatkhande et al., 2002).

Photocatalyst	Bandgap Energy (eV)	Photocatalyst	Bandgap Energy (eV)
Si	1.1	Fe <sub>2</sub> O <sub>3</sub>	2.2
TiO <sub>2</sub> (rutile)	3.0	ZnO	3.2
TiO <sub>2</sub> (anatase)	3.2	CdS	2.4
WO <sub>3</sub>	2.7	SrTiO <sub>3</sub>	3.4
ZnS	3.7	WSe <sub>2</sub>	1.2
SnO <sub>2</sub>	3.5	$\alpha$ -Fe <sub>2</sub> O <sub>3</sub>	3.1

The general mechanism of photocatalyst is shown in Figure 2.3. When the light (photon) with energy, that is equal or greater than the photocatalyst

bandgap, is adsorbed by the photocatalyst, electrons are excited from the valence band to the conduction band. This phenomenon generates electron-hole pairs. These charges,  $e^-$  and  $h^+$ , will reach the surfaces of photocatalyst and reacts with either water, oxygen, or hydroxyl groups from pollutants. The holes ( $h^+$ ) react directly with water or hydroxyl to produce  $OH^\bullet$  radicals while the electrons ( $e^-$ ) will reduce the oxygen gives  $O_2^\bullet$  radicals.

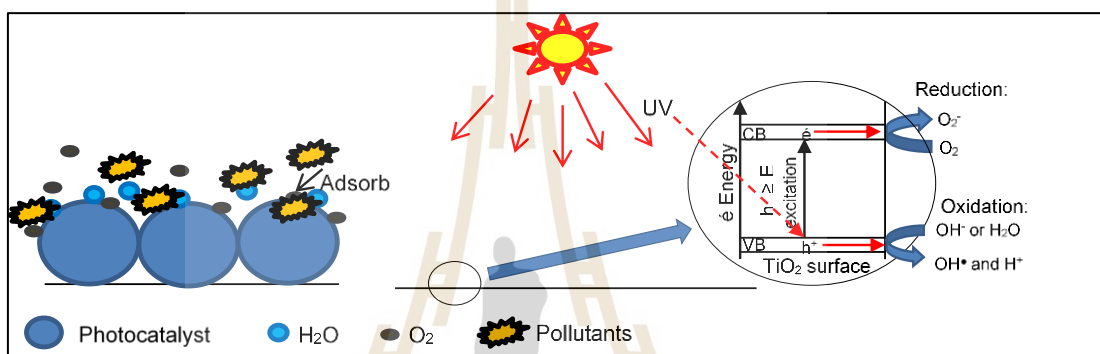
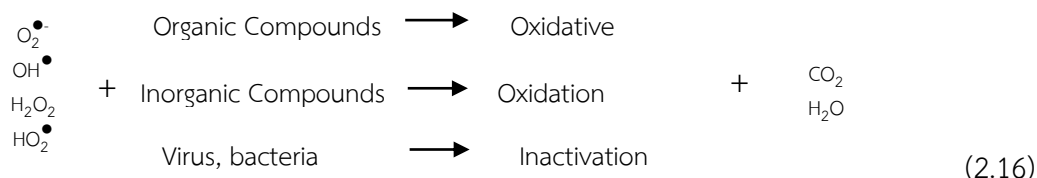


Figure 2.3 Mechanism of Photocatalyst (Klondon et al., 2016).

This mechanism could be described by the following reactions.





From reaction (2.7) to (2.15), four products can be used as an oxidizing agent since they are capable to oxidize any organic and inorganic materials. Reaction (2.16) describes the reaction that occurs when materials in pollutants react with these oxidizing agents. The result of the last reaction conduct to  $\text{CO}_2$  and  $\text{H}_2\text{O}$  presents, and in some cases, an inorganic acid.

There are two states in heterogeneous photocatalysis which are the ground state and excited state. The process of states' change can be described mathematically by using kinetic chemical reactions. Kinetics of reactions often start from first-order kinetics which is commonly used for observing reactions in homogenous phases (Bhatkhande et al., 2002; Castellote & Bengtsson, 2011). However, in heterogeneous photocatalysis, the kinetics of reactions must be significantly different. Studies of kinetics often used the Langmuir-Hinshelwood mechanism for photocatalytic reactions in the suspension system.

Langmuir-Hinshelwood's mechanism was introduced by Langmuir (1921) and was developed by Hinshelwood (1926). The Langmuir-Hinshelwood process assumes that two molecules adsorb nearby sites in this mechanism, and the adsorbed molecules undertake a bimolecular reaction. Typically used when discussing the mechanism of a photocatalytic reaction in a suspension system. The photocatalytic reaction necessitates the simultaneous participation of organic and oxygen molecules (Davis & Davis, 2003). Because oxygen is abundant in nature, its concentration can be assumed to be constant throughout photocatalysis. Photocatalysis requires the adsorption of organic compounds on the semiconductor

surface. A Langmuir isotherm is thought to govern the adsorption-desorption (A–D) equilibrium. The following equation is used to calculate the amount of substance that will be adsorbed at the catalyst's surface (Davis & Davis, 2003; Langmuir, 1916).

$$r = -\frac{dC}{dt} = k_r C \quad (2.17)$$

$$\theta = \frac{C}{C_m} = \frac{KC}{1+KC} \quad (2.18)$$

$$r = -\frac{dC}{dt} = \frac{k_r KC}{1+KC} \quad (2.19)$$

where  $r$  is the photocatalytic rate (mg/L.min),  $k_r$  is the reaction rate constant (mg/L.min),  $C$  is the concentration of adsorbate that was adsorbed (mg/L) at time  $t$ ,  $C_m$  is the maximum concentration of adsorbate that were adsorbed to make a monolayer (mg/L),  $K$  is adsorption rate constants of Langmuir (L/mg), and  $C$  is the concentration of adsorbate solution at time  $t$ . The integrated expression of equation (2.19) can calculate the constant  $k_r$  and  $K$  by limit  $C = C_0$  at  $t = 0$  and  $C = C$  at  $t = t$ .

$$\ln \left( \frac{C_0}{C} \right) + K(C_0 - C) = k_r K t \quad (2.20)$$

The LH kinetics on the first order has condition  $KC \ll 1$ . If so, equation (2.19) becomes  $r = k_r KC$  and be integrated into first-order kinetics and is given by:

$$\ln \frac{C_0}{C_t} = k t \quad (2.21)$$

where  $k$  ( $k_r K$ ) is the rate constant ( $\text{min}^{-1}$ ) and  $t$  is the degradation time (min).

### 2.1.3 Application of Photocatalyst

Major users of photocatalyst products used it as a sustainable technology for environmental purification especially to remove pollutants in air and water. This application can remove both organic and inorganic matters from air and water. In the case of air cleaning, photocatalyst can be mixed with concrete or cement (Boonen & Beeldens, 2014; Shen et al., 2012). Photocatalyst also has been used water splitting to produce hydrogen and oxygen as an alternative fuel (Fujishima & Honda, 1972; Moniz et al., 2015). Some photocatalyst was researched and produce to disinfectant and self-cleaning product to remove microbial and dirt (Paz & Heller, 1997). In the medical area, photocatalyst can activate photosensitizer creates reactive oxygen species that can kill the surrounding cells of the tumor (Ibhadon & Fitzpatrick, 2013).

### 2.1.4 Photocatalyst Research

A study about heterogeneous photocatalyst was published first time by Fujishima and Honda in 1972. They developed a photoelectrochemical cell with semiconducting n-type  $\text{TiO}_2$  to use in water photolysis (Fujishima & Honda, 1972). Matthews (1986) started research  $\text{TiO}_2$  (Degussa P25) thin film on photooxidation of organic matters by using a UV lamp. In this study, also was known that each flow rate obeyed first-order kinetics and more precisely interpreted in the integrated form of the Langmuir expression (Matthews, 1987).  $\text{TiO}_2$  is still the main semiconductor material for photocatalytic research in the 1990s. Most of them were focused on photodegradation of Volatile Organic Compounds in the gases phase for air purification (Alberici & Jardim, 1997; Augugliaro et al., 1999; Blanco et al., 1996; Hager & Bauer, 1999).

Following the triumph of  $\text{TiO}_2$ ,  $\text{ZnO}$  is another photocatalyst that draws the attention of researchers. Hossain prepares a hexagonal  $\text{ZnO}$  nanorod that has been confirmed to have an optical bandgap of 3.30 eV, similar to pure  $\text{ZnO}$  (Hossain & Hossein, 2015).  $\text{ZnO}$ -doped also has been researched. While co-doped Bi and Ag were conducted to increase the conductivity of  $\text{ZnO}$  thin film by Lin (Lin et al., 2015). Lavand made a progress in the preparation of visible light photocatalyst of

C/ZnO/CdS nanocomposite. CdS were used to expand the photo-response of C doped ZnO to the visible region (Lavand & Malghe, 2015).

$\alpha$ -Fe<sub>2</sub>O<sub>3</sub> is a new promising semiconductor that was thought to be an ideal photocatalyst because of its abundance, low cost, and narrow bandgap (2.20 eV). However, it has a short charge carrier diffusion length and recombination with rapid charge (Pal et al., 2014).

## 2.2 TiO<sub>2</sub>

Titanium dioxide, also known as titanium (IV) oxide, has a molecular weight of 79.87 g/mol and represents the naturally occurring oxide with the chemical formula TiO<sub>2</sub>. TiO<sub>2</sub> is a mineral that exists in nature at room temperature as three main different crystallines such as rutile, anatase, and brookite. Their crystallographic properties can be seen in Table 2.2 (Khataee & Mansoori, 2011).

**Table 2.2** Crystallographic properties of rutile, anatase, and brookite.

Crystal Structure	Density (kg/m <sup>3</sup> )	System	Space Group	Cell Parameters (nm)		
				a	b	c
Rutile	4240	Tetragonal	$D_{4h}^{14}$ mnm	0.4584		0.2953
Anatase	3830	Tetragonal	$D_{4h}^{19}$ amd	0.3758		0.9514
Brookite	4170	Orthorhombic	$D_{2h}^{15}$ Pbca	0.9166	0.5436	0.5135

Each crystal structure contains 6-coordinate titanium but rutile is the most common form (Greenwood & Earnshaw, 1997). A titanium atom is surrounded by six oxygen atoms in a distorted octahedral configuration to form the basic block. (Diebold, 2003). Rutile TiO<sub>2</sub> crystal is widely available, both in nature and produced commercially.



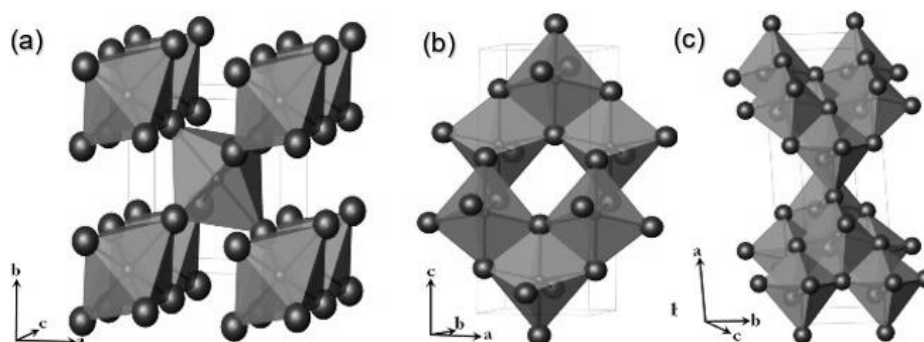


**Figure 2.4** Structures of (a) Rutile, (b) Anatase, and (c) Brookite (Aravindan et al., 2015).

The properties of semiconductors in  $\text{TiO}_2$  are considered in photocatalyst application. Different structures exhibit different photocatalytic activities towards the same organic material under identical conditions. Yet, in most photocatalytic studies, anatase form shows more photocatalytic activity compared to rutile. Even though anatase form has a higher bandgap energy (3.2 eV) compared with rutile (3.0 eV), rutile being constantly much less photoactive than anatase then efficiency in photo-adsorbing and photo-desorbing oxygen not much better than anatase. Since the high performance of a good photocatalyst is related simultaneously (i) to a good capacity of adsorbing reactants and (ii) to a good ability to absorb photons to create photoinduced electrical charges, it appears that anatase corresponds to the best candidate (Sclafani & Herrmann, 1996).

$\text{TiO}_2$  has wideband energy (3.2 eV) means that only 5% of the solar spectrum could be used as the light source for photocatalyst. For installation, a UV lamp was needed to enhance the photoactivity of  $\text{TiO}_2$ . Another way, to increase photo activity in the visible area, modification of the electronic structure must be applied such as impure doping (metal/non-metal), surface modification, hybrid composite (integration with other materials), etc. (Hernandez et al., 2016).

TiO<sub>2</sub> is a good photocatalyst with numerous applications. TiO<sub>2</sub>'s key advantages are its great chemical stability (inertness) when exposed to acidic and basic substances, nontoxicity, low cost, and strong oxidizing power, which make it a viable choice for many photocatalytic applications (Castellote & Bengtsson, 2011; Khataee & Mansoori, 2011). TiO<sub>2</sub> is an industrially mass-produced substance that is easy to get, cheap, and simple to create in the laboratory. TiO<sub>2</sub> as a photocatalyst is a powerful oxidant that is less expensive and more environmentally friendly than chlorine in water treatment (Lee & Park, 2013).

As explain before, the properties of semiconductors in TiO<sub>2</sub> can be considered in photocatalyst area. These properties will have a different result depends on the phase of TiO<sub>2</sub>. The differences in titanium dioxide rutile and anatase structures have a significant impact on their physicochemical qualities. In general, anatase is more active than rutile, but there is no agreement on why this is so. In Luttrell et al. (2014), they get that anatase activity increases for films up to 5 nm thick, but rutile films attain their maximal activity for layers as thin as 2.5 nm. This demonstrates that charge carriers stimulated deeper in the bulk of anatase contribute more to surface reactions than charge carriers excited in rutile (Luttrell et al., 2014).

TiO<sub>2</sub> as photocatalyst is found in a variety of polymorphs, the most prevalent of which are anatase- and rutile-crystal structures. Rutile has lower electron mobility, a greater dielectric constant, and a higher density than anatase. The point of zero charge of TiO<sub>2</sub> increases as the rutile content of the sample increases. In the case of rutile, charge recombination rates are lower. But rutile is a highly effective photocatalyst for the activation of molecular oxygen. However, anatase looks to be a more potent oxidant. Excitation of rutile/anatase composites results in desirable charge separation, which involves electron transfer from rutile to anatase. The inclusion of rutile increases the amount of oxygen adsorbed at the composite when compared to anatase. The oxidation properties of the rutile /anatase combination, on the other hand, outperform those of pure rutile. The anatase/rutile ratio can be adjusted to optimize the composite's overall photocatalytic activity.

### 2.2.1 Application of TiO<sub>2</sub>

TiO<sub>2</sub> was used as a promising material in many applications. The common application including antibacterial purposes, self-cleaning coatings, solar cells, gas sensors, as a white pigment in paints and cosmetics products, and corrosion-protective coatings (Diebold, 2003). TiO<sub>2</sub> also is important in earth sciences, play role in the biocompatibility of bone implants, used in controlled drug-release and cancer-cell treatment and environmental remediation (Khataee & Mansoori, 2011).

### 2.2.2 Related Research of TiO<sub>2</sub> as Photocatalyst

In the photocatalyst area, many semiconductors can be used. However, TiO<sub>2</sub> is appropriate for efficient photocatalytic reaction in the environmental application. Several researchers research TiO<sub>2</sub> in its application as a photocatalyst in environmental remediation. The semiconductor properties of TiO<sub>2</sub> are necessary for the removal of organic pollutants (Khataee & Mansoori, 2011). Both pure and composite TiO<sub>2</sub> are developed through research, improve the use of TiO<sub>2</sub> in these areas.

Matthews started research TiO<sub>2</sub> (Degussa P25), primarily anatase, thin film on photooxidation of organic matters in water. Because of the photocatalytic properties of TiO<sub>2</sub>, which has a band energy gap in the UV range, he researched these phenomena by using a UV lamp. Thin film of TiO<sub>2</sub> was chosen to minimize filtration and resuspension in the water purification process. In this study, also was known that each flow rate of aromatic organic compounds obeyed first-order kinetics and was more precisely interpreted in the integrated form of the Langmuir expression (Matthews, 1987).

The use of a UV lamp in the purification process is sometimes inconvenient to apply in the real stage. Modifications of TiO<sub>2</sub> to enhance its photocatalytic properties in visible light were conducted. Platinum (Pt) and other noble metals were introduced as the first metal-doped that was used to enhance the photocatalytic activity of TiO<sub>2</sub>. Following other metals and non-metals, research about doped TiO<sub>2</sub> was conducted. In recent years, modification of doped titania has

become popular among researchers. Modification of doped material, or can be called composite, was known not only to enhance its photocatalytic activity but also its adsorptivity with other materials.

Iron (Fe) doped  $\text{TiO}_2$  were prepared by Qing (2012) with the sol-gel method. This research was carried out by using methylene blue in water as the research object. The photocatalytic activity was conducted in an incandescent lamp environment, 2cm from the solution surface. While 0.05wt% Fe increased the degradation 1.45 times than pure  $\text{TiO}_2$ . This research also confirmed the first-order kinetic law within the concentration range between 5 and 15 mg/L (Qing, 2012).

When coated photocatalyst reduces its photocatalytic activity, Larumbe (2014) researched  $\text{Fe}_3\text{O}_4/\text{SiO}_2/\text{N-TiO}_2$  composite that can magnetically separate. This result enhanced the absorption in the visible range. This research is interesting because there is a combination between photocatalytic response under visible light and the possibility of the extract by an external magnetic field (Larumbe et al., 2014).

### 2.3 $\text{SiO}_2$

Silica or silicon dioxide ( $\text{SiO}_2$ ) is a compound of silicon and oxygen. From its crystallographic properties, synthesis modes, and petrographic importance, it belongs to the silicate family. Silica has seven structures of polymorphism and two classes of porous framework structures. Different structures are known as quartz, tridymite, cristobalite, coesite, keatite, stishovite, melanophlogite, fibrous, lamellar silica, zeolites, or clathrates (Hobbs et al., 1998). Numerous industrial applications taking advantage of the specific properties of this material have been and are still being developed.

Silica has a well-characterized surface and can be modified to the presence of hydroxyl groups. A bonding with hydrogen produces the silanol group on the silica surface. These groups can help silica to be embedded with water in a multilayer. Silanols are proposed to be water adsorption sites. Besides water adsorption,

adsorption of various small organic molecular on silica surfaces was studied (Parida et al., 2006). To enhance the adsorptivity of  $\text{TiO}_2$ ,  $\text{SiO}_2$  will be added.  $\text{SiO}_2$  also is known as the material that can improve the photocatalytic process of  $\text{TiO}_2$  because it can increase the specific surface area of photocatalyst (Aziz & Sopyan, 2009). At the same time, helps to obtain a large surface area as well as to improve the surface adsorption (Zhou et al., 2006).

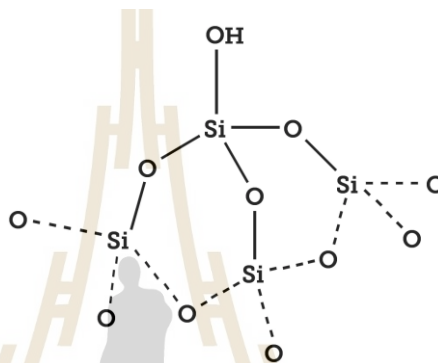


Figure 2.5 Silicon dioxide (Fortis Life Sciences, 2021).

Table 2. 3 Specific surface area of  $\text{TiO}_2/\text{SiO}_2$  photocatalyst (Klondon et al., 2016)

Ratio $\text{TiO}_2/\text{SiO}_2$	Specific Surface Area ( $\text{m}^2/\text{g}$ )
Pure $\text{TiO}_2$	12.86
1:0.25	82.72
1:0.5	126.15
1:1	182.72
1:1.5	215.86
1:2	238.09
Pure $\text{SiO}_2$	301.75

Vine and rice husks can be used to produce silicon dioxide. When rice husk is burnt at high temperatures, it contains silica. Rice husk is a plentiful raw material that

is also readily available in the community with reasonably priced. Titanium dioxide will be enriched with silica from rice husk to improve the photocatalytic process's efficiency. The addition of SiO<sub>2</sub> has the effect of increasing surface area. As a result, TiO<sub>2</sub>'s photocatalytic activity and ability to retain absorbed water, which rises during UV irradiation, improved (Machida et al., 1999). Table 2.3 shows the effect of SiO<sub>2</sub> from rice husk to the specific surface area of TiO<sub>2</sub>/SiO<sub>2</sub> photocatalyst.

## 2.4 Graphene Sheets

Graphene is a thick honeycomb crystal structure composed of a monolayer of carbon atoms. It can be seen as an individual atomic plane removed from graphite, as unrolled single-wall carbon nanotubes, or as a huge flat fullerene molecule. (Novoselov et al., 2005). The name 'graphene' is frequently applied improperly to ultrathin graphite layers. Strictly speaking, it refers to a quasi-two-dimensional isolated monolayer of hexagonally organized carbon atoms (Warner et al., 2013).

Because the conduction and valence bands contact at the Dirac points and exhibit linear dispersion, graphene is a zero-gap semiconductor (Novoselov et al., 2005). The carbon-carbon chemical bonds are due to hybridized orbitals generated by the superposition of 2s with 2p<sub>x</sub> and 2p<sub>y</sub> orbitals (electron shell configuration of carbon is [He] 2s<sup>2</sup> 2p<sup>2</sup>). The remaining free 2p<sub>z</sub> orbitals present  $\pi$  symmetry orientation and the overlap of these orbital states between neighboring atoms plays a major role in the electronic properties of graphene (Rocha et al., 2016).

The first study of graphene membranes was conducted by Meyer et al. (Meyer et al., 2007). Graphene was exfoliated across a metal support grid and investigated these structures by using nano area electron diffraction (ED). Currently, not only graphene which has a 2D layer in their structures. A reduced form of Graphene Oxide (GO) is an alternative material to graphene due to the ease with which their products can be scaled up. Reduction of GO can be accomplished by using a strong chemical reducing agent e.g. hydrazine, that leads to significant



removal of oxygen (Warner et al., 2013). rGO is conductive but exhibits strongly less conductivity than exfoliated graphene.

## 2.5 Preparation of Photocatalyst

### 2.5.1 Sol-Gel Method

Preparation of TiO<sub>2</sub>-based photocatalysts can be done in a variety of ways, including electrochemical, thin film by vacuum arc plasma evaporator, precipitation, thermal (ethanol thermal, hydrothermal, and solvothermal), chemical solvent and chemical vapor decomposition (CSD & CVD), ultrasonic irradiation, extremely low temperature, and sol-gel. Nonetheless, the advantages of preparing TiO<sub>2</sub> by sol-gel method, such as synthesis of crystallized powder in nanosized particles of high purity at relatively low temperature, the possibility of stoichiometry controlling process, preparation of composite materials, and production of homogeneous materials, have prompted many researchers to use the method in the preparation of TiO<sub>2</sub>-based photo crystals. This research work on sol-gel production methods of TiO<sub>2</sub>-based photocatalysts provided the impetus for the current investigation.

One of the most often utilized processes is sol-gel, which is mostly used to manufacture thin film and powder catalysts. Some research demonstrated that several versions and adaptations of the method were utilized to generate pure thin films or powders in vast homogenous concentrations and under stoichiometry control. In general, the sol-gel process includes converting a system from a liquid sol phase to a solid gel phase. Precursors are often organometallic compounds, resulting in materials with varying physicochemical properties (Akpan & Hameed, 2010). TiO<sub>2</sub> nanoparticles with great homogeneity could be generated using the sol-gel process, and particle size could be easily modified. As a result, the current research focuses on sol-gel and sol-gel-related ways of doping TiO<sub>2</sub> photocatalysts, with an emphasis on the efficiency of the catalysts made by the approach in any given photocatalytic activity.



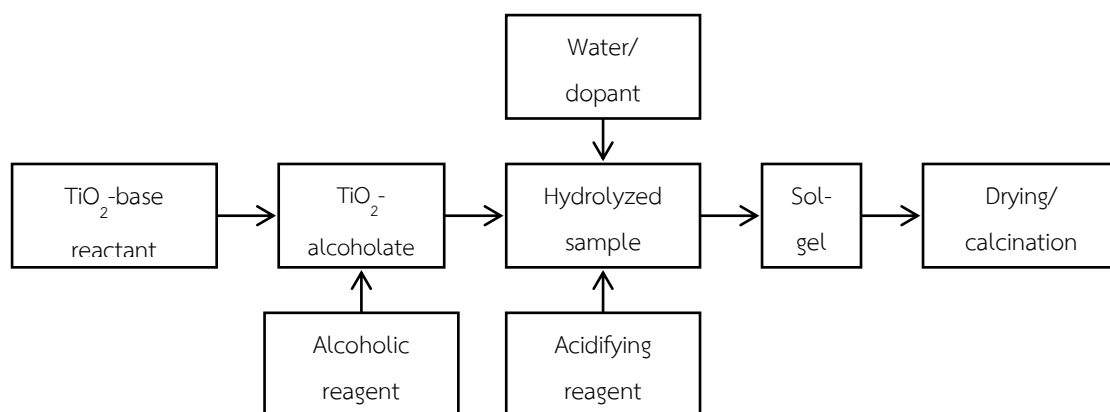


**Figure 2.6** Process Flow Chart for the Preparation of TiO<sub>2</sub> based photocatalyst by Sol-Gel methods.

Sol-gel processing is the most successful approach for producing nano-sized metal oxide semiconductors. The sol-gel method is a technique for improving the physicochemical and electrochemical properties of TiO<sub>2</sub> nanocrystalline. It enables a straightforward synthesis procedure of nanoparticles at ambient temperature and atmospheric pressure, and this technology does not require a sophisticated setup. It is a low-temperature technique used to obtain more crystalline products.

Due to the necessity for titanium dioxide small solid particles, high purity, low cost, and ability to be blended with other substances, the sol-gel process is chosen as a method to produce TiO<sub>2</sub>.

### 2.5.2 Coating of Photocatalyst

In current applications, the slurry of TiO<sub>2</sub> is used because of its effectiveness. But the suspended particles can contaminate the phase. Filtration is one of the ways to separate the water and TiO<sub>2</sub> particles, yet it is not a practical and economic cost. To avoid that and increase catalyst durability, coated on solid supports as bound particles or thin films can become an alternate way. However, the photocatalytic activity of coated films is lower because it will have a lower specific surface area. These disadvantages can be overcome by add material that can enhance the surface area such as silica. Silica has an active site on its surface since

the silanol groups in silica can improve the adsorptivity and the photocatalytic activity of photocatalyst.

Commonly coating method is used substrates such as glass, activated carbon, various polymeric materials, and metals. Important properties of the substrate are a good adhesion of the  $\text{TiO}_2$  particles, resistance against sintering temperatures, a high specific surface area, and strong absorbance affinity towards the pollutants. Glass and silica substrates may be wanted because they are transparent. Activated carbon is very porous and has a high specific surface area and has been shown to increase the activity of the catalyst (Shan et al., 2010).

To deposit the titanium dioxide on the substrate, different techniques may be utilized. One of the most popular is dip-coating. It is commonly utilized for covering surfaces for use in heterogeneous photocatalysis since it is a low-cost and simple method. Dip coating results in a thin and controllable layer. Preparing a precursor solution of the photocatalytic substance to be deposited is required prior to the dip-coating process.

## 2.6 Monte Carlo Simulation

Monte Carlo (MC) simulation is a numerical method that relies on random sampling to arrive at an approximate solution of a given problem to obtain numerical results. This method is quite related to random experiments since the result is not known in advance. It also can be called a what-if analysis because the input parameters can be depended on the external factor (Raychaudhuri, 2008).

The idea of Monte Carlo simulation self is simple. The quantities can be expressed as the value of a random variable then generated independently from the distribution and take the average. The possible configurations of the system are sampled with a known weighting and from these samples, a variety of averaged quantities and histograms describing the structure can be formed. The extent of the phase space, which is sampled can be varied, but by far the largest number of studies have employed the canonical ensemble (constant  $N$ ,  $V$  and  $T$ ); the

isothermal-isobaric (constant  $N$ ,  $P$  and  $T$ ), and the grand canonical (constant  $T$ ,  $V$ ). The Metropolis algorithm is practically used to simulate various ensembles that are mostly used in adsorption.

### 2.6.1 Application of Monte Carlo in Photocatalyst

The reaction rate of photocatalytic reactions usually is calculated based on the degradation rate of the pollutants along the time. But the photocatalytic kinetics is more complicated. It involves many processes, including the generation, the transport, the recombination, and the interfacial charge transfer of electrons and holes. Because of that, although most kinetics data are experimental, the simulation gives an important role in analyzing experimental data and providing mechanistic information that is inaccessible in the experiment.

Dabrowski (Dabrowski et al., 1970) uses monte carlo simulation to study the mechanism of dehydration reaction in catalyst surface and compare it with the experimental result. It is shown that the monte carlo simulation success and indicates considerable potential in certain areas in certain modeling or simulation of catalytic behavior. It also explained that even though the number of experiments cannot be numbered since some data are experimental quantities, but the simulation can reduce the experimental burden.

In 2001, a simulation of  $\text{TiO}_2$  photocatalyst has been conducted by Ramirez-Custa (Ramirez-Cuesta et al., 2001). The model of many layers of  $\text{TiO}_2$  which grow during re-oxidation. The simulation remodeled well the morphology and rate of growth of  $\text{TiO}_2$  surfaces while the spillover species can react with low probability. On the other side, Bashiri (Bashiri & Rafiee, 2016) simulated  $\text{ZnO}$  nanocatalyst by Monte Carlo simulation. The simulation provided the mechanism of the reaction and the rate constant for each step was obtained. Since that, the system can be simulated in different conditions and get the effect of each parameter.

## 2.7 N- Nitrosamine

N-Nitrosamines are a class of chemical compounds with the chemical structure  $R_1-N(R_2)-N=O$ . The essential feature of N-nitroso compounds is the N-N=O structure; the R1 and R2 groups attached to the amine nitrogen may range from simple hydrogen (H) atoms to more complex chemical substituents (including ring structures that incorporate the nitrogen atom). Most nitrosamines are carcinogenic.

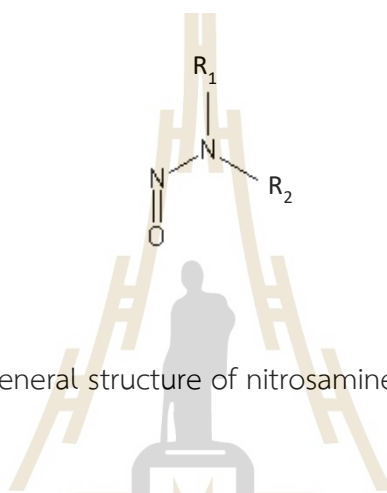


**Figure 2.7** General structure of nitrosamine (Luan et al., 2005).

Individual nitrosamines do not exist in isolation, but rather in combinations with other nitrosamines. N-Nitrosamines are disinfection byproducts that can be produced during the oxidation water treatment process. Nitrosamines can be found in latex products like balloons and rubbers, as well as numerous foods and other consumables like meat, fish and their products, alcoholic beverages, and cigarette smoke (Tricker et al., 1991; Verna, 1996). According to reaction pathway studies, N-nitrosamines can be formed through the reactions of natural and synthetic amine precursors found in natural and technical aquatic systems with chemical oxidants such as chloramines, chlorine, or ozone. When nitrites, which can be generated from nitrates, react with a secondary or tertiary amine, nitrosamines are formed. High temperatures, such as those used to fry meat, fish, and their products, and high acidity, such as that found in stomach acid, both contribute to the creation of n-nitrosamines (pH 1-2).



Nitrite creates nitrous acid ( $\text{HNO}_2$ ) in an acid-base environment, which is protonated and divides into the nitrosonium cation  $\text{NO}^+$  and water. Nitrosamine is formed when the nitrosonium cation combines with an amine.

Because this class of molecules includes powerful mutagens and carcinogens, there has been a surge in interest in N-nitrosamines over the last decade. Furthermore, to satisfy rising demand, drinking water utilities are increasingly relying on algal- or wastewater-affected waters, and it is thought that these impacted source waters contain increased quantities of nitrogenous precursors, potentially leading to N-nitrosamines.

### 2.7.1 N-Nitrosodiethylamine (NDEA)

N-Nitrosodiethylamine (NDEA), also known as diethylnitrosamine (DEN), is a yellow liquid with a boiling point of 175-177 °C, a specific gravity of 0.94, and the ability to dissolve in water, ethanol, diethyl ether, and organic solvents. NDEA has been found in a variety of goods that potentially expose humans to it, including mainstream and off-label tobacco smoke, beef, and whiskey (Tricker et al., 1991; Verna, 1996).

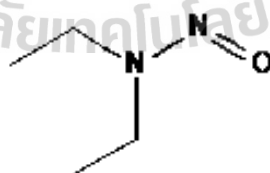


**Figure 2.8** Chemical structure of NDEA (National Center for Biotechnology Information, 2021).

**Table 2.4** Physical and Chemical properties of NDEA (Santa Cruz Biotechnology, 2010).

Property	Information
Molecular weight	102.14
Specific gravity	0.9422 20 °C
Boiling point	175 to 177 °C
Water solubility	Miscible
Vapor pressure	Negligible
Vapor density	>1

NDEA emits toxic nitrogen oxide fumes when heated. NDEA can affect DNA integrity, possibly through alkylation, and has been used in experimental studies to induce hepatic tumorigenesis. It is widely anticipated as a human carcinogen (Tanaka et al., 1988). The physical and chemical properties of N-nitrosodiethylamine are listed in the following table.

## 2.8 Characterization

### 2.8.1 X-Ray Diffraction (XRD)

XRD is a quick analytical technique that can offer information on unit cell dimensions and is mostly used for phase identification of crystalline materials (Dutrow & Clark, 2016). William Henry Bragg and his son William Lawrence Bragg created a much simpler method of analyzing and forecasting diffraction patterns from a crystal in 1913. According to the Bragg analogy, incident X-ray rays enter from the left and reflect from each plane in the family.

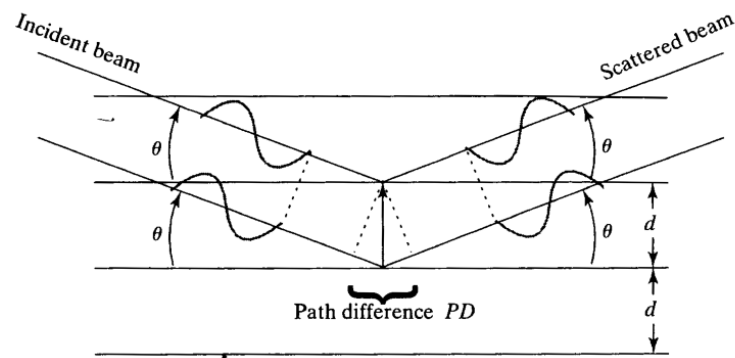


Figure 2.9 Bragg's Law of Diffraction (van Holde et al., 2006).

If we assume that the initial waves are in phase with one another and that the waves reflect from each plane in the family, we can rapidly construct the governing equation. These derivations result in the Bragg equation's solution:

$$n\lambda = 2d_{hkl} \sin \theta \quad (2.23)$$

where the integer  $n$  is the order of the diffracted beam and  $d$  is the distance between adjacent planes of atoms (the  $d$ -spacings) (van Holde et al., 2006)

X-rays are generated within a vacuum-sealed tube in X-ray powder diffraction equipment. This high voltage accelerates electrons, which subsequently strike a target, which is often constructed of copper. X-rays are produced when these electrons collide with the object. The wavelength of these X-rays is unique to the object. These X-rays are collimated before being directed towards the ground-to-a-fine powder substance. A detector detects the X-ray radiation; the signal is then processed, either by a microprocessor or electrically, to transform the signal to a count rate. An X-ray scan is a controlled change in the angle between the X-ray source, the sample, and the detector between predefined limitations (S., 2014).



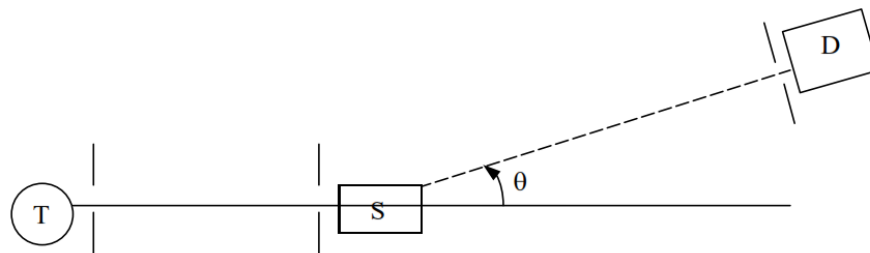


**Figure 2.10** The essential parts of a small angle scattering system. T = x-ray source, S = sample,  $\theta$  = the scattering angle, the slit used to define the incident and scattered beam, and D = detector (L. Li, 2005).

### 2.8.2 SEM

SEM is a Scanning Electron Microscope that used a focused beam of the electron as a light source. The electron will interact with atoms in the sample produce the signals that contain the information about surface topography and composition of the sample. When an electron hits onto a material, different interactions (signals) can occur, classified into two types: elastic and inelastic interactions (Krumeich, 2009). Secondary electrons (SE), reflected or back-scattered electrons (BSE), auger electrons, bremsstrahlung X-rays, photons of distinctive X-rays, and light (cathodoluminescence) (CL), absorbed current (specimen current), and transmitted electrons are all forms of signals produced by an SEM. Secondary electrons and backscattered electrons are often utilized for imaging samples: secondary electrons are best for displaying morphology and topography on samples, while backscattered electrons are best for presenting compositional contrasts in multiphase samples.

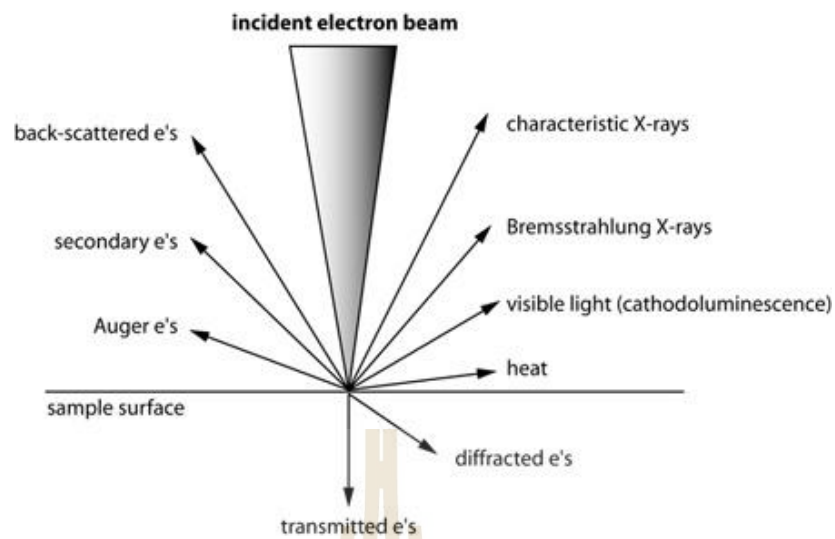


Figure 2.11 Types of interactions between electrons and a sample (Henry, 2016).

Sample preparation for SEM analysis can be simple or complex, depending on the nature of the samples and the data sought. The procurement of a sample that will fit into the SEM chamber and modest accommodation to prevent charge build-up on electrically insulating samples constitute minimal preparation.

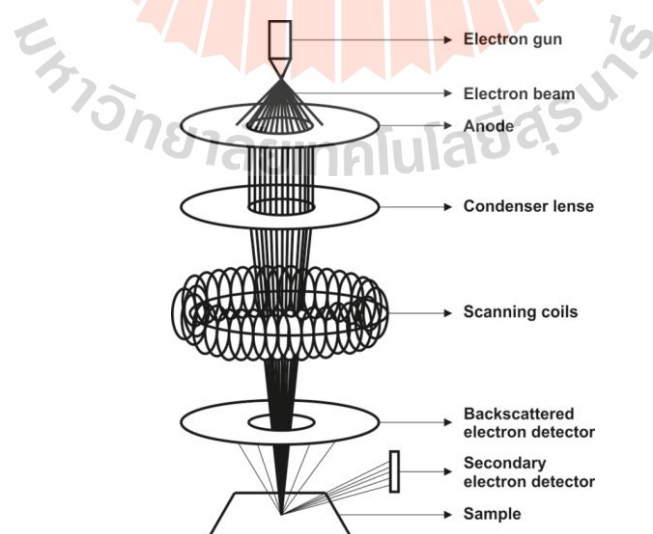


Figure 2.12 Mechanism of SEM (Carrara, 2017).

Using electrons, the device creates a greatly magnified image. An electron gun produces a beam of electrons at the top of the microscope. The electron beam travels in a vertical route through the vacuum-sealed microscope. The beam passes through electromagnetic fields and lenses, which focus it downward toward the sample. When the beam strikes the sample, electrons and X-rays are expelled. These X-rays, backscattered electrons, and secondary electrons are collected by detectors and converted into a signal that is delivered to a screen, like a television screen. This results in the final image.

### 2.8.3 TEM

The operation of the transmission electron microscope (TEM) is by accelerating a beam of electrons to sufficient energy so that when it strikes a very thin sample (<100 nm), electrons are allowed to pass through it (Holsgrove, 2017; Martinez, 2011). The interaction of electrons passed through the sample produces a picture, which is magnified and focused on an imaging device (Callahan et al., 2018; Rukari & Babita, 2013).

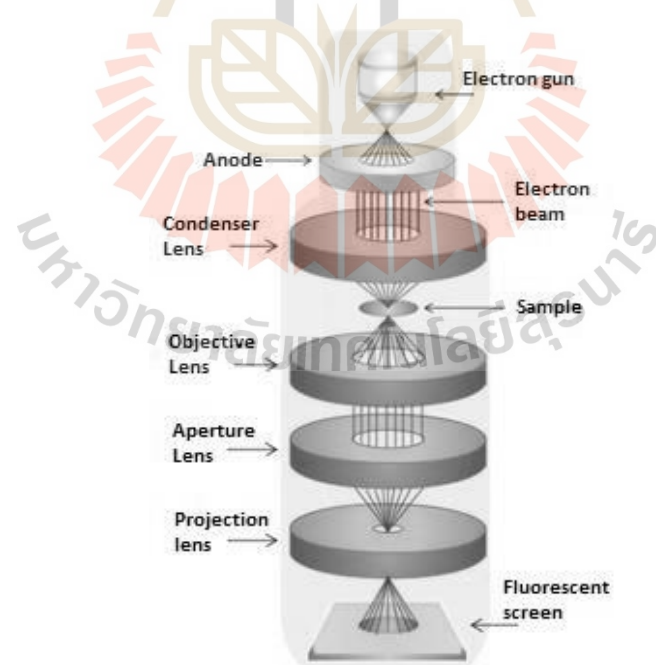


Figure 2.13 Transmission electron microscope (Sierra, 2019).

From top to bottom, a tungsten filament, or a lanthanum hexaboride (LaB<sub>6</sub>) source is used as an emission source in a TEM. If the gun is connected to a high voltage source (typically 100-300 kV), it will begin to emit electrons into the vacuum via thermionic or field electron emission if the current is sufficient. The condenser and aperture lenses modify the electron beam before it reaches the sample to increase light coherence, that is, to keep the waves in the same direction with a consistent phase difference. Following that, the electron beam reaches the sample, where numerous events take place, including elastic dispersion of electrons that damage the material and other processes in which electrons give some of their energy to internal electrons of the sample (inelastic). The scattered beams are then focused by the objective lens via a diffraction process conducted by the projection lens, which expands the electron beam and reflects it on the phosphor screen (Rukari & Babita, 2013; Sierra, 2019).

The TEM is a tool used to analyze the structure, composition, and properties of samples in various fields of study such as materials science, geology, the environment, medicine, electronics, and biology in general. Although TEM has been less widely used in the study of organic materials, owing to perceived difficulties with sample preparation and beam damage, recent studies of pharmaceutical compounds have shown not only that these difficulties can be overcome, but that TEM analysis can provide a range of useful information about samples that cannot be obtained by other commonly used analytical methods.

#### **2.8.4 Surface Area Analyzer**

Surface Area Analyzer is used to analyze the specific surface area and pore size distribution of the sample by using the principle of gas sorption based on BET (Brunauer, Emmett, and Teller) theory. The specific surface determined by BET relates to the total surface area (reactive surface) as all porous structures adsorb the small gas molecules. The concept self is an extension of the Langmuir theory, which is for monolayer molecular adsorption, to multilayer adsorption with the equation: (Brunauer et al., 1938; Lowell et al., 2004).

$$\frac{1}{V[(P_0/P)-1]} = \frac{c-1}{V_m c} \left(\frac{P}{P_0}\right) + \frac{1}{V_m c} \quad (2.24)$$

where  $P/P_0$  is the gas's relative pressure,  $V$  is the volume of gas adsorbed ( $m^3$ ),  $V_m$  is the volume of the monolayer adsorbed gas ( $m^3$ ) and  $c$  is BET constant related to the strength of interaction between gas and solid.

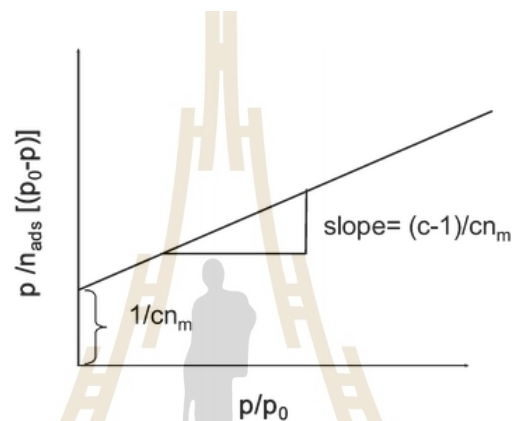


Figure 2.14 BET plot and the relation between  $c$  and  $n_m$  to slope and intercept of the y-axis (Weidenthaler, 2011).

By plotting  $\frac{1}{V[(P_0/P)-1]}$  and  $P/P_0$ , it will give a linear plot with the slope is  $(c-1)/V_m c$  and intercept is  $1/V_m c$ . From this value,  $V_m$  can be calculated as  $1/(\text{slope}/\text{intercept})$ , while  $c$  is calculated by  $(\text{slope}/\text{intercept})+1$ . Therefore, the total surface area,  $S_t$ , is then calculated from

$$S_t = \frac{V_m N_A \sigma}{V_{STP}}, \text{ m}^2 \quad (2.25)$$

where  $N_A$  is the number of Avogadro ( $6.023 \times 10^{23}$  molecules/mole),  $\sigma$  is the adsorption cross-section of gas ( $\text{m}^2/\text{molecule}$ ), and  $V_{\text{STP}}$  is the molar volume of gas at STP condition ( $2.2414 \times 10^{-2} \text{ m}^3/\text{mole}$ ). The specific surface area is finally normalized by sample mass by

$$S_{\text{BET}} = \frac{S_t}{m}, \text{ m}^2/\text{g} \quad (2.26)$$

Before the specific surface area of the sample can be determined, it is necessary to remove gases and vapors that may have become physically adsorbed onto the surface. Some weighing sample is placed then gas will flow through the sample until reaches some relative pressure. The gas most used in this analysis is nitrogen.

### 2.8.5 UV-Vis spectroscopy

UV/Vis spectroscopy is a technique that uses light absorption by an unknown chemical or sample. The sample is irradiated with electromagnetic rays of varying wavelengths in the visible (VIS) and adjacent spectrum areas, specifically ultraviolet (UV) and a portion of the lower infrared region (near IR). Light is partially absorbed depending on the substance (De Caro & Claudia, 2015). The several phenomena involved (reflectance, transmittance, and absorbance) are discussed, as well as the measurement equipment necessary. A suitable detector records the remaining light, for example, the transmitted light, as a function of wavelength, providing the sample's UV/VIS spectrum (Rouessac & Rouessac, 2013).

Light of a specified wavelength will pass through the sample, and the intensity of the light before and after they pass through will be compared. This direct transmittance  $I/I_0$  is usually expressed as a percentage (%T). The absorbance can be calculated from this value using the equation :

$$A = -\log \frac{\%T}{100} \quad (2.27)$$

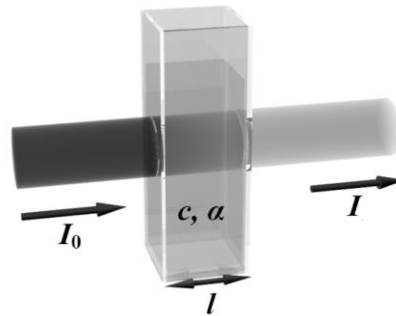


Figure 2.15 Lambert-Beer Laws (Gallik, 2011).

Absorbance is widely used to measure concentration in liquid solutions following the Beer-Lambert law (Gallik, 2011; Swinehart, 1962).

$$A = \epsilon Lc \quad (2.28)$$

where  $\epsilon$  is the molar extinction coefficient,  $L$  is the path length of the cell holder and  $c$  is the concentration of the solution. Molar absorptivity constant is normally not given for unknown samples. The common method of working with Lambert-Beer's law is the graphing method. The graphing method is called for when several sets of data involving standard solutions with similar wavelengths with the sample are available for concentration and absorbance. Graphing the data allows checking the assumption that Beer's Law is valid by looking for a straight-line relationship for the data. By plot concentration and each absorbance of standard and get linear graph, slope and intercept value can be used to calculate the concentration of sample by using

$$A = (\text{slope} \times c) + \text{Intercept} \quad (2.29)$$



## 2.8.6 Gas Chromatography

Gas chromatography (GC) is a chromatography technique used in analytical chemistry to separate and analyze substances that may be evaporated without decomposition. A gas chromatograph's main components are a gas source as the mobile phase, an inlet to deliver the sample to a column, the column where separations occur, an oven as a column thermostat, a detector to detect the presence of a chemical in the column effluent, and a data system to record and display the chromatogram (Eiceman, 2006). These components of a gas chromatograph have remained constant in function or purpose for the last 40 years, despite advances in design, materials, and methodology.

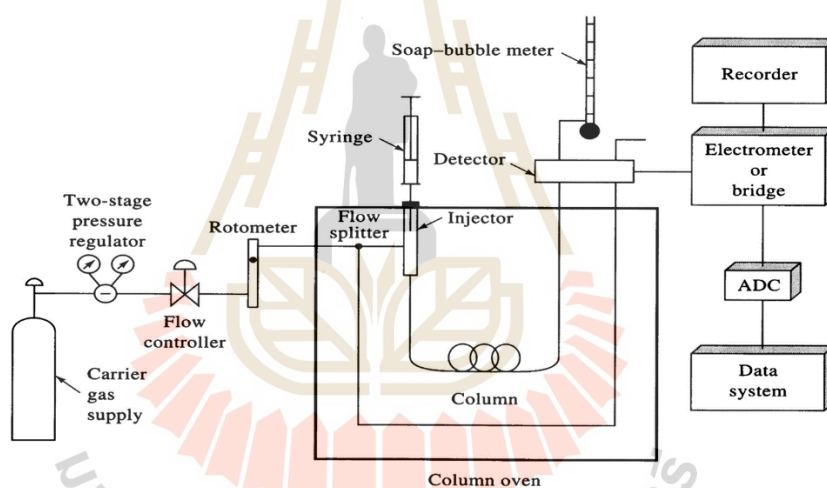
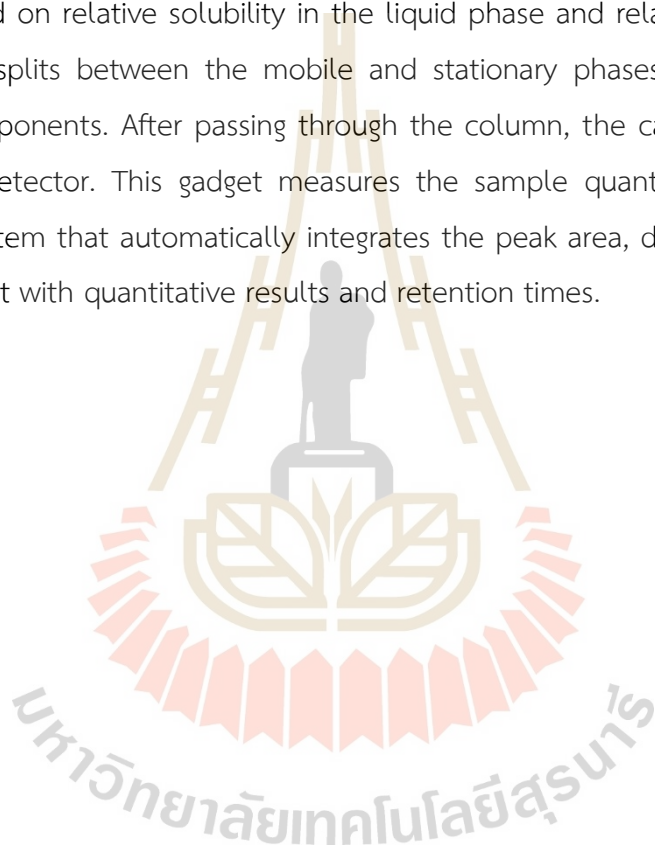


Figure 2.16 The components in gas chromatography.

Some of the benefits of chromatography include the measuring range (from ppm levels to 100 %), the detection of a large range of components, and the repeatability of the measurements. Sensitive detectors, such as the flame-ionization detector, can detect 50 ppb of organic chemicals with a relative standard deviation of less than 5 %. With minimal downtime, automated systems can handle more than 100 samples each day.

The gas chromatography function is as following: an inert carrier gas (such as helium) flows constantly via the injection port, the column, and the detector from a huge gas cylinder. The flow rate of the carrier gas is carefully adjusted to achieve repeatable retention times while minimizing detector drift and noise. The sample is injected into the heated injection port, where it is vaporized and moved into the column, which is normally a capillary column 15 to 30 m long with the inside covered with a thin (0.2  $\mu\text{m}$ ) film of high boiling liquid (the stationary phase). Based on relative solubility in the liquid phase and relative vapor pressures, the sample splits between the mobile and stationary phases and is divided into discrete components. After passing through the column, the carrier gas and sample pass via a detector. This gadget measures the sample quantity and develops an electrical system that automatically integrates the peak area, does calculations, and prints a report with quantitative results and retention times.



## CHAPTER III

### EFFECTIVE SOLAR LIGHT PHOTOCATALYSIS BY GSs ADDITION ON THE COMPOSITE TiO<sub>2</sub>/SiO<sub>2</sub>

#### 3.1 Abstract

This study investigated the synthesis of TiO<sub>2</sub>/SiO<sub>2</sub> using a sol-gel method with the addition of differences in the mass ratio of Titanium (Ti):Graphene Sheets (GSs) (1:0; 1:0.04; 1:0.07; 1:0.14) and calcination temperature (Tcal) (400 °C; 450 °C; 500 °C). The composites were examined using an X-ray powder diffraction (XRD), a scanning electron microscope, and an energy dispersive X-ray spectrometer (SEM-EDS). At the near point of  $2\theta$  (26°-27°), the TiO<sub>2</sub>/SiO<sub>2</sub>/GSs XRD pattern shows anatase and rutile phases, as well as graphite. The tendency of anatase phase according to GSs ratio and Tcal variables decreases as the GSs ratio and Tcal increases. The crystal size ranged from 24 to 41 nm. Methylene blue was decolorized under four conditions: dark, UV lamp, LED, and solar light. The photocatalytic activity obtained under solar light is comparable to that obtained under UV light. Within 3 hours, the photocatalyst with a ratio of 0.07 and Tcal of 450 °C provided the highest efficiency of MB degradation under solar light with 97.83 %. After four cycle times, the efficiency of reusable TiO<sub>2</sub>/SiO<sub>2</sub>/GSs shows a slight decrease.

#### 3.2 Introduction

Titanium dioxide (TiO<sub>2</sub>) is the semiconductor material that is widely used as a photocatalyst for the degradation of several pollutants. Semiconductor materials have a bandgap between conducting band and valence band (Pennington, 2015). These bands determined the electrical conductivity of materials. When the light in a

certain wavelengths illuminate  $\text{TiO}_2$  surface, that energy will induce the electrons on the valence band to excited into conducting band. These free electrons will move along the surface or near the surface of  $\text{TiO}_2$ , yet the hole of electrons is in the valence band (Kang et al., 2019; Schneider et al., 2014).

$\text{TiO}_2$  has attracted attention because of its desirable physicochemical properties such as thermal and chemical stability, relatively high photocatalytic activity, low toxicity, and low cost. However, the bandgap of  $\text{TiO}_2$  is generally a range of 3.0-3.2 eV (Castellote & Bengtsson, 2011; Dalton et al., 2002), which gives a work range as photocatalyst under UV range (100 – 400 nm). It almost makes  $\text{TiO}_2$  cannot effectively work under the radiation of solar light (only 3-5 % of the solar spectrum) (Singh & Dutta, 2018).

Somehow, nonmetal doping was effective to obtain a visible light response. In recent years, carbon in graphene form is popular doping material to decrease the bandgap of semiconductors, especially in photocatalyst applications. The graphene is considered as an impurity in  $\text{TiO}_2$  structural system, the bandgap of graphene will overlap with  $\text{TiO}_2$ , in this case, the conduction band of graphene will be lower than  $\text{TiO}_2$  then it will decrease the gap between the conduction band of graphene and valence band of  $\text{TiO}_2$  (Najafi et al., 2017). Its properties such as large BET area (which provides more active adsorption sites), chemical inertness, zero bandgaps (which acts as a sensitizer), high electron mobility (which prolongs electron lifetime), electron storage ability (which acts as an electron tank), and tunable structural give modified photocatalysts an added advantage (Au-pree et al., 2021; Tang et al., 2018). Therefore, the composite of graphene and semiconductors, especially  $\text{TiO}_2$ , is currently being considered as a potential photocatalyst in air and water purification. The graphene-based  $\text{TiO}_2$  composite exhibit enhanced photocatalytic activity in comparison with only  $\text{TiO}_2$  (Y. Zhang et al., 2010).

Photocatalyst in the case of environmental purification will act as adsorbent and photocatalyst. Those actions take place at the same time. Since the photocatalytic reaction will take place mostly near the surface of the photocatalyst. To enhance the adsorptive of  $\text{TiO}_2$ ,  $\text{SiO}_2$  will be added to increase the surface area

for adsorption (Zhou et al., 2006).  $\text{SiO}_2$  also is known as the material that can improve the photocatalytic process of  $\text{TiO}_2$  (Aziz & Sopyan, 2009).

The preparation of  $\text{TiO}_2/\text{SiO}_2$  has been studied under Klondon work (Klondon et al., 2016). The variables were the amount of GSs and the calcination temperature (Tcal). The effects of these variables on the methylene blue degradation during photocatalysis with a variation of applied light sources e.g. dark, UV lamp, LED lamp, and solar light were investigated.

### 3.3 Experimental Procedure

#### 3.3.1 Preparation of $\text{TiO}_2/\text{SiO}_2/\text{GSs}$

10 mL of Ti-n-butoxide is diluted by 35 mL of absolute ethanol, became solution A. The mixture of 3 mL of  $\text{HNO}_3$  concentrated, 35 mL of absolute ethanol 10 mL of deionized water and GSs pure called solution B. GSs was added with calculated mass ratio of Ti:GSs are 1:0; 1:0.04; 1:0.07; 1:0.14 and labeled as G0; G0.04; G0.07; and G0.14 respectively. Label G stand for GSs and the number stands for ratio number of GSs. The  $\text{SiO}_2$  was added into the mixed solution to make the ratio of  $\text{TiO}_2:\text{SiO}_2$  is 1:1.

$\text{TiO}_2/\text{SiO}_2/\text{GSs}$  photocatalyst was synthesized by the sol-gel method. Solution B with the variation ratio of GSs was added into solution A slowly under stirring and stirred for 1 hour. 1.5 g of  $\text{SiO}_2$  was added under stirring then kept the solution for one day. Finally, the solution is drying at 110 °C for 12 hours. This sample continues to calcine with the variation of temperature from 400 °C, 450 °C, and 500 °C (sample coding T400, T450, and T500 respectively) for 6 hours. The composite photocatalyst of  $\text{TiO}_2/\text{SiO}_2/\text{GSs}$  was finally obtained.

#### 3.3.2 Characterizations

The identification of the crystal phase of the composite was performed using a Bruker D2 PHASER XRD. In titanium dioxide, XRD provides information about the major peaks of the structure phase of  $\text{TiO}_2$ . The major peaks of pure anatase at  $2\theta$  consist of (101), (004), (200), (105), (204), (220), and (215)

planes. Meanwhile for rutile have intensity at (110), (101), (200), (111), (210), (211), and (220) planes (Au-pree et al., 2021; Boonprakob et al., 2017; Haider et al., 2015). The XRD patterns show different peak broadening which is inversely proportional to the average crystal size of TiO<sub>2</sub>/SiO<sub>2</sub>/GSs according to Scherrer equation (Najafi et al., 2017; Singh & Dutta, 2018) as in equation (3.1)

$$D_p = \frac{k\lambda}{\beta \cos\theta} \quad (3.1)$$

where  $D_p$  is the crystal size (nm),  $K$  is the Scherrer constant, like 0.89 for cubic crystallite shape (Rufai et al., 2020),  $\lambda$  is the x-ray wavelength (Cu  $K\alpha$  radiation source, 0.154178 nm),  $\beta$  is the full width at half maximum (FWHM), and  $\theta$  is the diffraction angle ( $2\theta$  of peak (101) of anatase is 25.30°). The following equation can be used to calculate the ratio of TiO<sub>2</sub> crystal phases from XRD results (Eshaghi et al., 2011; Singh & Dutta, 2018)

$$\% \text{ anatase phase} = \frac{100}{1 + (I_R / 0.791 I_A)} \quad (3.2)$$

where  $I_R$  and  $I_A$  are the strongest intensities of the rutile and anatase phases, respectively.

The structure of TiO<sub>2</sub>/SiO<sub>2</sub>/GSs was characterized by using FE-SEM JEOL JSM 7800F to analyze surface properties. The detector that was used is a backscattering detector because the sample has a high atomic number which backscattered electrons stronger thus appear brighter in the image. It can detect the contrast between areas with different compositions. EDS was used in conjunction with SEM to characterize the elemental composition. After an electron beam bombarded the sample, a relative abundance of x-ray emitted from the sample be

measured by the detector to determine the elemental composition of sampled volume.

Samples were prepared by dispersing the nano-powder in ethanol and a drop of this suspension is transferred on carbon-coated Cu grid micropores. Prepared samples were measured with the energy of 200 keV by using FEI-TEM-TECNAI G220, SUT. Selective area electron diffraction (SAED), bright field images, high-resolution TEM (HRTEM), Scanning TEM (STEM) images & energy dispersive X-ray (EDX) spectra were obtained.

The specific surface area ( $S_p$ ) and porosity of the nanoparticles were measured by using the  $N_2$  adsorption technique. By using a computer interfaced BELSORP-mini-II instruments, all samples were thoroughly degassed at 300 °C for 3 h. The specific surface area was calculated by using the BET method. The pore size distributions were obtained from the analysis of the adsorption branch of the isotherm by the BJH method. The samples were labeled by their ratio G0, G0.04, G0.07, and G0.14 with T400, T450, T500 as represented to Tcal 400 °C, 450 °C, and 500 °C, respectively.

### 3.3.3 Photocatalytic activity

The photocatalytic activity of the  $TiO_2/SiO_2/GSs$  was investigated by using the degradation of Methylene Blue (MB) solution. The MB solution was prepared by dissolved 20 mg of methylene blue ( $C_{16}H_{18}N_3SCl$ ) with 1L of deionized water to be stock solution 20 mg/L. This solution then was diluted to be standard from 2, 4, 6, 8, and 10 mg/L, also the initial condition (2.5 mg/L) for photocatalytic reaction.

The initial condition was done by analyzing the degradation of MB by variation of the amount of photocatalyst (0.05 g; 0.1 g; and 0.15 g) in a 100 mL MB solution of 2.5 mg/L under solar light. The initial concentration of MB also was determined by put 0.1 g of the photocatalyst into a 100 mL MB solution of 1 mg/L, 2.5 mg/L, and 4 mg/L.



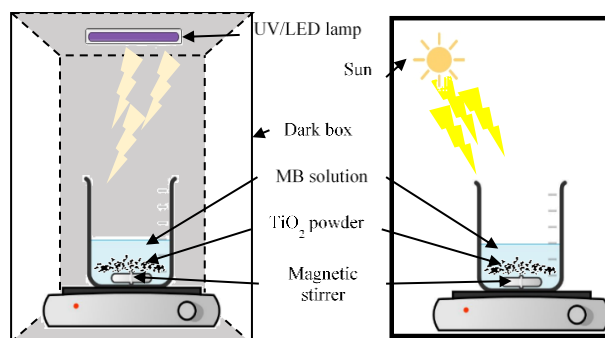


**Figure 3.1** Experimental setup for Methylene Blue degradation by TiO<sub>2</sub> photocatalyst in the dark box (left) and with different light sources (left) and an open system under solar light (right).

The 0.1 g of the composite was put into a 100 mL solution of 2.5 mg/L of MB in the reactor under the different applied light sources, e.g., UV lamp, LED lamp, and solar light. The dark condition was also tested to show how the adsorption takes place in photocatalyst when it has no light source. The UV lamp that is used has power 4 W and wavelength 366 nm while an LED lamp has power 35 W and wavelength 557 nm. The monitoring under solar light was restricted from 11 am to 4 pm according to peak sun-hours in Thailand (5 hours). The interval of measurement of MB concentration change was in every 30 minutes for 3 hours of data.

The 5 mL of decolorization solution was analyzed by using a T80+ PG instrument UV-Vis spectrophotometer with absorbance at a wavelength of 665 nm. The photocatalytic activity was measured as the decolorization of MB by the following equation:

$$\% \text{ decolorization} = \frac{C_0 - C_t}{C_0} \times 100\% \quad (3.3)$$

where  $C_0$  and  $C_t$  are the initial concentration and concentration at the time of MB, respectively. The variation of catalyst loading (0.05 to 0.15 g of TiO<sub>2</sub>/SiO<sub>2</sub>/GSs) and

the initial concentration of MB (1 to 4 mg/L) were investigated. The photocatalytic activity of optimum condition was also measured with three-time cycles.

The kinetics of photocatalytic degradation of MB was based on the most used Langmuir-Hinshelwood (LH) kinetics, is given by:

$$r = -\frac{dC}{dt} = \frac{k_r KC}{1+KC} \quad (3.4)$$

where  $r$  is the rate reaction (mg/L min) that changes by time  $t$  (min),  $C$  is the concentration at any time during degradation (mg/L),  $k_r$  is limiting rate constants of reaction at maximum coverage, and  $K$  is the equilibrium constant for adsorption of the substrate onto catalyst (K. V. Kumar et al., 2008).

The integrated expression of this equation can calculate the constant  $k_r$  and  $K$  in equation (3.4) by limit  $C = C_0$  at  $t = 0$  and  $C = C$  at  $t = t$ . the integrated can be expressed:

$$\ln \left( \frac{C_0}{C} \right) + K(C_0 - C) = k_r Kt \quad (3.5)$$

The LH kinetics on the first order has condition  $KC \ll 1$ . If so, equation (3.4) becomes  $r = k_r KC$  and be integrated into first-order kinetics and is given by:

$$\ln \frac{C_0}{C_t} = kt \quad (3.6)$$

where  $k$  ( $k_r K$ ) is the rate constant ( $\text{min}^{-1}$ ) and  $t$  is the degradation time (min).

### 3.4 Results and Discussion

The phase of  $\text{TiO}_2$  was known to effects the ability of  $\text{TiO}_2$  as a photocatalyst. XRD characterized the crystal phase of the composite of  $\text{TiO}_2/\text{SiO}_2/\text{GSs}$ , FE-SEM/EDS and TEM analyzed the physical structure and elemental components, while BET give the specific surface area of samples. The EDS result was shown on the %wt of Ti and C presence, which was analyzed on 5 points for each sample and presented as mean data. The preparation, especially for the ratio composition and calcination treatment, gives the effect into its surface properties.

#### 3.4.1 XRD Results

##### 3.4.1.1 Effect of Calcination temperature ( $T_{\text{cal}}$ )

Calcination has a role in affecting the performance of the material. In  $\text{TiO}_2$  preparation,  $T_{\text{cal}}$  affects the structure phase of anatase and rutile, especially based on their phase transition. The result in Figure 3.2 shows that a pure anatase phase exists at a lower temperature until  $T_{400}$  when a rutile peak is observed and increases along with the increase in  $T_{\text{cal}}$ . It explains how the tendency of  $\text{TiO}_2$  that stays as anatase phase at a lower temperature in the phase diagram and starts to transform into rutile at a higher temperature, as the percentage is presented in Figure 3.3. The percentage of anatase in the Figure 3.3 comes in comparison with the percentage of rutile phase in  $\text{TiO}_2$ . This temperature gives energy into  $\text{TiO}_2$  bonding to change form from metastable one (anatase) into the stable one (rutile).

Figure 3.3 also indicates that when the  $\text{TiO}_2/\text{SiO}_2/\text{GSs}$  composite is calcined at a higher temperature up to  $450\text{ }^\circ\text{C}$ , the larger crystal size may happen due to particle growth. The  $T_{\text{cal}}$  also affects not only changing the phase of  $\text{TiO}_2$  but also bonding between  $\text{TiO}_2$  and GSs, based on their ratio on the XRD result (Figure 3.2). At the  $T_{\text{cal}}$  at  $500\text{ }^\circ\text{C}$ , the crystal size is found to be decreased.

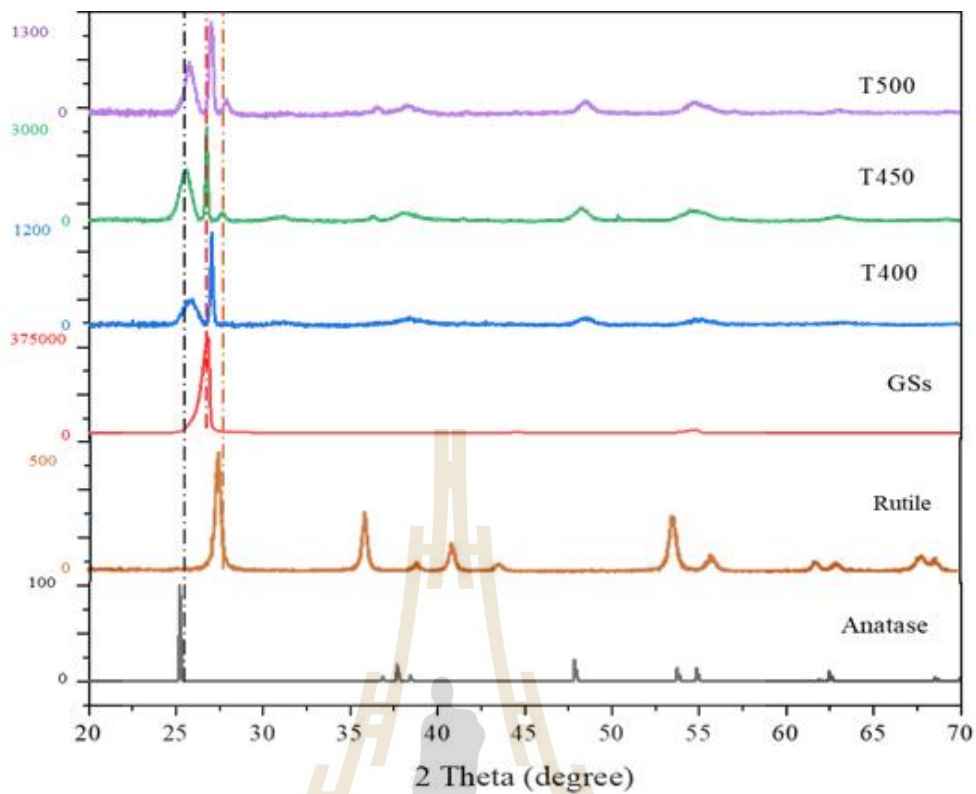


Figure 3.2 XRD pattern of TiO<sub>2</sub> photocatalyst G0.07 with a variation of Tcal

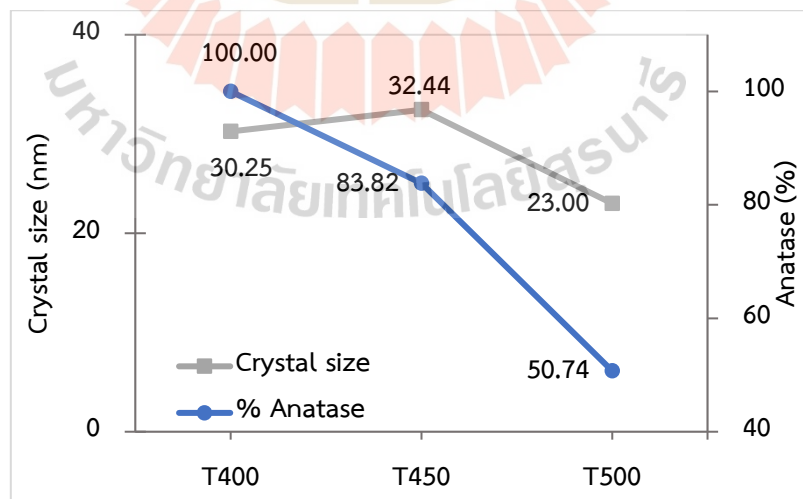
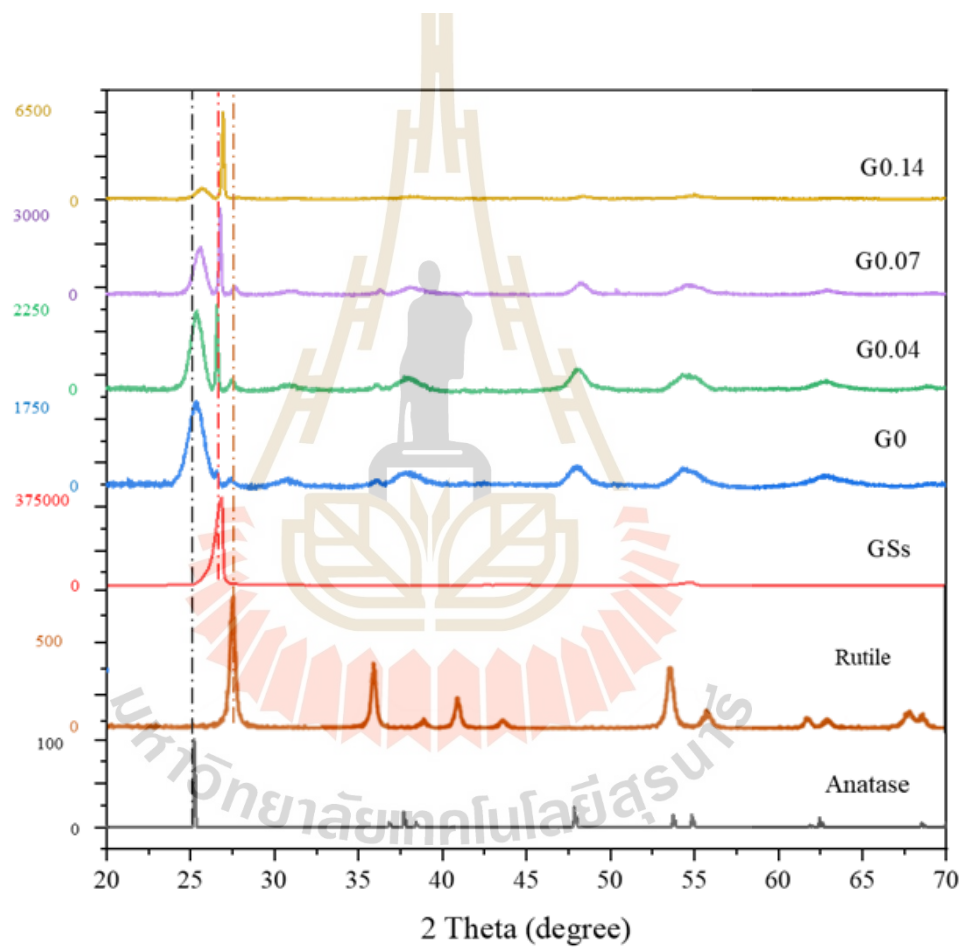


Figure 3.3 The interpretation data of XRD result (G0.07).

### 3.4.1.2 Effect of GSs ratio

The XRD results in Figure 3.4 can be used to determine the proportion of  $\text{TiO}_2$  and GSs in each sample based on their highest intensity. As in Figure 3.4, peak of GSs is getting higher according to the increase of GSs ratio. Meanwhile the number of Ti is fixed amount then the peak of anatase and rutile seems to decline as long as the GSs ratio increases. The sample's XRD patterns show a tendency of intensity and a decrease in FWHM, indicating an increase in crystal size, that shows in Figure 3.5.



**Figure 3.4** XRD pattern of  $\text{TiO}_2$  photocatalyst with a variation of GSs ratio ( $T_{450} \text{ } ^\circ\text{C}$ )

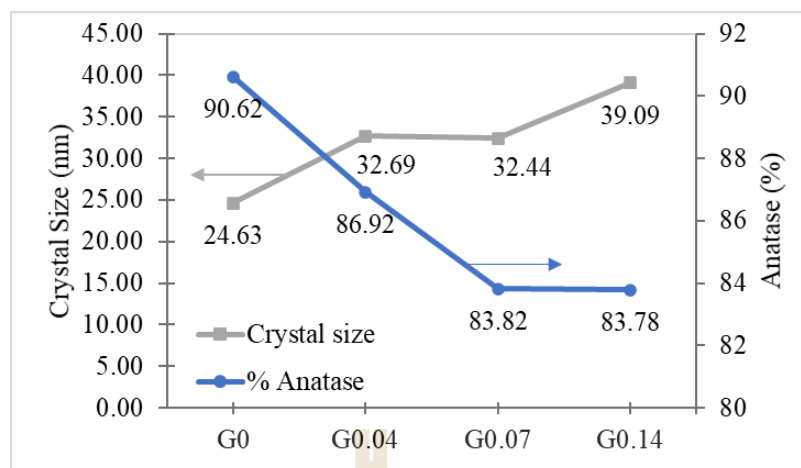


**Figure 3.5** The interpretation data of the XRD result.

The crystal size of the  $\text{TiO}_2/\text{SiO}_2/\text{GSs}$  composite was in the 25-40 nm range, as shown in Figure 3.5. The crystal size is increasing not only due to the crystal growth when  $\text{TiO}_2$  changing its phase from anatase to rutile but also the presence of GSs affect its size as the impurities in the system. Although in the XRD pattern (Figure 3.4) the peak of anatase and rutile are not visible clearly along the increasing of GSs ratio, based on the intensity data for each existing peak, the ratio of anatase and rutile has been calculated. In the form of  $\text{TiO}_2$  and GSs bonding, the GSs induce the  $\text{TiO}_2$  phase change from anatase to rutile, as can be seen in Figure 3.5 the percentage of anatase decrease, compatible with increasing of percentage of rutile in  $\text{TiO}_2$ .

### 3.4.2 SEM/EDS and TEM Results

According to the results of EDS, the increasing amount of C corresponds to an increasing GSs ratio, as shown in Figure 3.6 (left). The carbon content in the spectrum of sample G0 could be due to the residues of raw materials used to produce the sample. On the other hand, the presence of Ti (titanium) decreases with the presence of C content.

The sample's C content rises until T450, then falls at T500, shown in Figure 3.6 (right). This trend shows that Tcal affects the presence of C in the sample

regardless of the initial GSs ratio, which in this case is G0.07. It also clearly states that the rutile phase on the sample influences  $\text{TiO}_2$  bonding with GSs, as it shows that when Tcal is 400 °C, there is no rutile phase, and it increases at T450, proportionally with C content. Even so, the rutile phase appears to be increasing, despite a decrease in C content at T500. This behavior could indicate that the temperature in the furnace is high enough to ignite the combustion reaction between carbon and oxygen. The presence of Ti, on the other hand, exhibits a random trend for each parameter. Overall, the results indicate that crystal size is strongly influenced by C content, with the higher the C content, the larger the crystal size.

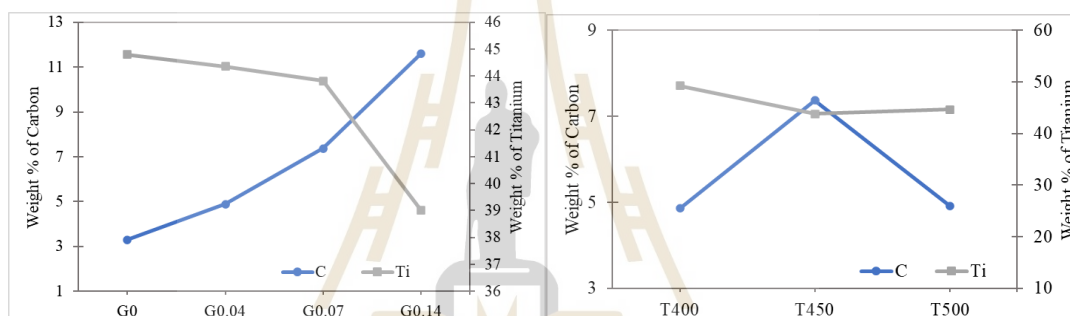


**Figure 3.6** EDS result of  $\text{TiO}_2/\text{SiO}_2/\text{GSs}$  at Tcal 450 °C (left) and G0.07 in different Tcal (right).

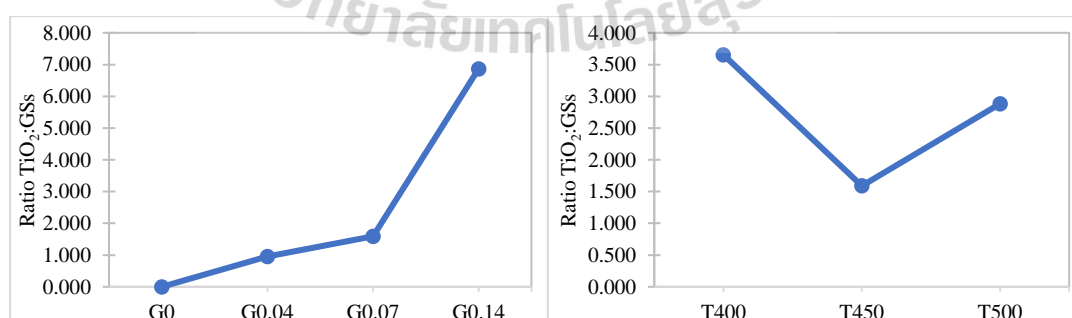


**Figure 3.7** Ratio of  $\text{TiO}_2$ :GSs at Tcal 450 °C (left) and G0.07 in different Tcal (right). (interpretation of XRD results)



For comparison, ratio of GSs was derived from XRD result and applied into Figure 3.7 for each Tcal and weight ratio of TiO<sub>2</sub>:GSs. For different ratio, the presence of GSs seems to be consistent with the weight ratio of Ti and GSs. It fits with the result of C in EDS, while C content is increasing along the increasing of ratio. In contrast with the result in different Tcal, GSs ratio from XRD is decreasing at 450 °C and up at 500 °C. It is different with the result in EDS, when C content is in the maximum value at 450 °C and start to decrease in 500 °C. This difference could be appeared as in XRD, the peak of each component is already fixed, and it can measure the intensity of each peak precisely, while in EDS, the calculation of percentage of each element are done on different site randomly.

The pattern in XRD results give the ratio of GSs at different Tcal as in Figure 3.7. at 400°C, the components are only anatase of TiO<sub>2</sub> and GSs. So, the ratio in T400 is higher than T450 since at 450 °C, there is one additional element which is rutile of TiO<sub>2</sub>, then ratio GSs is decreasing. While at T500, with the presence of anatase and rutile increases, the site to bond with GSs also increase. Then ratio of GSs is increasing along the increasing of Tcal.

Figure 3.8 and 3.10 shows the SEM images of the TiO<sub>2</sub>/SiO<sub>2</sub>/GSs composites, which shows how the GSs layering was formed. TEM images of composites are shown in Figure 3.9 and 3.11, aggregates consisting of many small TiO<sub>2</sub> composites were obtained.

As depicted in Figure 3.8, the graphite sheets (GSs) are observed as the ordered layers structure with an irregular shape. This property affects the TiO<sub>2</sub>/SiO<sub>2</sub>/GSs pattern, which tends to have layers because of the GSs presence. The composite pattern is shown in Figure 3.8(b-e) for the ratio of G0, G0.04, G0.07, and G0.14, respectively. Figure 3.9 is a nanoscale with a grain size less than 50 nm, following the results that have been shown in Figure 3.5.

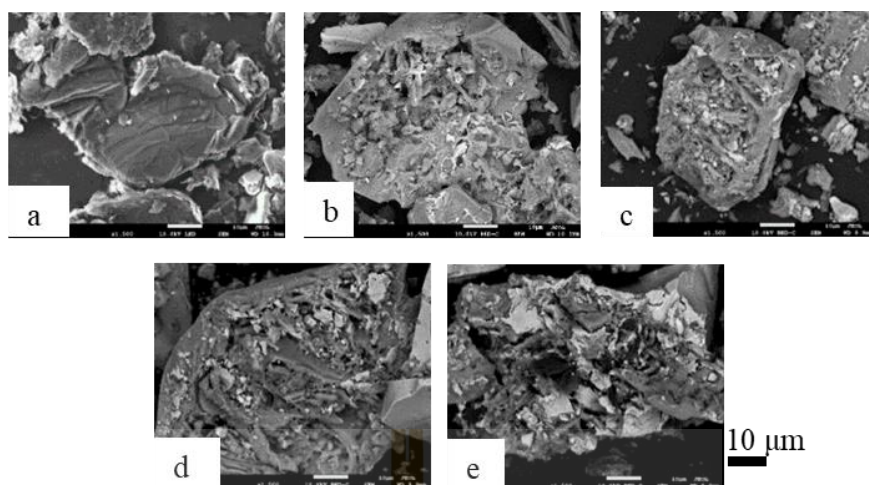


Figure 3.8 SEM images of (a) GSs and  $\text{TiO}_2/\text{SiO}_2/\text{GSs}$  composite (b) G0, (c) G0.04, (d) G0.07 and (e) G0.14 at  $T_{\text{cal}} 450\text{ }^\circ\text{C}$ .

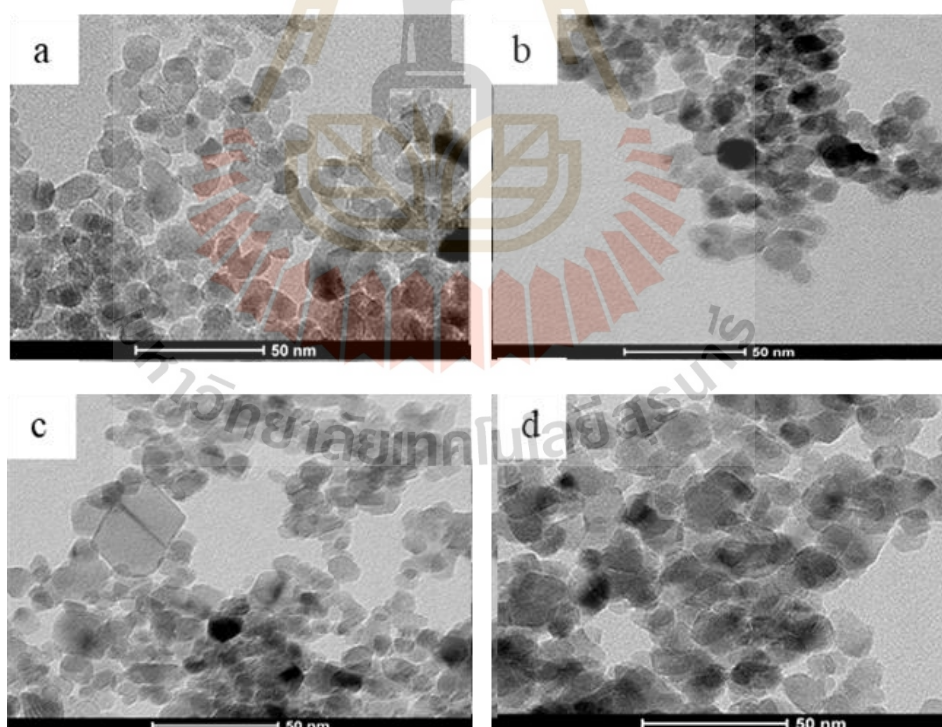
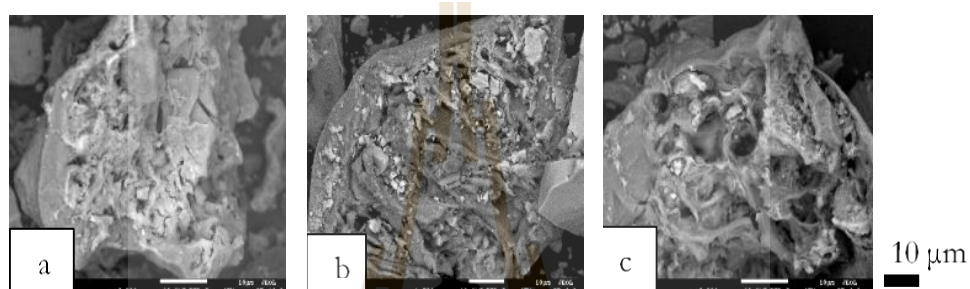
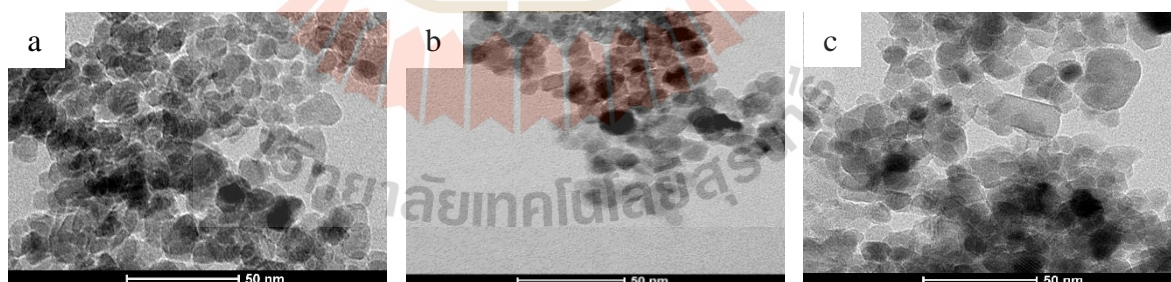


Figure 3.9 TEM images of  $\text{TiO}_2/\text{SiO}_2/\text{GSs}$  composite (a) G0, (b) G0.04, (c) G0.07 and (d) G0.14 at  $T_{\text{cal}} 450\text{ }^\circ\text{C}$ .

Figure 3.10 shows the SEM image of the G0.07 TiO<sub>2</sub> composite, which shows how the layering of GSs was formed at different T<sub>cal</sub>. The layer order is affected by an increase in T<sub>cal</sub>. The layer began to form at T450, accompanied by the presence of C content, as evidenced by the EDS result. However, as shown in Figure 3.10, the layer ordering form became less uniform as the C content decreased at high temperatures of 500 °C (c).



**Figure 3.10** SEM images of G0.07 TiO<sub>2</sub>/SiO<sub>2</sub>/GSs composite (a) T400, (b) T450, and (c) T500.



**Figure 3.11** TEM images of G0.07 TiO<sub>2</sub>/SiO<sub>2</sub>/GSs composite (a) T400, (b) T450, and (c) T500.

### 3.4.3 BET Results

#### 3.4.3.1 Effect of Calcination temperature (T<sub>cal</sub>)

Specific surface area (SSA) is a total surface area of a solid material per unit of mass. The size of the particles affects the value of SSA as well as the structure and porosity of the material. For different Tcal, crystal size happened to increase along with temperature but shrink when it reached 500 °C. It affects its SSA that the value decreases when the composite was calcined at 500 °C.

**Table 3.1** Specific surface area value of TiO<sub>2</sub>/SiO<sub>2</sub>/GSs with a variation of Tcal (G0.07)

Sample	Specific surface area (m <sup>2</sup> /g)	Mean pore D (nm)	Vm (cm <sup>3</sup> /g)	Total pore volume (cm <sup>3</sup> /g)
G0.07T400	1.28E+02	8.3557	23.251	0.280
G0.07T450	1.39E+02	8.4441	32.012	0.294
G0.07T500	1.26E+02	8.1570	23.052	0.269

#### 3.4.3.2 Effect of GSs ratio

Table 3 gives the result of SSA for TiO<sub>2</sub>/SiO<sub>2</sub>/GSs composite at different GSs ratios at Tcal 450 °C. The SSA has the same overall tendency as for the size of each composite. GSs presence improves the surface area of composite because GSs alone have a high specific surface area (2630 m<sup>2</sup>/g).

**Table 3.2** Specific surface area value of TiO<sub>2</sub>/SiO<sub>2</sub>/GSs with a variation of GSs ratio (T450 °C)

Sample	Specific surface area (m <sup>2</sup> /g)	Mean pore D (nm)	Vm (cm <sup>3</sup> /g)	Total pore volume (cm <sup>3</sup> /g)
G0T450	1.28E+02	7.5975	29.464	0.274
G0.04T450	1.38E+02	8.5563	31.767	0.263
G0.07T450	1.39E+02	8.4441	32.012	0.294
G0.14T450	1.46E+02	9.0459	33.629	0.297

### 3.4.4 Degradation of Methylene Blue (MB) Solution

#### 3.4.4.1 Optimum Condition

Under solar light, photocatalytic degradation is measured using a variable  $\text{TiO}_2/\text{SiO}_2/\text{GSs}$  catalyst loading in 100 mL of MB concentration (2.5 mg/L). Figure 3.12 shows that increasing the catalyst loading can increase degradation. This work can be used to determine the optimum catalyst loading for specific concentrations to avoid using too much catalyst while still achieving the best efficiency. At the first 30 minutes, the result is not clearly distinguishable. But along the time, the degradation for each loads start to be seen for the differences because while 0.05 already reach its maximum capacity, another loading just start to degrade MB. Within 3 hours, 0.1 g of catalyst loading G0.07T450  $\text{TiO}_2/\text{SiO}_2/\text{GSs}$  for 100 mL of 2.5 mg/L MB yields the best degradation of 97.83 %.

The initial concentration influences degradation efficiency with a fixed catalyst loading (0.1 g  $\text{TiO}_2/\text{SiO}_2/\text{GSs}$  /100 mL MB). Figure 3.13 shows how the lowest concentration (1 mg/L) yields a similar result to 2.5 mg/L (97-99 %), while the highest concentration (4 mg/L) yields only 56%. It demonstrates how an excess of MB leads to a specific amount of photocatalyst overcapacity. This result indicates that for 2.5 mg/L MB, 0.1 g of G0.07T450  $\text{TiO}_2/\text{SiO}_2/\text{GSs}$  is effective in degrading 100 mL MB.

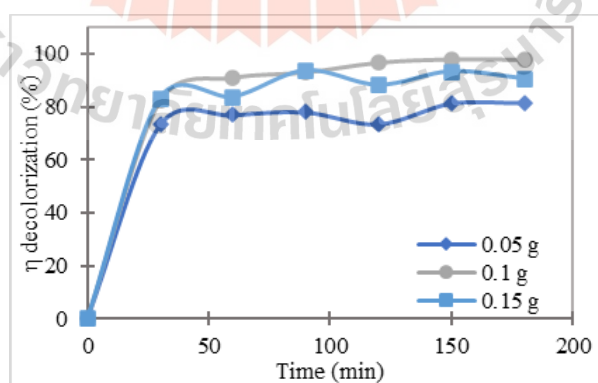


**Figure 3.12** The effect of the amount of  $\text{TiO}_2$  photocatalyst for degradation of MB.



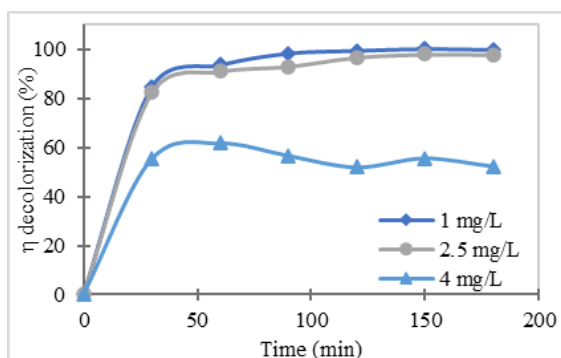


**Figure 3.13** The effect of the concentration of MB on the degradation process.

When the energy bandgap of the photocatalyst is equal to or greater than the energy bandgap of the photocatalyst, light can be one of the most important factors in the photocatalytic process. The energy bandgap in  $\text{TiO}_2$  is 3.2 eV, indicating that ultraviolet (UV) light is appropriate. This work focuses on adding carbon to reduce the bandgap that can be used under visible light range (GSs). Figure 3.14 shows that G0.04T500 can photo-catalytically decolorize MB under solar light with a 90.3 % efficiency in 3 hours. Because of MB adsorption to the  $\text{TiO}_2/\text{SiO}_2/\text{GSs}$  surface, the concentration drops dramatically in the dark. It will be color changing.

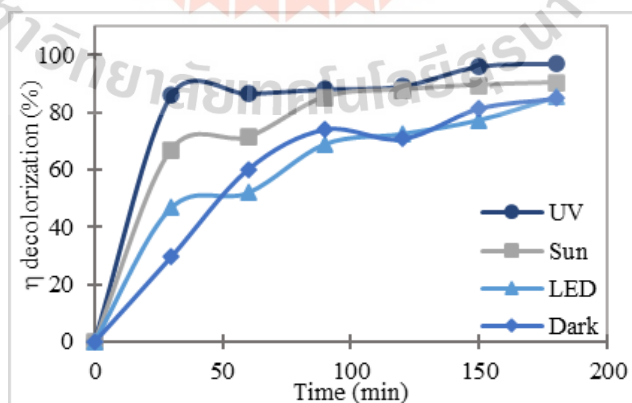


**Figure 3.14** The effect of degradation under four conditions; dark, UV lamp (366 nm), solar light, and LED lamp on  $\text{TiO}_2$  G0.04T500.

In comparison, degradation occurred under a specific LED lamp. It yields the similar results as the test performed in the dark. It means that under an LED lamp, the main process that occurs is adsorption, like a dark condition, with a little bit photodegradation process. It can be because the energy of LED is not enough to trigger photocatalytic reaction ( $E_{LED} < E_{bandgap}$ ). Meanwhile, solar light produces excellent results due to its broad wavelength, which is beneficial to photocatalysts. The reaction was also performed under a UV lamp to provide a brief result on how  $TiO_2$  photocatalyst reacts within its work range. More than 86 % of the MB was adsorbed and degraded in the first hour of the reaction, according to the results.

Adsorption on photocatalyst plays an important role in the photocatalytic process.  $TiO_2$  adsorbs MB on its surface before photocatalytic degradation. The observation of degradation under dark conditions in this experiment can demonstrate how  $TiO_2/SiO_2/GSs$  photocatalyst adsorption occurs. The photocatalytic degradation did not occur in this step due to a lack of light energy, and the surface of the photocatalyst was saturated by MB. Meanwhile, under light conditions (UV, LED, and solar), the efficiency of degradation was slightly higher than in the dark condition because there was a photocatalytic degradation process of MB into other compounds along its desorption and be replaced by other MB due to the adsorption process. As a result, for this condition over a much longer time than the testing time in this work, all MB molecules may be degraded by photocatalysis. However, the MB that was adsorbed on the catalyst surface in the dark may still exist as surface molecules attached to the catalyst. And this process in the dark is not degrade MB molecules into unharmed material and still contaminated photocatalyst or washed water when the photocatalyst will be reused for next process.

Under dark conditions, the process can be described as adsorption of  $TiO_2/SiO_2/GSs$  photocatalyst. Figure 3.15 depicts the adsorption process during the first hour of the reaction. When compared to the EDS result of the amount of C content at the same Tcal, it shows the same trend for T400 but begins to show a different tendency with adsorption at T450 and higher. Instead, it demonstrates that



the adsorption process slows down at some point in Tcal for the same ratio. Overall, G0.07T450 has the highest adsorption capacity, with a crystal size of 34.26 nm and an adsorption capacity of 69.93 % at first hour degradation.

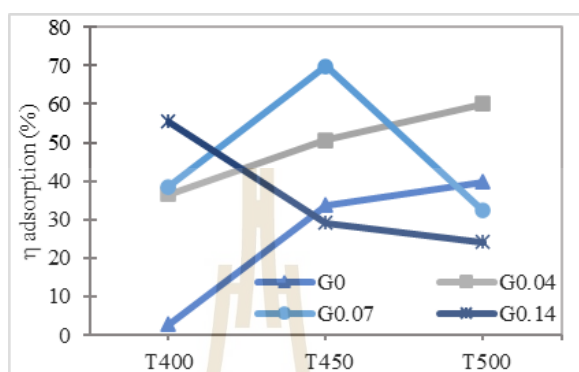


**Figure 3.15** Adsorption of  $\text{TiO}_2/\text{SiO}_2/\text{GSs}$  under the dark condition at the first hour of degradation for each ratio and Tcal.

#### 3.4.4.2 Effect of Tcal

Tcal contributes significantly to the formation of a different  $\text{TiO}_2$  structure, which affects photocatalytic activity. Figure 3.16 depicts the effect of Tcal on G0.07 of  $\text{TiO}_2/\text{SiO}_2/\text{GSs}$ . T450 had the highest degradation with 97.83 % at 3 hours degradation.

Under solar light, T450 produces the best results for the degradation of MB. It demonstrates how the crystal phase of  $\text{TiO}_2$  affects degradation because T400 is pure anatase and has the lowest degradation compared to other Tcal that has developed a rutile phase on  $\text{TiO}_2$ . Because there is a combustion reaction at high temperatures, the amount of C content was lower at 500 °C, even though it has a high rutile phase, and degradation of MB was lower than T450. The rate constant of G0.07 for each Tcal is shown in Figure 3.17 (left). The rate constant was then used to calculate the model data for each sample's degradation rate, which was plotted in Figure 3.17 (right) and compared to the experimental data.

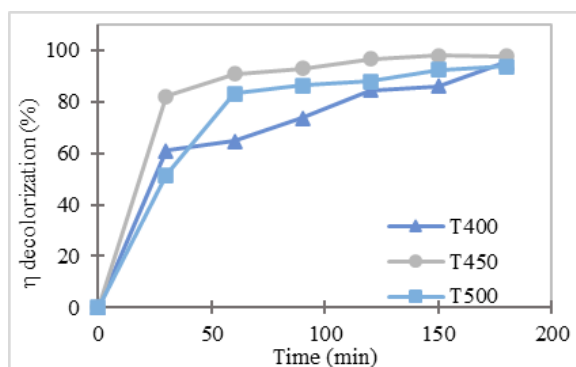


Figure 3.16 The effect of Tcal on  $\eta$  degradation for G0.07  $\text{TiO}_2/\text{SiO}_2/\text{GSs}$ .

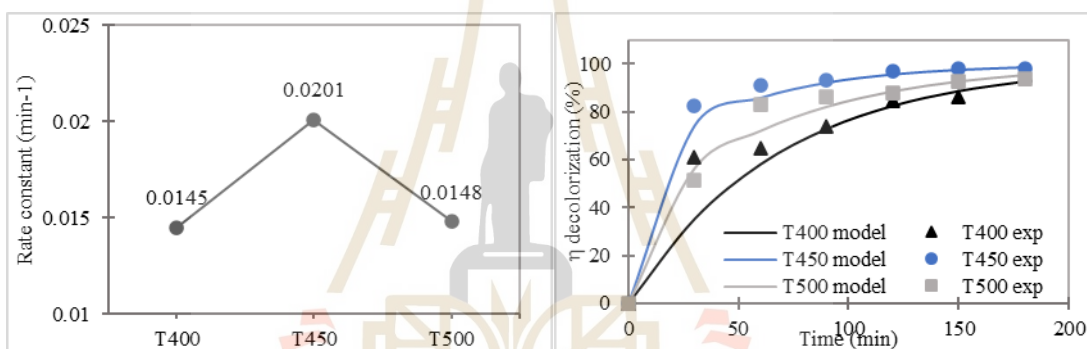
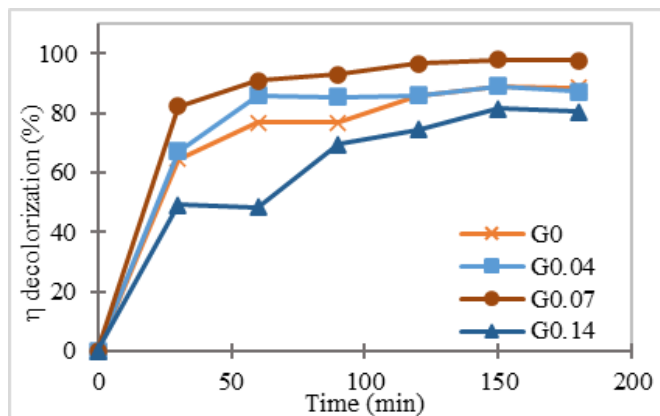


Figure 3.17 The rate constant of G0.07  $\text{TiO}_2/\text{SiO}_2/\text{GSs}$  for each Tcal (left) and validity between experiment data and model data (right).

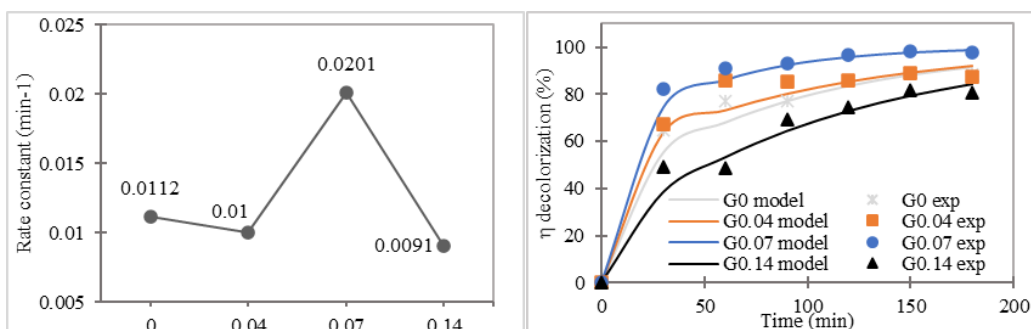
#### 3.4.4.3 Effect of GSs Ratio

Figure 3.18 shows how the  $\text{TiO}_2/\text{SiO}_2/\text{GSs}$  with different ratio of GSs affects the degradation of MB. The results show that G0.07T450 has the highest photocatalytic activity under solar light for MB degradation. It also implies that the photocatalytic activity of  $\text{TiO}_2/\text{SiO}_2/\text{GSs}$  is the best on anatase: rutile phase ratio of 83.8 %:16.2 %, and the sample's optimum C content is 7.96 %wt. The higher the C content, the worse the result of MB degradation because G0.07 and G0.14 have similar anatase: rutile ratios while the C content is different.



**Figure 3.18** The effect of ratio Ti:GSs to  $\eta$  degradation (%) for T450.

The outcome of degradation can influence the kinetics of the reaction. The rate constant of each ratio can be calculated using equation (3.5), as shown in Figure 3.19 (left). G0.07T450 at 0.0201 min<sup>-1</sup> is the highest rate constant for a photocatalytic reaction. The value of the rate constant was then used to calculate the degradation rate model for each sample. The model data was then compared to the experiment data, as depicted in Figure 3.19 (right), where the lines represent model data, and the symbols represent experiment data. It demonstrates that the LH model equation is reasonable for describing the experimental data for all tests in this work.



**Figure 3.19** The rate constant of  $\text{TiO}_2/\text{SiO}_2/\text{GSs}$  for each ratio at T450 (left) and validity between experiment data and model data (right).

#### 3.4.4.4 Effect of Reusable/Stability

In general, the photocatalyst is stable and can be reused until its particle is damaged. The experiment to test the reusable of the photocatalyst was carried out as follows: after the first batch of G0.07T450  $\text{TiO}_2/\text{SiO}_2/\text{GSs}$  used for MB degradation was completed, the photocatalyst was washed by ethanol and then by water to neutralize the pH before being heated at 100 °C to remove water. This 0.1 g reused photocatalyst was used to degrade a new MB solution for 3 hours under solar light at a fixed initial concentration of 2.5 mg/L. Three cycles of this activity were observed. Figure 3.20 depicts the degradation efficiency of the second drop from the first cycle reaching 93.1 %, then dropping to 92.4 % in the third cycle and dropping again in the fourth cycle to 87.65 %. However, the efficiency decreases slightly; the differences could be due to an error during the photocatalyst washing process. The G0.07T450 photocatalyst has a stable structure and can be used multiple times, according to the results of this series of experiments. As a result, it can be used in a variety of applications.

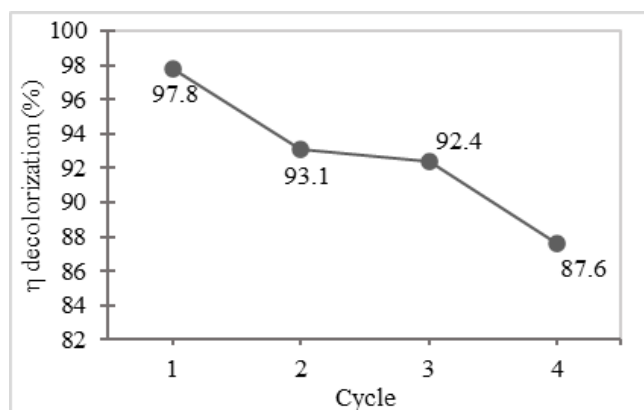


**Figure 3.20** Effect of recycled G0.07T450 TiO<sub>2</sub> photocatalyst on  $\eta$  degradation.

### 3.5 Conclusion

The TiO<sub>2</sub>/SiO<sub>2</sub>/GSs composite was created using the sol-gel method, which was then calcined. The morphology was studied at various Ti:GSs composition ratios and calcination temperatures (Tcal). The TiO<sub>2</sub>/SiO<sub>2</sub>/GSs composite demonstrates that the presence of GSs affected the layer pattern, while the EDS spectrum confirms the presence of Ti and C on the composite's surface. The percentage of rutile phase tendency increases as the amount of GSs increases, while the percentage of anatase phase decreases. Meanwhile, an increase in Tcal does not affect the percentage of the rutile phase. The average crystal size tends to increase with increasing Tcal until 450 °C when it begins to shrink. The average crystal size affects proportionally to specific surface area value and happened GSs improve this value. Under solar light, the degradation of MB demonstrates a good result of photocatalytic activity.

Furthermore, the MB degradation using the TiO<sub>2</sub>/SiO<sub>2</sub>/GSs photocatalyst under solar light is dependent on optimum parameters such as the sample's crystalline phase, crystal size, and C content. The photocatalyst prepared with a Ti:GSs ratio of 0.07 and Tcal at 450 °C achieves the highest efficiency of MB degradation with 97.83 % in 3 hours (G0.07T450). After four cycle times, the ability of reusable TiO<sub>2</sub>/SiO<sub>2</sub>/GSs shows a slight decrease in efficiency.

## CHAPTER IV

### REMOVAL NITROSODIETHYLAMINE (NDEA) BY COATED OF TiO<sub>2</sub>/SiO<sub>2</sub>/GSs COMPOSITE PHOTOCATALYST ONTO SUPPORTING MATERIALS

#### 4.1 Abstract

The sol-gel method was used to synthesize TiO<sub>2</sub>/SiO<sub>2</sub>/GSs with a mass ratio of Titanium:(GSs) of 1:0.07 and calcined at 450 °C. The synthesized powder was coated onto the sponge substrate by dipping with Polyvinyl alcohol as a binder prepared with sponge substrate thicknesses of 0.3, 0.5, 0.8, and 1 cm. The microstructure was examined using a Scanning Electron Microscope (SEM), and the phase composition was determined using an x-ray Diffraction Spectrometer (XRD). The TiO<sub>2</sub>/SiO<sub>2</sub>/GSs XRD pattern reveals the presence of anatase phase and rutile (83.82 %: 16.18 % ), with an average crystal size of 34.26 nm. The SEM photograph of the synthesized powder provided a brief overview of the structure pattern of TiO<sub>2</sub>/SiO<sub>2</sub>/GSs, which follows the layer pattern of GSs, whereas the dipped samples demonstrate the tendency of powder-coated along the surface of sponge fibers. NDEA was degraded in 300 minutes(5 hours) using a TiO<sub>2</sub>/SiO<sub>2</sub>/GSs compact with a degradation efficiency of 95.52 %.

#### 4.2 Introduction

Photocatalyst requires light emission to activate the catalyst function. The bandgap energy of materials determines the source of light. In photocatalysis applications, all semiconductors in nanomaterial form can be used (Jain & Vaya, 2017). TiO<sub>2</sub> is a material that has been attracted widely used due to possessing desirable physicochemical properties such as thermal and chemical stability, relatively high photocatalytic activity, low toxicity, and low cost(Bezerra et al., 2017).

However,  $\text{TiO}_2$  has a bandgap of 3.0-3.2 eV, which gives it a work range as a photocatalyst in the UV range (100 – 400 nm) (Castellote & Bengtsson, 2011; Kang et al., 2019). It almost makes  $\text{TiO}_2$  cannot effectively work under the radiation of solar light (no more than 4 % yield of the solar spectrum). Meanwhile, visible light adsorption on semiconductors with gap energies less than or equal to 3 eV can occur. Many methods have been introduced in much research to increase the photocatalytic activity of  $\text{TiO}_2$  under visible light, such as impure doping (metal/non-metal), surface modification, hybrid composite (integration with other materials), and so on (Aziz & Sopyan, 2009; Kovacic et al., 2018; Negishi et al., 2019).

Non-metal doping was effective to obtain a visible light response. Carbon in graphene form has recently become a more popular doping material for decreasing the bandgap of semiconductors, particularly in photocatalyst applications (Lee & Park, 2013; Najafi et al., 2017; Ribao et al., 2018). Because the bond between graphene and oxide on the system produces dipole force, graphene is considered an impurity in the  $\text{TiO}_2$  system. This force causes their bandgaps to overlap. When the conduction band of graphene is lower than the conduction band of  $\text{TiO}_2$ , the gap between the conduction band of graphene and the valence band of  $\text{TiO}_2$  is reduced. The properties of graphene are high thermal and electrical conductivity, high specific surface area, and high charge carrier mobility at room temperature (Brownson & Banks, 2014). As a result, a graphene-semiconductor composite, particularly  $\text{TiO}_2$ , is currently being considered as a potential photocatalyst in air and water purification applications. In comparison to ordinary  $\text{TiO}_2$ , the graphene based  $\text{TiO}_2$  composite has higher photocatalytic activity.

$\text{TiO}_2$  in the powder form has difficulty dispersing in the suspension and needs another technique to separate it (Larumbe et al., 2014). To avoid free nanoparticles as the colloidal in suspension water, nano- $\text{TiO}_2$  particles are usually coated on a substrate or integrated into thin films and other materials (Doll & Frimmel, 2004). The Coating of  $\text{TiO}_2$  makes it simple to install and recycle, but it reduces photocatalytic activity due to a reduction in effective surface area. By incorporating a material with a high surface area into  $\text{TiO}_2$  and/or reducing the crystal structure to a nanoscale



(nanostructured),  $\text{TiO}_2$  has the potential to achieve a high photocatalytic activity in the coated form. To enhance the adsorptive and surface area of  $\text{TiO}_2$ ,  $\text{SiO}_2$  will be added as the material that can improve the photocatalytic process of  $\text{TiO}_2$  (Aziz & Sopyan, 2009). At the same time,  $\text{SiO}_2$  act as a carrier of  $\text{TiO}_2$  and helps to obtain a large surface area as well as to improve the surface adsorption (Zhou et al., 2006).

General methods to coating are used various substrates materials such as glass, activated carbon, polymeric materials, and metals and dipped into a slurry of photocatalyst materials. Glass and activated carbon are the materials that usually be used as a substrate (Shan et al., 2010). Because of its high surface area and suitability for Coating of  $\text{TiO}_2/\text{SiO}_2/\text{GSs}$  boned with polyvinyl alcohol (PVA) as a binder, the sponge was used as an alternative substrate in this study. PVA is a water-soluble polymer with distinctive strong cohesiveness and film toughness, as well as other properties such as high smoothness, oil and solvent resistance, air barrier capabilities, abrasion resistance, and the protective colloid property. The sponge was chosen because it has more fibers that can be bonded with  $\text{TiO}_2/\text{SiO}_2/\text{GSs}$  and pore with a large surface area, which increases the area in contact with pollutants. The primary goal of this work will be to conduct a focused study on the effect of photocatalyst Coating and the effect of sponge thickness on the photodegradation of methylene blue (MB) under a variety of light sources (dark, UV lamp, LED lamp, and solar light).

### 4.3 Experimental Procedure

#### 4.3.1 Coating of $\text{TiO}_2/\text{SiO}_2/\text{GSs}$

A 3 g of polyvinyl alcohol was dissolved in 100 ml distilled water. The solution was stirred and boiled on the hot plate at 80 °C for 24 hours. 4 g of  $\text{TiO}_2/\text{SiO}_2/\text{GSs}$  (ratio Ti:GSs 1:0.07, Tcal 450 °C) was mixed with 10 ml of distilled water and 4.4 ml of polyvinyl alcohol solution. After that,  $\text{TiO}_2/\text{SiO}_2/\text{GSs}$  slurry was prepared with the ball mill for 24 hours. The sponge substrate was dipped into the slurry and dried at 110 °C for 22-24 hours.

#### 4.3.2 Characterization of $\text{TiO}_2/\text{SiO}_2/\text{GSs}$ Compact

The structure of  $\text{TiO}_2/\text{SiO}_2/\text{GSs}$  was characterized by using FE-SEM JEOL JSM 7800F to analyze surface morphology as labeled by their thickness of 0.3, 0.5, 0.8, and 1.0 cm.

#### 4.3.3 Optimum Condition of Photocatalytic Activity

The photocatalytic activity of  $\text{TiO}_2/\text{SiO}_2/\text{GSs}$  dipped sponge (size 2 cm x 3 cm x thickness) was investigated by using a Methylene Blue (MB). The 0.1 g of synthesized composite powder was put into a 100 ml solution of 3 mg/l of MB under solar light. The monitoring under solar light was restricted from 11 am to 4 pm according to peak sun-hours in Thailand (5.23 hours). The reaction time was in every 30 minutes for 3 hours of taking data. The 5 mL of degradation solution was analyzed by using a T80+ PG instrument UV-Vis spectrophotometer with absorbance at a wavelength of 665 nm.

#### 4.3.4 Removal NDEA in Contaminated Water

The  $\text{TiO}_2$  sample that will be used in this experiment is a sample with a thickness of 0.5 cm (t0.5). Prepare the main solution of NDEA with a concentration of 5 ppm. Prepare each 200 mL of the standard solution of NDEA with the concentration 0 ppb, 2 ppb, 4 ppb, 6 ppb, 8 ppb, and 10 ppb. Put into the refrigerator. Prepare three of 250 mL samples of NDEA with a concentration of around 1 ppm in beaker glass. Take 25 mL of each NDEA sample, put it into a dark bottle (code sample 1t0, 2t0, 3t0). Put the NDEA solution (sample) outdoor. Put 2 pieces of  $\text{TiO}_2$  sample t0.5 into the NDEA solution, start to count the stopwatch. Every 15, 30, 60, 90-, 120-, 180-, and 300-minutes. Take  $\pm$  25 mL of each NDEA sample, put into dark bottle (code sample 1tx, 2tx, 3tx; x means time (15, 30, 60, etc.)). After finishing the experiments, take all samples to be analyzed by GC-MS. Analysis of the standard and sample solution by GC to get the peak of each.

Analysis sample was using Bruker 450-GC/Bruker 320-MS. In a DB-WAXetr (extended temperature range high polarity polyethylene glycol, 30 m 0.25 mm, 0.50 m film thickness), the volume sample injected was 2 L in the splitless mode of operation, with an injector temperature of 250 °C and a splitless period of 1 min. The solvent delay time was set to 6 minutes. The temperature program for the

oven was as follows: 60 °C held for 1 minute; then ramped to 100 °C at 10 °C min<sup>-1</sup> and held for 1 minute, and finally ramped to 245 °C at 15 °C min<sup>-1</sup> and held for 2 minutes. At a constant flow rate of 1 mL min<sup>-1</sup>, helium (99.99 %, Praxair, Spain) was employed as the carrier gas.

## 4.4 Results and Discussion

### 4.4.1. The Characteristics and Properties of TiO<sub>2</sub>/SiO<sub>2</sub>/GSs Composite

To coat TiO<sub>2</sub>/SiO<sub>2</sub>/GSs powder into a compact one, sponge substrates with dimensions of 2 cm x 3 cm x thickness (t) were dipped into a TiO<sub>2</sub>/SiO<sub>2</sub>/GSs composition slurry. The thickness (t) was varied by 0.3, 0.5, 0.8, and 1 cm (the sample was labeled by t0.3, t0.5, t0.8, and t1 respectively). SEM images show how the photocatalyst was coated into the sponge substrate. Figure 4.1 shows the image of the fibers of the sponge and how the TiO<sub>2</sub>/SiO<sub>2</sub>/GSs were coated on the surface of the fiber.

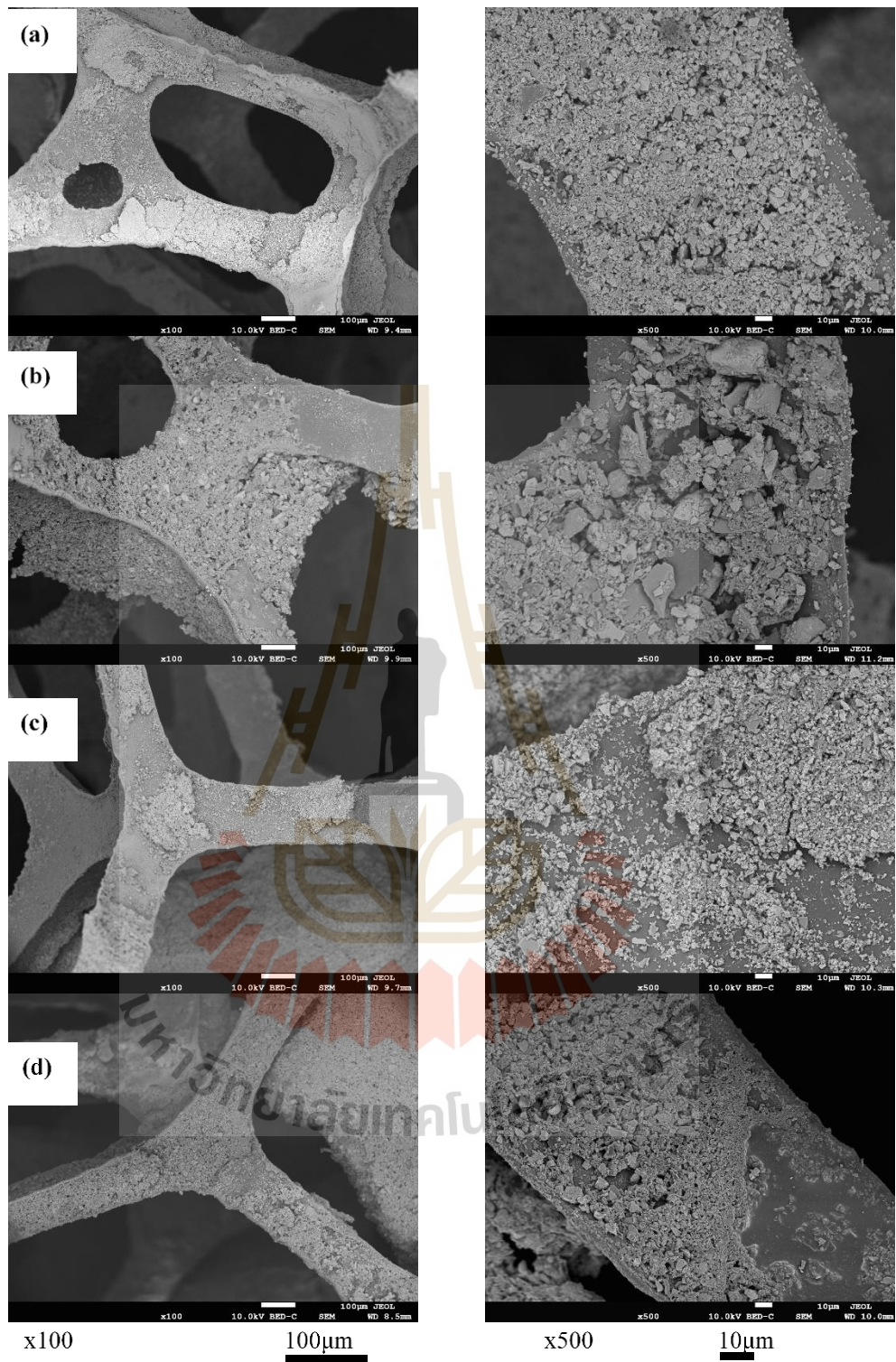
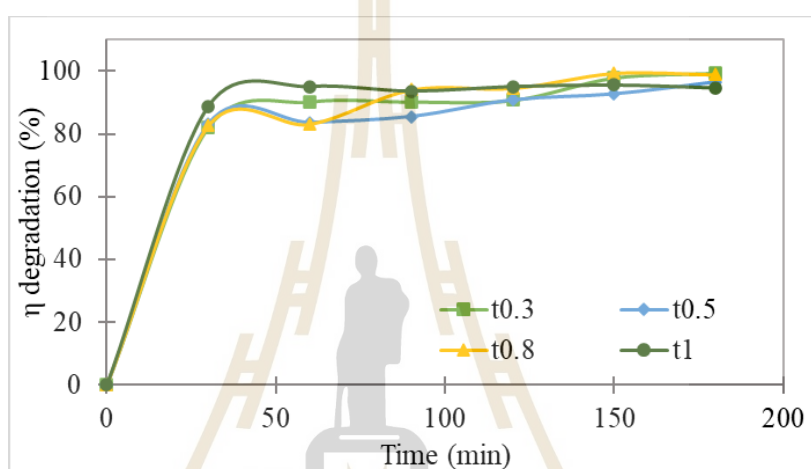


Figure 4.1 SEM images of sponge substrate of  $\text{TiO}_2/\text{SiO}_2/\text{GSs}$  sample (a)  $t_{0.3}$ , (b)  $t_{0.5}$ , (c)  $t_{0.8}$ , and (d)  $t_1$  (cm).



#### 4.4.2. Optimum Condition of Photocatalytic Activity

A PVA binder was used to coat  $\text{TiO}_2/\text{SiO}_2/\text{GSs}$  into sponge fibers. The area of fibers in the sponge that was coated with photocatalyst influenced the sponge's thickness. The effect of sponge thickness on  $\text{TiO}_2/\text{SiO}_2/\text{GSs}$  photocatalyst activity is shown in Figure 4.2. The result shows how the thickness affects degradation early on, but the results will be quite similar after 3 hours ( $\eta$  94-99 %).



**Figure 4.2** The effect of thickness of  $\text{TiO}_2/\text{SiO}_2/\text{GSs}$  compact on the sponge to  $\eta$  degradation (%).

At the early stage of degradation (30-60 mins), t1 had already degraded nearly 95 % of the MB, whereas another sample had only degraded 83 %. It happened that the amount of  $\text{TiO}_2/\text{SiO}_2/\text{GSs}$  coated on t1 was higher than others. After some time,  $\eta$  degradation for all thickness start to have similar number because when t1 already in complete phase at the early minutes, in another thickness MB start to degraded slowly and reach it peak (start to degrade completely) on the last minutes. As depicted at Figure 4.2 where in 2-3 hours,  $\eta$  degradation for each thickness are similar, no have distinguishable result. According to this result, the best thickness to use for degradation is t0.5 because it has the

potential to continue to degrade and is also thick enough (not too thick or thin) so that sunlight can hit every surface.

#### 4.4.3. Removal NDEA in contaminated water

NDEA solution was degraded by using  $\text{TiO}_2/\text{SiO}_2/\text{GSs}$  compact with the thickness of 0.5 cm under sunlight. Figure 4.3 shows the  $\eta$  degradation (%) of NDEA for 300 minutes. 95.52 % of NDEA was degraded is the highest  $\eta$  degradation that reached at minute 300.

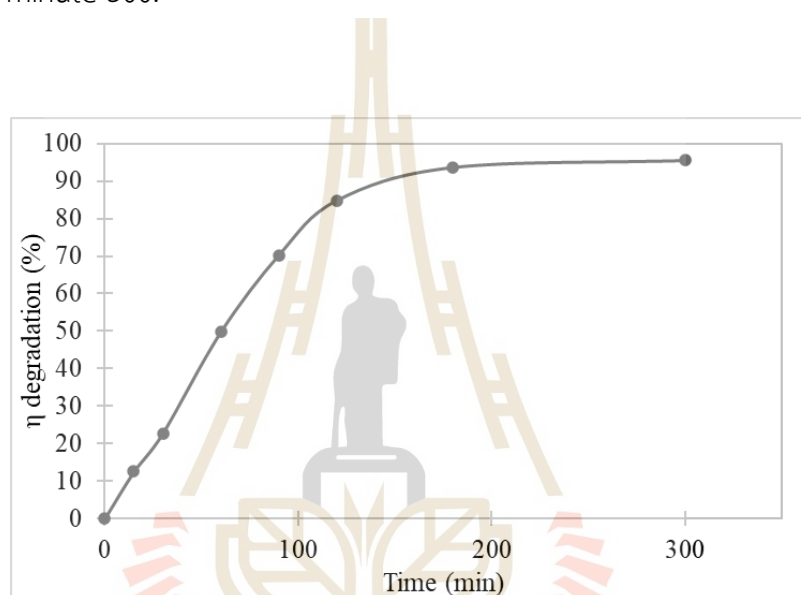


**Figure 4.3** Degradation of NDEA by  $\text{TiO}_2/\text{SiO}_2/\text{GSs}$  (G0.07T450) compact (t0.5).

The rate constant of each ratio can be calculated using equation (3.5), as shown in Figure 4.4 (a). The rate constant for this NDEA degradation process is  $0.0159 \text{ min}^{-1}$ . The value of the rate constant was then used to calculate the degradation rate model for each sample. The model data was then compared to the experiment data, as depicted in Figure 4.4 (b), where the lines represent model data, and the symbols represent experiment data. It demonstrates that the LH model equation is reasonable for describing the experimental data for all tests in this work.

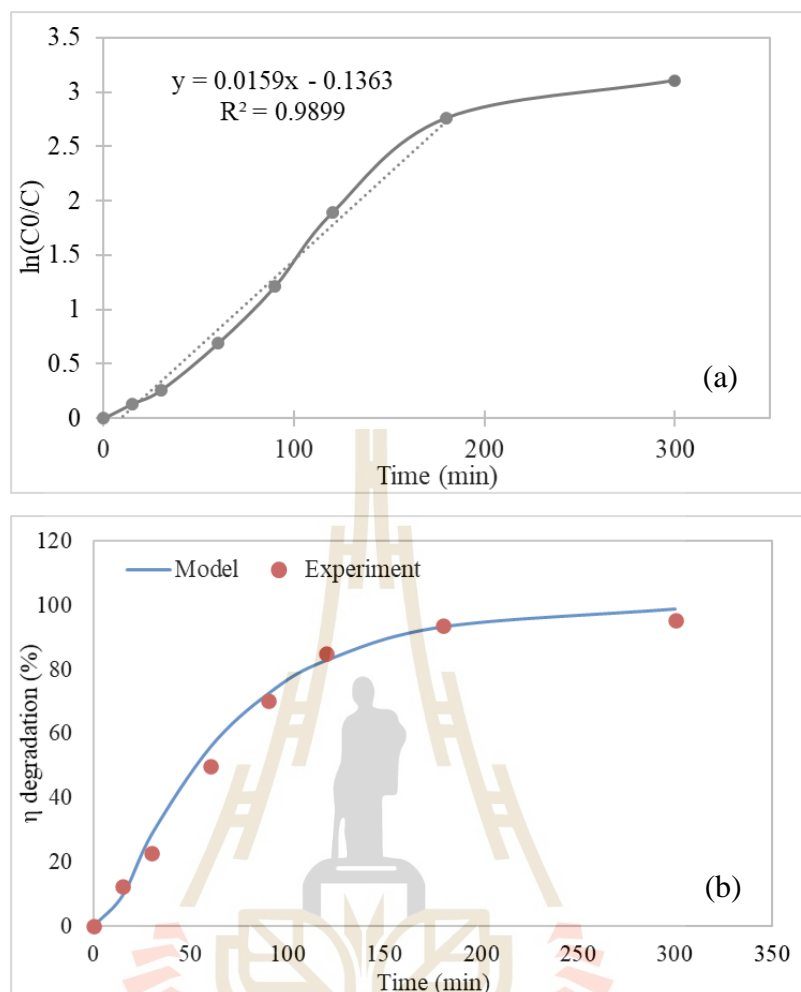


**Figure 4.4** (a) Rate constant of degradation of NDEA by  $\text{TiO}_2/\text{SiO}_2/\text{GSs}$  compact (t0.5)  
 (b) validity between experiment data and model data.

#### 4.5 Conclusion

$\text{TiO}_2/\text{SiO}_2/\text{GSs}$  samples were prepared by dipping them on a sponge substrate and then drying them. The SEM image of the  $\text{TiO}_2/\text{SiO}_2/\text{GSs}$  compact shows how the photocatalyst coated the sponge fibers. The degradation of MB produced a good photocatalytic activity under solar light emission. t1 had the highest efficiency of 95.04 % in the first 60 minutes. Within 3 hours, all samples had reached their saturation points of 98-99 %. It demonstrates how the thickness affects degradation proportionally to the amount of  $\text{TiO}_2/\text{SiO}_2/\text{GSs}$  coated, as well as the surface area of



the compact, which improves absorption and the photocatalytic reaction of  $\text{TiO}_2/\text{SiO}_2/\text{GSs}$  composite in the dark condition with 86 % adsorption. The recycling of each thickness of  $\text{TiO}_2$  compact shows a degradation efficiency of 90 % until three times reused. Furthermore, the degradation of the  $\text{TiO}_2/\text{SiO}_2/\text{GSs}$  compact on the sponge under solar light is thickness dependent. Degradation of NDEA was done in 300 minutes by using  $\text{TiO}_2/\text{SiO}_2/\text{GSs}$  compact with the chosen thickness of 0.5 cm and get the efficiency of 95.52 % degradation.



## CHAPTER V

### SIMULATION OF PHOTOCATALYTIC REACTION ON TiO<sub>2</sub>/SiO<sub>2</sub>/GSs PHOTOCATALYST

#### 5.1 Abstract

TiO<sub>2</sub>/SiO<sub>2</sub>/GSs as the photocatalyst material has two important properties which are photocatalytic activity and adsorption. The research is conducted to model the structural and the activity between a solid photocatalyst and pollutant molecules in the liquid phase. The structure was proposed based analysis result of TiO<sub>2</sub>/SiO<sub>2</sub>/GSs and sketched by the initial model of each component. The orientation and conformation of photocatalyst and the free electron which are produced during light illumination were investigated by using Monte Carlo simulation based on the structure of TiO<sub>2</sub>/SiO<sub>2</sub>/GSs and randomness of a free electron. The electron will move around the structure, following a multi-trapping mechanism, before transferring to oxygen and water. It can be imagined that the free electron can move not far from the surface and the pollutant molecules will attract near the surface then both will interact with each other to induce a photocatalytic reaction.

#### 5.2 Introduction

Photocatalyst has two main properties that are very important when its material interacts with another substance which is photocatalytic activity and adsorption. Photocatalytic activity is the ability of materials to create an electron-hole pair under light conditions. These pairs can generate a free radical on the system. While adsorption is the ability of the material to adsorb molecules or ions onto the surface of materials (Guo et al., 2020; Moma & Baloyi, 2019). Usually, these properties are helpful when degradation of substances with light support.

TiO<sub>2</sub> is a semiconductor material. Semiconductor materials have a bandgap

between conducting band and the valence band (Messenger & Abtahi, 2010). These bands determined the electrical conductivity of materials. Since there is a bandgap between these bands, the electron cannot move freely to conduct the electricity. The light provides the energy within its spectrum. When the light in a certain wavelength is illuminated by  $\text{TiO}_2$ , that energy will induce the electrons on the valence band to be excited into conducting band. These free electrons will move along the surface or near the surface of  $\text{TiO}_2$ , yet the hole of electrons is in the valence band. The free electrons, before moving back into the valence band, will interact with the substances near-surface of  $\text{TiO}_2$  like oxygen or water molecules and produce some radical on the surface of  $\text{TiO}_2$ . Similar to the electron, the hole will act as a proton and react with water molecules to produce free radicals, following by the reaction (2.7) to (2.15). On other hand, the degradation process was following by the reaction (2.16).

$\text{TiO}_2$  as the photocatalyst will produce electron-hole pairs when the light source illuminates it. It is because of the characteristic of  $\text{TiO}_2$  in the term as a semiconductor material. These characteristics and electron-hole pair production,  $\text{TiO}_2$  can be used for the degradation of pollutants to environmental purification. The mechanism of electron-hole production until the degradation process by using  $\text{TiO}_2$  has been conducted with the experimental studies on these materials.

The computational studies can provide a more detailed atomic level about photocatalytic activity and the degradation process of  $\text{TiO}_2$  on the system. This study is time-saving and economic to learn more about mechanisms while in the experiment there will be factors that affect collecting data. Monte Carlo simulation can be used to mimic photocatalytic activity and reaction in  $\text{TiO}_2$  photocatalyst. In this work, the free electron was generated before then the initial adsorption and degradation of pollutants orientation were determined. These simulations were validated with the experimental result.

### 5.3 Experimental Procedure

The crystal structure of  $\text{TiO}_2/\text{SiO}_2/\text{GSs}$  was replicated in x, y, z directions. Since the photocatalytic process produces the free electrons which were moved freely, the free electrons were placed randomly in a fixed position by assumed that position right before interacting with the system. The  $\text{TiO}_2/\text{SiO}_2/\text{GSs}$  and free electrons are placed on the system which is assumed in the liquid phase. The system is consisting of water, dissolved oxygen, and pollutants molecules. These molecules will close together with little free space between them. The pollutants will move randomly and at a certain distance will react with free electrons.

The molecules in the liquid phase will move and slide past each other. With the force of photocatalyst, the pollutants molecules will attract into  $\text{TiO}_2/\text{SiO}_2/\text{GSs}$ . The pollutant molecules near-surface of  $\text{TiO}_2/\text{SiO}_2/\text{GSs}$  because of adsorption and some free electron from the photocatalytic reaction will interact with then produce degradation product, oxygen and/or water molecules. During the illumination of light into  $\text{TiO}_2/\text{SiO}_2/\text{GSs}$ , the free electron production will continue and interact with pollutants.

Aside from photocatalytic activity, adsorption is also an important role when the photocatalyst interacts with another substance and can be modeled by using Monte Carlo simulation. The investigation of the orientation of  $\text{TiO}_2/\text{SiO}_2/\text{GSs}$  and the electron using computer programming based on the structure of  $\text{TiO}_2/\text{SiO}_2/\text{GSs}$  and electron's position near-surface of  $\text{TiO}_2/\text{SiO}_2/\text{GSs}$ . The fixed position of the electron is chosen as the light illuminated  $\text{TiO}_2/\text{SiO}_2/\text{GSs}$  and produces the free electrons and that position shows right before interacting with the system. The system is conditioned as in the liquid phase when the molecules in the system are close together yet still can move past each other. Interaction between the system and free electrons produces degradation products whose position will be near the surface of  $\text{TiO}_2/\text{SiO}_2/\text{GSs}$ . By the properties of  $\text{TiO}_2/\text{SiO}_2/\text{GSs}$ , the adsorption force will attract other substances and the desorption force will release it. So, the pollutant molecules will be absorbed into the surface of  $\text{TiO}_2/\text{SiO}_2/\text{GSs}$  after that the degradation product will be assumed release from the surface without reacting with

another free electron. The free electron will be fixed on the traps and molecules in the system will move and interact randomly then the photocatalytic reaction will occur. The degradation product was desorbed from  $\text{TiO}_2$  and replaced with another pollutant. The process is confined to no more pollutants on the system.

## 5.4 Results and Discussion

### 5.4.1 Structural Model and Mechanism of $\text{TiO}_2/\text{SiO}_2/\text{GSs}$

The structural model can be hypothesized based on the results of experimental result analysis, as shown in Figure 5.1. Because the reaction heat was lower than the minimum carbide to be formed ( $1200\text{ }^\circ\text{C}$ ) (H. Zhang et al., 2008), the C modeled on GSs could be bonded to the oxygen on  $\text{TiO}_2$ . The more C on GSs, the more the unit cell is stretched, making the crystal lattice larger than the original and enhancing the phase transition from anatase to the more stable rutile phase. The presence of  $\text{SiO}_2$  also bonds to  $\text{TiO}_2$ , resulting in oxygen-oxygen bonding.

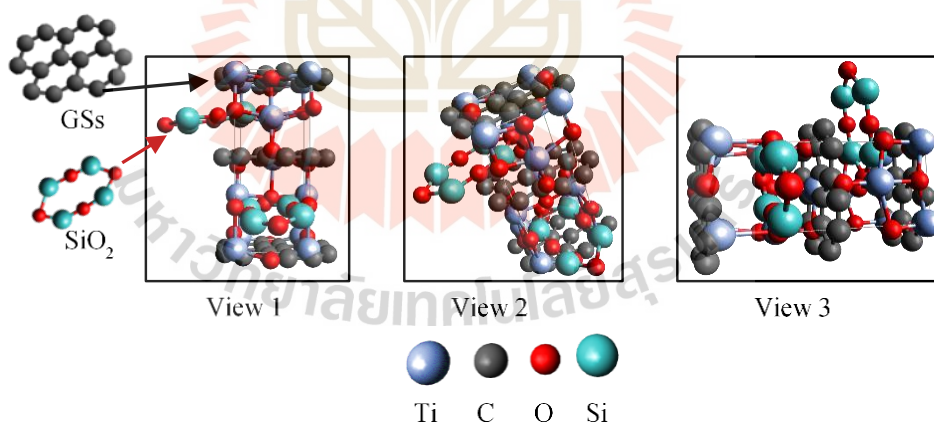


**Figure 5.1** The proposed structural model of  $\text{TiO}_2/\text{SiO}_2/\text{GSs}$  in a one-unit cell of anatase phase.

The semiconductor photocatalyst mechanism is based on the energy of the bandgap between the valence and conductive bands.  $\text{TiO}_2$  is a semiconductor with a bandgap energy of 3.2 eV, allowing it to function as a photocatalyst in the UV work range. In this study, GSs were doped to reduce the bandgap so that it could work on the visible light spectrum. Carbon on GSs in the form of a hexagonal lattice is attracted to oxygen on  $\text{TiO}_2$ , resulting in the formation of a dipole-dipole force between them. Figure 5.2 depicts the explanation for this bond. The bond generates a dipole moment, which disrupts bonding stability in  $\text{TiO}_2$  and reduces the bandgap on  $\text{TiO}_2$  (Shang et al., 2018). The bonding of oxygen on  $\text{TiO}_2$  and oxygen on  $\text{SiO}_2$  has taken place. A defect in  $\text{TiO}_2$  influences the bandgap decrease. It is supported by the fact that the crystal size of  $\text{TiO}_2/\text{SiO}_2/\text{GSs}$  composite is affected by the presence of GSs, which causes a defect in  $\text{TiO}_2$  and creates the state of dipole moment into bandgap, as shown in Figure 5.2. As a result, the  $\text{TiO}_2/\text{SiO}_2/\text{GSs}$  composite can function as a photocatalyst when exposed to solar light (visible light range).

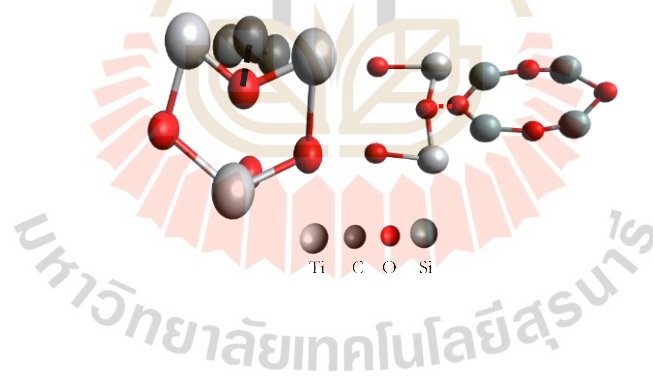
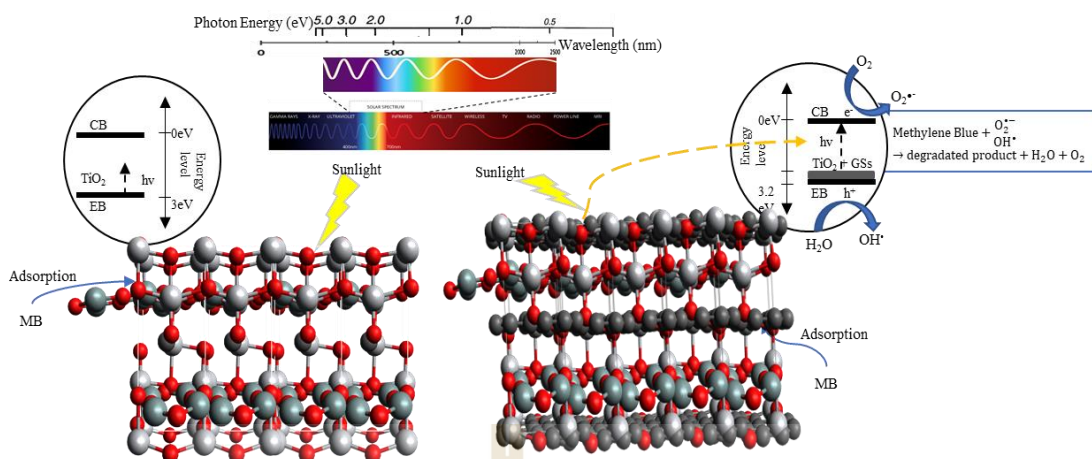


Figure 5.2 Bonding on  $\text{TiO}_2/\text{SiO}_2/\text{GSs}$  photocatalyst.



**Figure 5.3** Mechanism of photocatalytic degradation of MB by  $\text{TiO}_2/\text{SiO}_2/\text{GSs}$  composite.

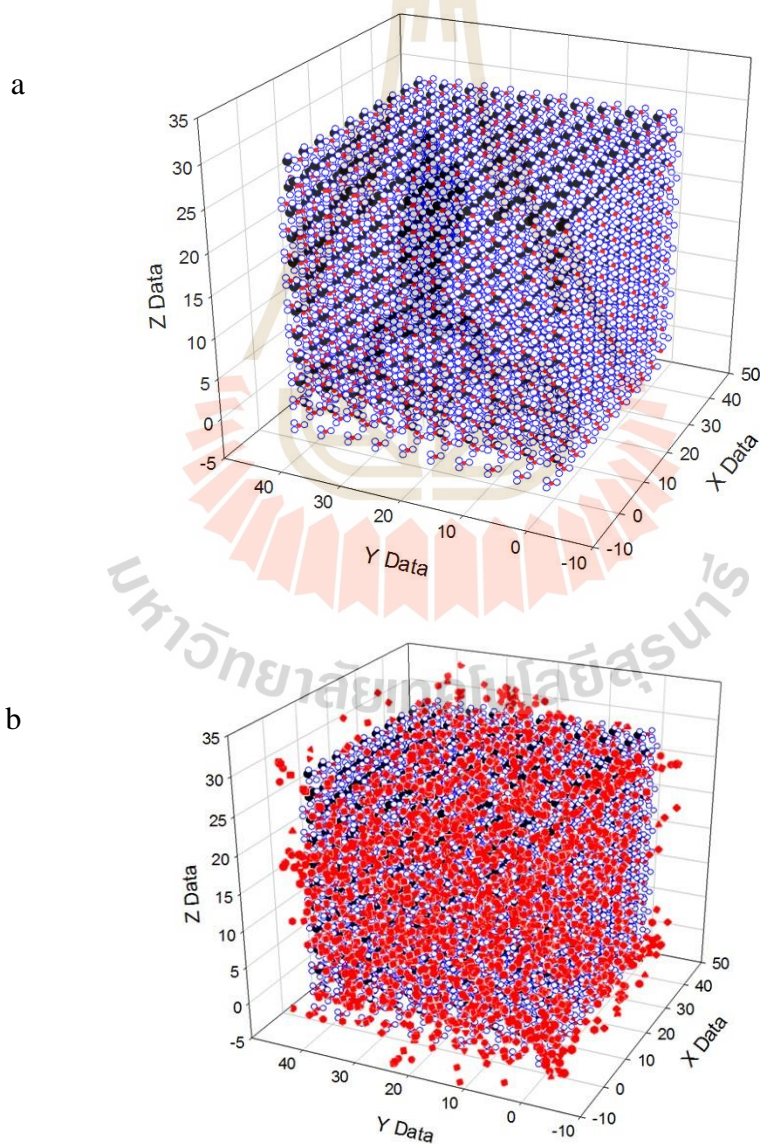
Later, the mechanism of photocatalytic degradation was explained in Figure 5.3. The figure shows how the presence of GSs affects the bandgap of  $\text{TiO}_2$ , how solar light can fill the gap to excite the electron into the conduction band, and how the photocatalytic reaction occurs. In the meantime,  $\text{TiO}_2/\text{SiO}_2$  without GSs has a 3.2 eV bandgap and can only be used with a UV lamp (387 nm or less) (Shang et al., 2018; Tayade et al., 2009). When used under solar light, pollutant concentrations can be reduced due to an adsorption process in the  $\text{TiO}_2/\text{SiO}_2$  photocatalyst. There was also a UV work range in solar light (3-5%) that could activate the photocatalytic reaction. Furthermore, the percentage of the anatase-rutile phase, the GSs ratio in the composite, and morphology such as crystal size can all influence photocatalytic activity.

#### 5.4.2 Simulation of Photocatalytic Reaction $\text{TiO}_2/\text{SiO}_2/\text{GSs}$

This study was done to see the simulation of the photocatalytic reaction of  $\text{TiO}_2$ -GSs in pollution degradation. In this study, computer programs are used to simulate events to predict potential outcomes by using random events. FORTRAN was used to write the program that has been arranged based on Monte Carlo Method.



The first thing is to set the system that contains  $\text{TiO}_2$ -GSs coated which is like the experimental system (cube shape which coated with  $\text{TiO}_2$ -GSs). Then determine the pollutant molecules in the system that scattered randomly without binding with  $\text{TiO}_2$ -GSs catalyst. Assign each movement of pollutant randomly with no overlapping with another pollutant. While the pollutants move, each time contact a photocatalyst, there will be a reaction and the pollutant will disappear from the system given by the time until all molecules are gone. The simulation that happened in the system can be studied in the following Figure 5.4.



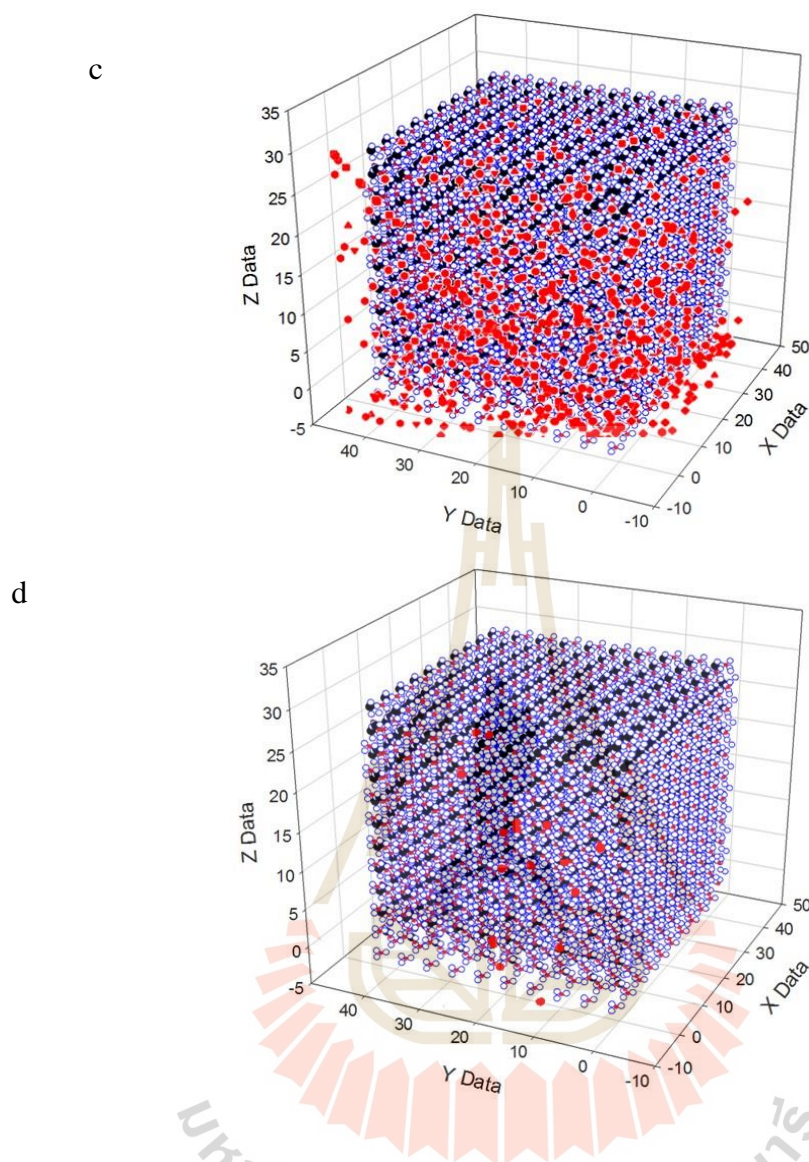


**Figure 5.4** System of  $\text{TiO}_2$ -GSs(cube) and pollutants (red dot). (a)  $\text{TiO}_2$  GSs photocatalyst, (b) initial condition when the pollutants were added into the system, (c) photodegradation were in process, and (d) the system almost reach its settle point.

## 5.5 Conclusion

The study determined the structure of  $\text{TiO}_2/\text{SiO}_2/\text{GSs}$  and simulate the photocatalytic reaction on the system. Bonding between each molecule was proposed by dipole-dipole force for  $\text{TiO}_2$  and GSs also oxygen-oxygen bonding

between  $\text{TiO}_2$  and  $\text{SiO}_2$ .  $\text{TiO}_2$  in anatase form act as the main crystal yet others are impurities that cause defects which leads to the changing properties of the photocatalyst. The system that contains this structure was created and the pollutant molecules within the system move around while each contact with  $\text{TiO}_2/\text{SiO}_2/\text{GSs}$  annihilated until it settled down.



## CHAPTER VI

### CONCLUSION AND RECOMMENDATION

#### 6.1 Conclusion

NDEA is one pollutant whose removal only focused on the photolysis process (UV irradiator). Photocatalyst is another choice to use for the removal of NDEA. The main of this thesis is to acquire  $\text{TiO}_2/\text{SiO}_2/\text{GSs}$  composite that can be used under sunlight without installing any instrument. This composite was created using the sol-gel method then coated into a sponge as supporting material.

$\text{TiO}_2/\text{SiO}_2/\text{GSs}$  were studied at various Ti:GSs composition ratios and calcination temperatures ( $T_{\text{cal}}$ ). XRD, SEM-EDS, and BET were used to analyze the morphology of the composite. The  $\text{TiO}_2/\text{SiO}_2/\text{GSs}$  composite shows that the presence of GSs influences the layer pattern, while the EDS spectrum verifies the presence of Ti and C on the composite's surface. As the amount of GSs rises, the percentage of rutile phase propensity increases, whereas the percentage of anatase phase declines. Meanwhile, increasing  $T_{\text{cal}}$  has little influence on the rutile phase's percentage. The average crystal size increases with rising  $T_{\text{cal}}$  until 450 °C when it starts to decrease.

Furthermore, the  $\text{TiO}_2/\text{SiO}_2/\text{GSs}$  photocatalyst's ability to degrade MB under solar light is reliant on optimal factors such as the sample's crystalline phase, crystal size, and C concentration. The photocatalyst produced with a Ti:GSs ratio of 0.07 and  $T_{\text{cal}}$  at 450 °C (G0.07T450) obtains the greatest MB degrading efficiency of 97.83 % in 3 hours. The ability of reusable  $\text{TiO}_2/\text{SiO}_2/\text{GSs}$  exhibits a minor drop in efficiency after four-cycle cycles.

$\text{TiO}_2/\text{SiO}_2/\text{GSs}$  powder has an excellent ability to do photodegradation under sunlight. But practically, using photocatalyst powder has a disadvantage in terms of

separation by solutions. The coating is one option to compact  $\text{TiO}_2/\text{SiO}_2/\text{GSs}$  powder to get solid photocatalyst which can easily separate and reuse. Samples were prepared by dipping them on a sponge substrate and then drying them. The SEM image of the  $\text{TiO}_2/\text{SiO}_2/\text{GSs}$  compact shows how the photocatalyst coated the sponge fibers. The degradation of MB produced a good photocatalytic activity under solar light emission. Within 3 hours, all samples had reached their saturation points of 98-99 %. It shows how the thickness impacts degradation proportionately to the quantity of  $\text{TiO}_2/\text{SiO}_2/\text{GSs}$  coated as well as the surface area of the compact, which enhances adsorption and the photocatalytic reaction of  $\text{TiO}_2/\text{SiO}_2/\text{GSs}$  composite in the dark with 86 % adsorption. The recycling of each layer of  $\text{TiO}_2$  compact results in a degradation efficiency of 90% after three reuses. Furthermore, under solar light, the deterioration of the  $\text{TiO}_2/\text{SiO}_2/\text{GSs}$  compact on the sponge is thickness dependent. NDEA was degraded in 300 minutes using a  $\text{TiO}_2/\text{SiO}_2/\text{GSs}$  compact with a substrate thickness of 0.5 cm and degradation effectiveness of 95.52 %. This result shows that the presence of GSs in  $\text{TiO}_2$  can improve the working range of photocatalyst into sunlight range, either in powder or compacted form.  $\text{SiO}_2$  can improve the adsorption of photocatalyst in powder form while sponge substrate also can help to enhance the surface area in compacted form. This work is proven can be used in the removal of NDEA in contaminated solutions.

## 6.2 Recommendation

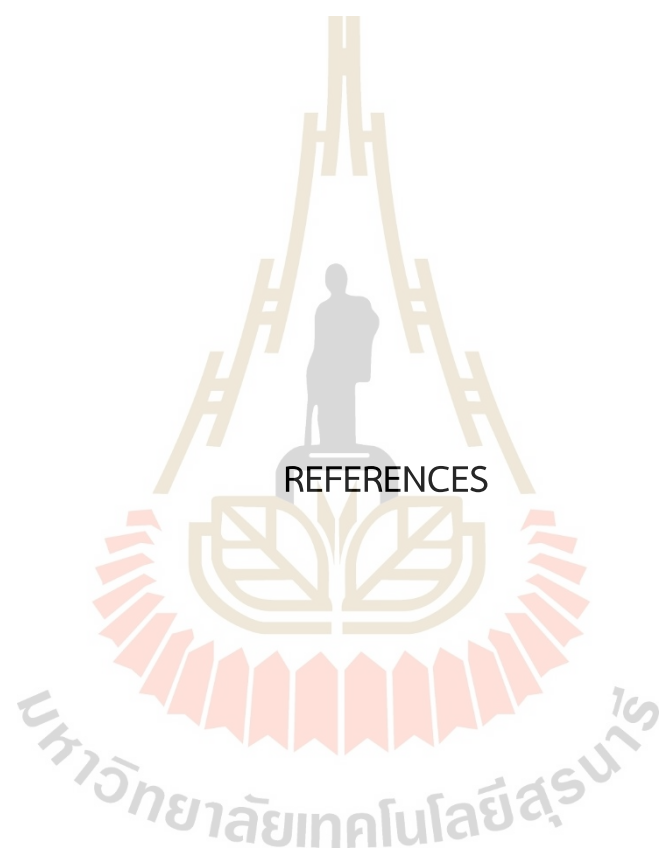
Some recommendations for future work are summarized as follows:

1. In this thesis, the optimum condition of  $\text{TiO}_2/\text{SiO}_2/\text{GSs}$  preparation by the sol-gel method has been acquired. Therefore, it would be of interest to design the prototype to produce and use it in a purification system.
2. This thesis investigated the chemical composition and morphology of  $\text{TiO}_2/\text{SiO}_2/\text{GSs}$ . It would be of great interest to further investigate the other properties of  $\text{TiO}_2/\text{SiO}_2/\text{GSs}$  photocatalyst including mechanical and electrical properties because this could be a piece of useful information for these materials.

3. The Monte Carlo program was used to investigate a photocatalyst reaction in this study. This is a preliminary model that will need to be refined to predict the photocatalytic process under the desired conditions.

4. Propose a new model that is consistent with the experimental results and can be used to better describe photocatalytic phenomena or propose a new model for this work that applies to the actual application.





REFERENCES



## REFERENCES

- Akpan, U. G., and Hameed, B. H. (2010). The Advancements in Sol-Gel Method of Doped-TiO<sub>2</sub> Photocatalysts. *Applied Catalysis A: General*, 375(1), 1–11.
- Alam, M. J., and Cameron, D. C. (2002). Preparation and Characterization of TiO<sub>2</sub> Thin Films by Sol-Gel Method. *Journal of Sol-Gel Science and Technology*, 25(2), 137–145.
- Alberici, R. M., and Jardim, W. F. (1997). Photocatalytic Destruction of VOCs in The Gas-Phase Using Titanium Dioxide. *Applied Catalysis B: Environmental*, 14(1–2), 55–68.
- Andrzejewski, P., and Nawrocki, J. (2018). N-Nitrosomethylethylamine (NMEA) and N-Nitrosodiethylamine (NDEA), Two New Potential Disinfection Byproducts; Formation During Water Disinfection with Chlorine. *Global NEST Journal*, 7(1), 17–26.
- Aravindan, V., Lee, Y.-S., Yazami, R., and Madhavi, S. (2015). TiO<sub>2</sub> Polymorphs in ‘Rocking-Chair’ Li-Ion Batteries. *Materials Today*, 18(6), 345–351.
- Au-pree, S., Narakaew, P., Thungprasert, S., Promanan, T., Chaisena, A., and Narakaew, S. (2021). Enhanced Photocatalytic Activity of C-Doped TiO<sub>2</sub> under Visible Light Irradiation: A Comparison of Corn Starch, Honey, and Polyethylene Glycol as a Carbon Sources. *Engineering Journal*, 25(1), 53–68.
- Augugliaro, V., Coluccia, S., Loddo, V., Marchese, L., Martra, G., Palmisano, L., and Schiavello, M. (1999). Photocatalytic Oxidation of Gaseous Toluene on Anatase TiO<sub>2</sub> Catalyst: Mechanistic Aspects and FT-IR Investigation. *Applied Catalysis B: Environmental*, 20(1), 15–27.
- Aziz, R., and Sopyan, I. (2009). Synthesis of TiO<sub>2</sub>SiO<sub>2</sub> Powder and Thin Film Photocatalysts by Sol-Gel Method. *Indian Journal of Chemistry Section A*,

48A, 951–957.

- Bartsch, H., and Montesano, R. (1984). Relevance of Nitrosamines to Human Cancer. *Carcinogenesis*, 5(11), 1381–1393.
- Bashiri, H., and Rafiee, M. (2016). Kinetic Monte Carlo Simulation of 2,4,6-Trichloro Phenol Ozonation in The Presence of ZnO Nanocatalyst. *Journal of Saudi Chemical Society*, 20(4), 474–479.
- Bezerra, P., Cavalcante, R., Garcia, A., Wender, H., Martines, M., Casagrande, G., Giménez, J., Marco, P., Oliveira, S., and Machulek Jr., A. (2017). Synthesis, Characterization, and Photocatalytic Activity of Pure and N-, B-, or Ag-Doped TiO<sub>2</sub>. *Journal of the Brazilian Chemical Society*. 28(9), 1788-1802.
- Bhatkhande, D. S., Pangarkar, V. G., and Beenackers, A. A. (2002). Photocatalytic Degradation for Environmental Applications - A Review. *Journal of Chemical Technology & Biotechnology*, 77(1), 102–116.
- Blanco, J., Avila, P., Bahamonde, A., Alvarez, E., Sánchez, B., and Romero, M. (1996). Photocatalytic Destruction of Toluene and Xylene at Gas Phase on a Titania-Based Monolithic Catalyst. *Catalysis Today*, 29(1–4), 437–442.
- Boonen, E., and Beeldens, A. (2014). Recent Photocatalytic Applications for Air Purification. *Belgium. Coatings*, 4(3), 553–573.
- Boonprakob, N., Chomkitichai, W., Ketwaraporn, J., Wanaek, A., Inceesungvorn, B., and Phanichphant, S. (2017). Photocatalytic Degradation of Phenol over Highly Visible-Light Active BiOI/TiO<sub>2</sub> Nanocomposite Photocatalyst. *Engineering Journal*, 21(1), 81–91.
- Breider, F., and Von Gunten, U. (2017). Quantification of Total N-Nitrosamine Concentrations in Aqueous Samples via UV-Photolysis and Chemiluminescence Detection of Nitric Oxide. *Analytical Chemistry*, 89(3), 1574–1582.
- Brownson, D. A. C., and Banks, C. E. (2014). The handbook of graphene electrochemistry. London: Springer.

- Brunauer, S., Deming, L. S., Deming, W. E., and Teller, E. (1940). On a Theory of the van der Waals Adsorption of Gases. *Journal of the American Chemical Society*, 62(7), 1723–1732.
- Brunauer, S., Emmett, P. H., and Teller, E. (1938). Adsorption of Gases in Multimolecular Layers. *Journal of the American Chemical Society*, 60(2), 309–319.
- Callahan, P. G., Stinville, J.-C., Yao, E. R., Echlin, M. P., Titus, M. S., De Graef, M., Gianola, D. S., and Pollock, T. M. (2018). Transmission Scanning Electron Microscopy: Defect Observations and Image Simulations. *Ultramicroscopy*, 186, 49–61.
- Castellote, M., and Bengtsson, N. (2011). Principles of TiO<sub>2</sub> Photocatalysis. In *Applications of Titanium Dioxide Photocatalysis to Construction Materials*. (RILEM State-of-the-Art Reports 5). Springer Publishing.
- Chemistry Libretexts. (2020). Le Chatelier's Principle. [https://chem.libretexts.org/Bookshelves/Physical\\_and\\_Theoretical\\_Chemistry\\_Textbook\\_Maps/Supplemental\\_Modules\\_\(Physical\\_and\\_Theoretical\\_Chemistry\)/Equilibria/Le\\_Chateliers\\_Principle](https://chem.libretexts.org/Bookshelves/Physical_and_Theoretical_Chemistry_Textbook_Maps/Supplemental_Modules_(Physical_and_Theoretical_Chemistry)/Equilibria/Le_Chateliers_Principle). Accessed on 29-03-2021.
- Chen, D., Chen, Y., Li, Y., and Ye, S. (2015). Preparation and Photocatalytic Properties of a Visible Light-Responsive and Magnetically Separated Photocatalyst of F-Fe<sub>2</sub>O<sub>3</sub>/SiO<sub>2</sub>/GSs/TiO<sub>2</sub>. *Micro and Nano Letters*, 10(5), 267–271.
- Dabrowski, J., Butt, J. B., and Bliss, H. (1970). Monte Carlo Simulation of a Catalytic Surface: Activity and Selectivity of Gamma;-Alumina for Dehydration. *Journal of Catalysis*, 18(3), 297–313.
- Dalton, J. ., Janes, P. ., Jones, N. ., Nicholson, J. ., Hallam, K. ., and Allen, G. . (2002). Photocatalytic Oxidation of NO<sub>x</sub> Gases Using TiO<sub>2</sub>: A Surface Spectroscopic Approach. *Environmental Pollution*, 120(2), 415–422.
- Davis, M. E., and Davis, R. J. (2003). *Fundamentals of Chemical Reaction Engineering*. McGraw-Hill Higher Education.

- De Caro, C., and Claudia, H. (2015). UV/VIS Spectrophotometry-Fundamentals and Applications. METTLER TOLEDO.
- Diebold, U. (2003). The Surface Science of Titanium Dioxide. *Surface Science Reports*, 48(5–8), 53–229.
- Do, D. D. (1998). Fundamentals of Diffusion and Adsorption in Porous Media. In *Adsorption Analysis: Equilibria and Kinetics*, 2, 337–414. Imperial College Press.
- Doll, T. E., and Frimmel, F. H. (2004). Development of Easy and Reproducible Immobilization Techniques Using TiO<sub>2</sub> for Photocatalytic Degradation of Aquatic Pollutants. *Acta Hydrochimica et Hydrobiologica*, 32(3), 201–213.
- Dutrow, B. L., and Clark, C. M. (2016). X-ray Powder Diffraction (XRD). *Integrating Research and Education*. [http://serc.carleton.edu/research\\_education/geochemsheets/techniques/XRD.html](http://serc.carleton.edu/research_education/geochemsheets/techniques/XRD.html).
- Eiceman, G. A. (2006). Instrumentation of Gas Chromatography. *Encyclopedia of Analytical Chemistry*. John Wiley & Sons, Ltd.
- Emerson. (2012). Emerson Process Management. [http://www2.emersonprocess.com/siteadmincenter/PMDanalyzerDocuments/DAN\\_AN\\_42-NGC-AN-OG-FUNDAMENTALS.pdf](http://www2.emersonprocess.com/siteadmincenter/PMDanalyzerDocuments/DAN_AN_42-NGC-AN-OG-FUNDAMENTALS.pdf).
- Eshaghi, A., Mozaffarinia, R., Pakshir, M., and Eshaghi, A. (2011). Photocatalytic Properties of TiO<sub>2</sub> Sol-Gel Modified Nanocomposite Films. *Ceramics International*, 37(1), 327–331.
- French, A. P., and Taylor, E. F. (1978). An Introduction to Quantum Physics. W. W. Norton & Company Inc.
- Fujishima, A., and Honda, K. (1972). Electrochemical Photolysis of Water at a Semiconductor Electrode. *Nature*, 238(5358), 37–38.
- Gallik, S. (2011). Spectrophotometry. Cell Biology OLM. 4. [http://stevegallik.org/cellbiologyolm\\_spectrophotometry.html](http://stevegallik.org/cellbiologyolm_spectrophotometry.html). Accessed on

7-5-2021

- Greenwood, N. N., and Earnshaw, A. B. T. (1997). 21-Titanium, Zirconium, and Hafnium. *Chemistry of The Elements*, 2, 954–975. Reed Educational and Professional Publishing Ltd.
- Guo, Y., Li, H., Ma, W., Shi, W., Zhu, Y., and Choi, W. (2020). Photocatalytic Activity Enhanced Via Surface Hybridization. *Carbon Energy*, 2(3), 308–349.
- Hager, S., and Bauer, R. (1999). Heterogeneous Photocatalytic Oxidation of Organics for Air Purification by Near UV Irradiated Titanium Dioxide. *Chemosphere*, 38(7), 1549–1559.
- Haider, A., Jameel, Z. N., and Taha, Y. (2015). Synthesis and Characterization of TiO<sub>2</sub> Nanoparticles via Sol-Gel Method by Pulse Laser Ablation. *Engineering and Technology Journal*, 33.
- Henry, D. (2016). Integrating Research and Education. [http://serc.carleton.edu/research\\_education/geochemsheets/electroninteractions.html](http://serc.carleton.edu/research_education/geochemsheets/electroninteractions.html). Accessed on 3-8-2018.
- Hernandez, R., Elizalde, E. A., Domínguez, A., Olvera-Rodríguez, I., Esquivel, K., and Guzman, C. (2016). Photoelectrocatalytic Degradation of Methyl Red Dye Using Au Doped TiO<sub>2</sub> Photocatalyst. 12th *Congreso Internacional de Ingeniería (CONIIN)*, 1–5.
- Hobbs, L. W., Jesurum, C. E., Pulim, V., and Berger, B. (1998). Local Topology of Silica Networks. *Philosophical Magazine A*, 78(3), 679–711.
- Holsgrove, K. M. (2017). Transmission Electron Microscopy Study of Domains in Ferroelectrics. Queen's University Belfast.
- Hossain, M. F., and Hossein, M. T. (2015). Preparation of Hexagonal Zinc Oxide Nanorods by Uncovered Hydrothermal Method on Seedless Glass Substrate. 2015 *International Conference on Electrical Engineering and Information Communication Technology (ICEEICT)*, 1–4.

- Ibhadon, A., and Fitzpatrick, P. (2013). Heterogeneous Photocatalysis: Recent Advances and Applications. *Catalysts*, 3(1), 189–218.
- Jain, A., and Vaya, D. (2017). Photocatalytic Activity of TiO<sub>2</sub> Nanomaterial. *Journal of the Chilean Chemical Society*, 62(4), 3683–3690.
- Kang, X., Liu, S., Dai, Z., He, Y., Song, X., and Tan, Z. (2019). Titanium Dioxide: From Engineering to Applications. *Catalysts*, 9(2), 191.
- Khataee, A., and Mansoori, G. A. (2011). Nanostructured Titanium Dioxide Materials. World Scientific.
- Klondon, R., Junpirom, S., and Mongkolkachit, C. (2016). Degradation of Methylene Blue in Suspended-TiO<sub>2</sub> Solution by Photocatalysis.
- Kovacic, M., Kopicic, N., Kusic, H., Stangar, U. L., Dionysiou, D. D., and Bozic, A. L. (2018). Reactivation and Reuse of TiO<sub>2</sub>-SnS<sub>2</sub> Composite Catalyst for Solar-Driven Water Treatment. *Environmental Science and Pollution Research*, 25(3), 2538–2551.
- Krumeich, F. (2009). Properties of Electrons, Their Interactions with Matter and Applications in Electron Microscopy. <http://www.microscopy.ethz.ch/downloads/Interactions.pdf>. Accessed on 4-6-2018.
- Kumar, K. V., Porkodi, K., and Rocha, F. (2008). Langmuir–Hinshelwood Kinetics – A Theoretical Study. *Catalysis Communications*, 9(1), 82–84.
- Kumar, S. G., and Devi, L. G. (2011). Review on Modified TiO<sub>2</sub> Photocatalysis under UV/Visible Light: Selected Results and Related Mechanisms on Interfacial Charge Carrier Transfer Dynamics. *Journal of Physical Chemistry A*, 115(46), 13211–13241.
- Langmuir, I. (1916). The Constitution and Fundamental Properties of Solids and Liquids. Part I. Solids. *Journal of the American Chemical Society*, 38(11), 2221–2295.
- Larumbe, S., Monge, M., & Gomez-Polo, C. (2014). Magnetically Separable

- Photocatalyst Fe<sub>3</sub>O<sub>4</sub>/SiO<sub>2</sub>/N-TiO<sub>2</sub> Hybrid Nanostructures. *IEEE Transactions on Magnetics*, 50(11), 1–4.
- Lavand, A. B., and Malghe, Y. S. (2015). Visible Light Photocatalytic Degradation of 4-Chlorophenol Using C/ZnO/CdS Nanocomposite. *Journal of Saudi Chemical Society*, 19(5), 471–478.
- Lee, S.-Y., and Park, S.-J. (2013). TiO<sub>2</sub> Photocatalyst for Water Treatment Applications. *Journal of Industrial and Engineering Chemistry*, 19(6), 1761–1769.
- Li, L. (2005). Structural Analysis of Cylindrical Particles by Small Angle X-ray Scattering. Universität Bayreuth. <https://epub.uni-bayreuth.de/874/1/diss.pdf>. Accessed on 7-8-2018.
- Li, X., He, X., Dong, Y., Jia, L., and He, Q. (2016). Analysis of N-Nitrosodiethylamine by Ion Chromatography Coupled with UV Photolysis Pretreatment. *Journal of Food and Drug Analysis*, 24(2), 311–315.
- Lin, T., Hsu, W., Lee, C., Ding, Y., Huang, S., Lan, W., and Wang, M. (2015). Photocatalytic Study of Silver and Bismuth Codoped Zinc Oxide by Spray Pyrolysis. *2015 International Symposium on Next-Generation Electronics (ISNE)*, 1–2.
- Lowell, S., Shields, J. E., Thomas, M. A., and Thommes, M. (2004). Surface Area Analysis from the Langmuir and BET Theories. In *Characterization of Porous Solids and Powders: Surface Area, Pore Size and Density*, 1, 58–81. Springer.
- Luan, F., Zhang, R., Zhao, C., Yao, X., Liu, M., Hu, Z., and Fan, B. (2005). Classification of The Carcinogenicity of N-Nitroso Compounds Based on Support Vector Machines and Linear Discriminant Analysis. *Chemical Research in Toxicology*, 18(2), 198–203.
- Martinez, I. G. G. (2011). Synthesis and Characterization of Boron- and Aluminum-Based Nanostructures. Technische Universität Dresden.
- Matthews, R. W. (1987). Photooxidation of Organic Impurities in Water Using Thin



- Films of Titanium Dioxide. *The Journal of Physical Chemistry*, 91(12), 3328–3333.
- Messenger, R. A., and Abtahi, A. (2010). Photovoltaic Systems Engineering, Third Edition. CRC Press. <https://books.google.co.th/books?id=JxLOBQAAQBAJ>. Accessed on 8-6-2019.
- Meyer, J. C., Geim, A. K., Katsnelson, M. I., Novoselov, K. S., Booth, T. J., and Roth, S. (2007). The structure of Suspended Graphene Sheets. *Nature*, 446(7131), 60–63.
- Moma, J., and Baloyi, J. (2019). Modified Titanium Dioxide for Photocatalytic Applications. In *Photocatalysts-Applications and Attributes*. IntechOpen.
- Moniz, S. J. A., Shevlin, S. A., Martin, D. J., Guo, Z.-X., and Tang, J. (2015). Visible-Light-Driven Heterojunction Photocatalysts for Water Splitting – A Critical Review. *Energy & Environmental Science*, 8(3), 731–759.
- Moura, L. M. D. E., and Suyanto, A. H. (2004). Fundamental of Photocatalytic Water Splitting by Visible Light. In *Chemistry of Catalytic System 2: Photocatalysis*. Wiley Online.
- Muller, N., Nowack, B., and Saari, J. (2010). Photocatalysis for Water Treatment. *Journal of Environmental Science, Computer Science and Engineering & Technology*, 7(3), 478-484.
- Najafi, M., Kermanpur, A., Rahimipour, M. R., and Najafizadeh, A. (2017). Effect of TiO<sub>2</sub> Morphology on Structure of TiO<sub>2</sub>-Graphene Oxide Nanocomposite Synthesized Via a One-Step Hydrothermal Method. *Journal of Alloys and Compounds*, 722, 272–277.
- nanoComposix. (2021). Silica Physical Properties. <http://www.pslc.ws/macrog/glass.htm>. Accessed on 29-11-2021.
- National Aeronautics and Space Administration Goddard Space Flight Center. (2013). <https://imagine.gsfc.nasa.gov/science/toolbox/emspectrum1.html>. Accessed on 20-10.

- National Center for Biotechnology Information. (2021). PubChem Compound Summary for CID 5921, N-Nitrosodiethylamine. <https://pubchem.ncbi.nlm.nih.gov/compound/5921>.
- Negishi, N., Sugawara, M., Miyazaki, Y., Hiram, Y., and Koura, S. (2019). Effect of Dissolved Silica on Photocatalytic Water Purification with a TiO<sub>2</sub> Ceramic Catalyst. *Water Research*, 150, 40–46.
- Novoselov, K. S., Geim, A. K., Morozov, S. V., Jiang, D., Katsnelson, M. I., Grigorieva, I. V., Dubonos, S. V., and Firsov, A. A. (2005). Two-Dimensional Gas of Massless Dirac Fermions in Graphene. *Nature*, 438(7065), 197–200.
- Ola, O., and Maroto-Valer, M. M. (2015). Review of Material Design and Reactor Engineering on TiO<sub>2</sub> Photocatalysis for CO<sub>2</sub> Reduction. *Journal of Photochemistry and Photobiology C: Photochemistry Reviews*, 24, 16–42.
- Pal, M., Rakshit, R., Mandal, M., and Mandal, K. (2014). Surface Modification of  $\alpha$ -Fe<sub>2</sub>O<sub>3</sub> Nanoparticles to Develop as Intrinsic Photoluminescent Probe and Unprecedented Photocatalyst. *IEEE Transactions on Magnetics*, 50(11), 1–4.
- Parida, S. K., Dash, S., Patel, S., and Mishra, B. K. (2006). Adsorption of organic molecules on silica surface. *Advances in Colloid and Interface Science*, 121(1–3), 77–110.
- Paz, Y., and Heller, A. (1997). Photo-Oxidatively Self-Cleaning Transparent Titanium Dioxide Films on Soda-Lime Glass: The Deleterious Effect of Sodium Contamination and Its Prevention. *Journal of Materials Research*, 12(10), 2759–2766.
- Pennington, A. M. (2015). Increased Visible-Light Photocatalytic Activity of TiO<sub>2</sub> Via Bandgap Manipulation [Rutgers University].
- Qing, L. (2012). Kinetic Mechanism of Photo-catalytic Oxidation for Soluble Methylene Blue by Iron-Doped TiO<sub>2</sub>. *2012 International Conference on Computer Distributed Control and Intelligent Environmental Monitoring*, 390–392.
- Ramirez-Cuesta, A. J., Bennett, R. A., Stone, P., Mitchell, P. C. H., and Bowker, M.

- (2001). STM Investigation and Monte-Carlo Modeling of Spillover in a Supported Metal Catalyst. *Journal of Molecular Catalysis A: Chemical*, 167(1-2), 171-179.
- Raychaudhuri, S. (2008). Introduction to Monte Carlo Simulation. *2008 Winter Simulation Conference*, 91-100.
- Ribao, P., Rivero, M. J., and Ortiz, I. (2018). Enhanced Photocatalytic Activity Using GO/TiO<sub>2</sub> Catalyst for The Removal of DCA Solutions. *Environmental Science and Pollution Research*, 25(35), 34893-34902.
- Rocha, C. G., Rummeli, M. H., Ibrahin, I., Sevincli, H., Kuntsmann, J., Kuntsmann, J., Bachmatiuk, A., Potschke, M., Li, W., Makharza, S. A. M., Roche, S., Buchner, B., and Cuniberti, G. (2016). Tailoring the Physical Properties of Graphene. (Eds.), *Graphene; Synthesis and Applications*, 1. CRC Press.
- Rouessac, F., and Rouessac, A. (2013). *Chemical Analysis: Modern Instrumentation Methods and Techniques*. John Wiley & Sons.
- Rufai, Y., Chandren, S., and Basar, N. (2020). Influence of Solvents' Polarity on the Physicochemical Properties and Photocatalytic Activity of Titania Synthesized Using Deinbollia Pinnata Leaves. *Frontiers in Chemistry*, 8.
- Rukai, T., and Babita, A. (2013). Review Article Transmission Electron Microscopy-An Overview. *International Research Journal for Inventions in Pharmaceutical Sciences*, 1(2), 1-7.
- S., P. M. (2014). X-ray Diffraction Analysis Principle Instrument and Applications. [https://www.researchgate.net/publication/260659249\\_X-ray\\_Diffraction\\_Analysis\\_Principle\\_Instrument\\_and\\_Applications](https://www.researchgate.net/publication/260659249_X-ray_Diffraction_Analysis_Principle_Instrument_and_Applications). Accessed on 9-8-2018.
- Santa Cruz Biotechnology, I. (2010). N-Nitrosodiethylamine. <https://datasheets.scbt.com/sc-257861.pdf>. Accessed on 9-8-2018.
- Schneider, J., Matsuoka, M., Takeuchi, M., Zhang, J., Horiuchi, Y., Anpo, M., and Bahnemann, D. W. (2014). Understanding TiO<sub>2</sub> Photocatalysis: Mechanisms and Materials. *Chemical Reviews*, 114(19), 9919-9986.

- Sclafani, A., and Herrmann, J. M. (1996). Comparison of The Photoelectronic and Photocatalytic Activities of Various Anatase and Rutile Forms of Titania in Pure Liquid Organic Phases and in Aqueous Solutions. *The Journal of Physical Chemistry*, 100(32), 13655–13661.
- Shan, A. Y., Ghazi, T. I. M., and Rashid, S. A. (2010). Immobilisation of Titanium Dioxide onto Supporting Materials in Heterogeneous Photocatalysis: A Review. *Applied Catalysis A: General*, 389(1–2), 1–8.
- Shang, C., Xu, B., Lei, X., Yu, S., Chen, D., Wu, M., Sun, B., Liu, G., and Ouyang, C. (2018). Bandgap Tuning in MoSSe Bilayers: Synergistic Effects of Dipole Moment and Interlayer Distance. *Physical Chemistry Chemical Physics*, 20(32), 20919–20926.
- Shen, S., Burton, M., Jobson, B., & Haselbach, L. (2012). Pervious Concrete with Titanium Dioxide as a Photocatalyst Compound for a Greener Urban Road Environment. *Construction and Building Materials*, 35, 874–883.
- Sierra, C. F. E. (2019). Fundamentals of Transmission Electron Microscopy, The Technique with The Best Resolution in The World. 1–6.
- Sing, K. S. W. (1985). Reporting Physisorption Data for Gas/Solid Systems with Special Reference to The Determination of Surface Area and Porosity (Recommendations 1984). *Pure and Applied Chemistry*, 57(4), 603–619.
- Singh, A. K. (2016). Experimental Methodologies for The Characterization of Nanoparticles. in *Engineered Nanoparticles*. Elsevier.
- Singh, R., and Dutta, S. (2018). Synthesis and Characterization of Solar Photoactive TiO<sub>2</sub> Nanoparticles with Enhanced Structural and Optical Properties. *Advanced Powder Technology*, 29(2), 211–219.
- Swinehart, D. F. (1962). The Beer-Lambert Law. *Journal of Chemical Education*, 39(7), 333.
- Tanaka, A., Hisanaga, A., Inamasu, T., Hirata, M., and Ishinishi, N. (1988). A Comparison of The Carcinogenicity of N-Nitrosodiethylamine and N-

- Nitrosodimethylamine after Intratracheal Instillation into Syrian Golden Hamsters. *Food and Chemical Toxicology*, 26(10), 847–850.
- Tang, B., Chen, H., Peng, H., Wang, Z., and Huang, W. (2018). Graphene Modified TiO<sub>2</sub> Composite Photocatalysts: Mechanism, Progress and Perspective. *Nanomaterials*, 8(2), 105.
- Tayade, R. J., Natarajan, T. S., and Bajaj, H. C. (2009). Photocatalytic Degradation of Methylene Blue Dye Using Ultraviolet Light Emitting Diodes. *Industrial & Engineering Chemistry Research*, 48(23), 10262–10267.
- Tricker, A. R., Ditrich, C., and Preussmann, R. (1991). N -Nitroso Compounds in Cigarette Tobacco and Their Occurrence in Mainstream Tobacco Smoke. *Carcinogenesis*, 12(2), 257–261.
- Turchi, C. S., and Ollis, D. F. (1990). Photocatalytic Degradation of Organic Water Contaminants: Mechanisms Involving Hydroxyl Radical Attack. *Journal of Catalysis*, 122(1), 178–192.
- van Holde, K. E., Johnson, W. C., and Ho, P. S. (2006). Principles of Physical Biochemistry. Pearson Education, Inc.
- Verna, L. (1996). N-Nitrosodiethylamine Mechanistic Data and Risk Assessment: Bioactivation, DNA-Adduct Formation, Mutagenicity, and Tumor Initiation. *Pharmacology & Therapeutics*, 71(1–2), 57–81.
- Wainright, T. (1986). The Chemistry of Nitrosamine Formation: Relevance to Malting and Brewing. *Journal of the Institute of Brewing*, 92, 49–64.
- Warner, J. H., Bachmatiuk, A., Schäffel, F., and Rummeli, M. H. (2013). Chapter 1 - Introduction. In *Graphene; Fundamentals and emergent applications*, 1, 1–4). Elsevier.
- Weidenthaler, C. (2011). Pitfalls in the Characterization of Nanoporous and Nanosized Materials. *Nanoscale*, 3(3), 792.
- WHO. (2008). N -Nitrosodimethylamine in Drinking-water. In *Background document for*

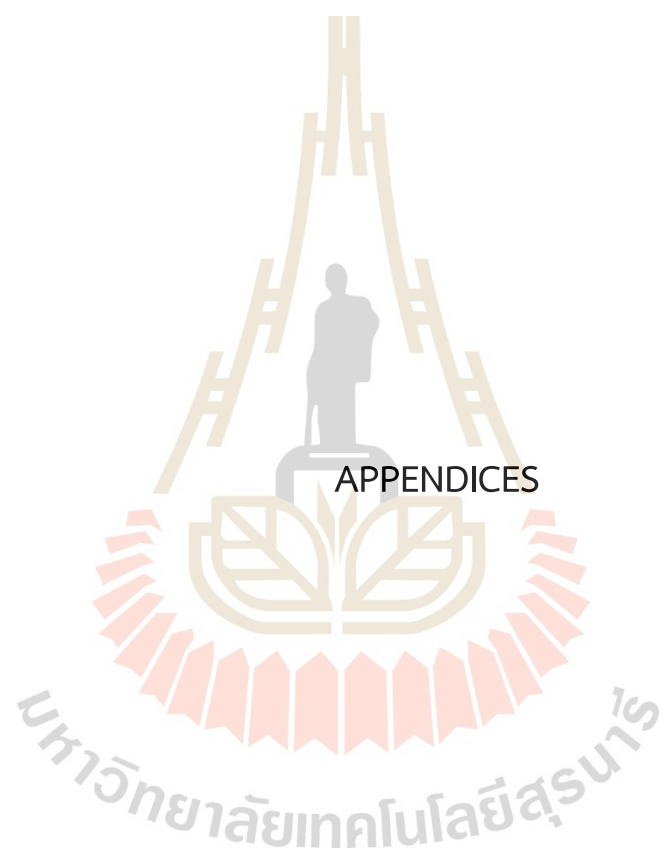
*development of WHO Guidelines for Drinking-water Quality*. World Health Organization.

Zhang, H., Li, F., Jia, Q., & Ye, G. (2008). Preparation of Titanium Carbide Powders by Sol-Gel and Microwave Carbothermal Reduction Methods at Low Temperature. *Journal of Sol-Gel Science and Technology*, 46(2), 217–222.

Zhang, Y., Tang, Z.-R., Fu, X., and Xu, Y.-J. (2010). TiO<sub>2</sub>-Graphene Nanocomposites for Gas-Phase Photocatalytic Degradation of Volatile Aromatic Pollutant: Is TiO<sub>2</sub>-Graphene Truly Different from Other TiO<sub>2</sub>-Carbon Composite Materials? *ACS Nano*, 4(12), 7303–7314.

Zhou, L., Yan, S., Tian, B., Zhang, J., and Anpo, M. (2006). Preparation of TiO<sub>2</sub>-SiO<sub>2</sub> Film with High Photocatalytic Activity on PET Substrate. *Materials Letters*, 60(3), 396–399.

Zhu, S., and Wang, D. (2017). Photocatalysis: Basic Principles, Diverse Forms of Implementations and Emerging Scientific Opportunities. *Advanced Energy Materials*, 7(23), 1700841.



APPENDICES



## APPENDIX A

RAW DATA OF ANALYSIS OF TiO<sub>2</sub>/SiO<sub>2</sub>/GSs POWDER

## A.1 Data XRD

Equation (A.1) and (A.2) was used for analyzing XRD data.

$$D = \frac{\kappa\lambda}{\beta \cos\theta} \quad (\text{A.1})$$

D is the crystal size (nm),  $\kappa = 0.89$ ,  $\lambda = 0.154178$  nm,  $\beta$  is the full width at half maximum (FWHM), and  $\theta$  is the diffraction angle at peak  $2\theta$ .

$$\% \text{ of anatase phase} = \frac{100}{1 + (I_R / 0.791 I_A)} \quad (\text{A.2})$$

$I_R$  and  $I_A$  are the strongest intensities of the rutile and anatase phases, respectively.

Table A.1 Data analysis XRD.

GSs	Tcal (°C)	Index	FWHM	Peak ( $2\theta$ )	Intensity	Anatase vs Rutile (%)	D (nm)	$D_{\text{avg}}$ (nm)
		1	1.061	25.314	1724.8	90.622	8.02	
OG	450	2						
		3	0.194	27.435	141.014	9.378	44	26.01

Table A.2 Data analysis XRD (cont).

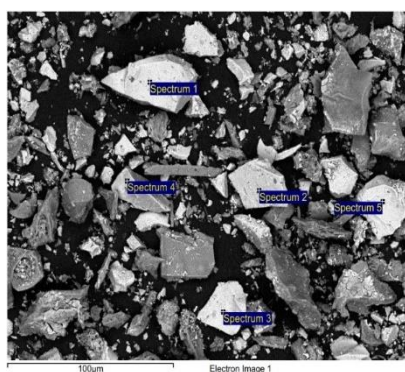
		1	0.817	25.374	1999.98	86.922	10.42	
0.04G	450	2	0.134	26.566	2144.32		63.66	
		3	0.29	27.475	237.718	13.078	29.49	34.523
	400	1	0.865	25.94	400.585	100	9.85	
		2	0.158	27.051	1463.81		54.05	31.95
		1	0.771	25.617	1652.43	83.821	11.05	
0.07G	450	2	0.135	26.748	3027.31		62.99	
		3	0.298	27.657	251.978	16.179	28.73	34.257
		1	0.596	25.738	251.091	50.745	14.3	
	500	2	0.274	27.01	1278.1		31.2	
		3	0.312	27.859	192.541	49.255	27.39	24.297
		1	0.701	25.698	766.774	83.785	12.15	
0.14G	450	2	0.147	26.93	6068.21		57.9	41.28
		3	0.159	27.839	117.23	16.215	53.79	

Note. T<sub>cal</sub> 1, 2, and 3 are Anatase, Graphene, and Rutile respectively

## A.2 Data EDS

Table A.3 Data analysis EDS of TiO<sub>2</sub>/SiO<sub>2</sub>/GSs.

G0T450



G0.04T450

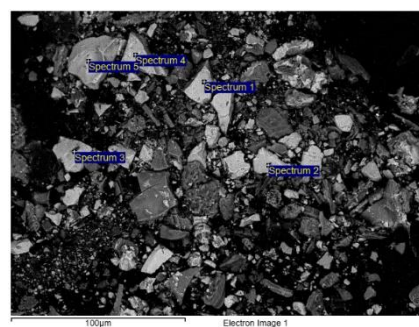
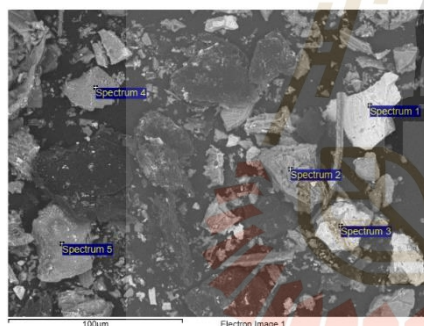


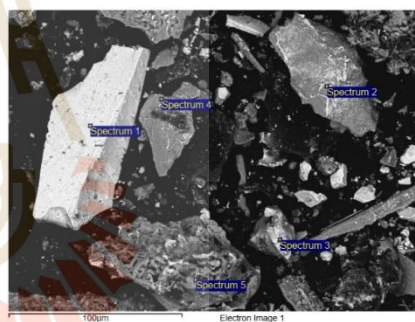
Table A.4 Data analysis EDS of TiO<sub>2</sub>/SiO<sub>2</sub>/GSs (cont).

Spectrum	C	O	Si	Ti	Spectrum	C	O	Si	Ti
1	2.03	45.61		52.37	1	2.61	42.2		55.19
2	3.01	55.61	0.46	40.92	2	4.44	55.78	11.9	27.89
3	5.85	53.34	0.62	40.19	3	3.34	48.7	0.42	47.54
4	3.57	56.07	0.86	39.51	4	7.41	50.89	0.43	41.28
5	2.05	46.31	0.63	51.02	5	6.65	42.78	0.7	49.87
Min	2.03	45.61	0.46	39.51	Max	7.41	55.78	11.9	55.19
Max	5.85	56.07	0.86	52.37	Min	2.61	42.2	0.42	27.89
Mean	3.3	51.39	0.64	44.8	Mean	4.89	48.07	3.36	44.35
Stdv	1.57	5.07	0.16	6.33	Stdv	2.08	5.71	5.69	10.47

G0.07T400



G0.07T450



Spectrum	C	O	Si	Ti	Spectrum	C	O	Si	Ti
1	8.55	34.77	48.15		1	8.2	23.52	3	18.3
2	1.86	40.3	55.16		2				
3	4.27	42.95	48.48		3	6.54	22.77	1.33	69.35
4	4.78	45.2	0.74	49.29	4				
5		36.9	32.39		5				
Max	8.55	45.2	55.16	49.29	Max	8.2	23.52	3	69.35
Min	1.86	34.77	0.74	49.29	Min	6.54	22.77	1.33	18.3
Mean	4.86	40.02	36.98	49.29	Mean	7.37	23.15	2.17	43.83
Stdv	2.77	4.26	21.92		Stdv	1.17	0.53	1.18	36.1

Table A.5 Data analysis EDS of TiO<sub>2</sub>/SiO<sub>2</sub>/GSs (cont).

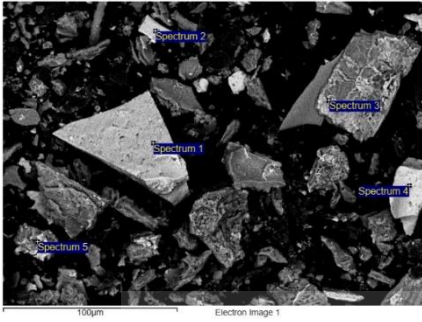
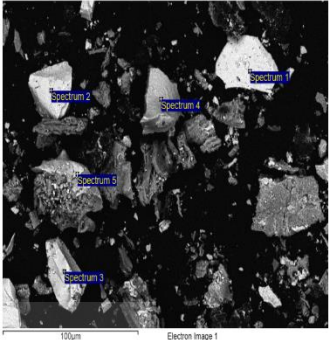
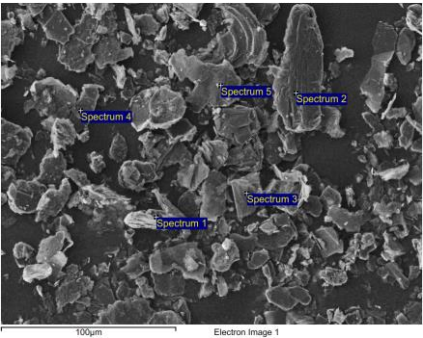
G0.07T500					G0.14T450				
									
Spectrum	C	O	Si	Ti	Spectrum	C	O	Si	Ti
1		41.79	47.45		1	13.68	44.9	0.5	40.91
2	2.19	35.14	1.09	61.58	2	8.14	53.11	0.78	37.97
3	5.29	17.93	48.97	27.81	3	5.5	38.01	1.44	55.04
4	6.9	58.13	26.23		4	6.98	29.53	0.64	62.85
5	5.31	55.02	36.37		5	12.96	48.46	0.42	38.16
Max	6.9	58.13	48.97	61.58	Max	13.68	53.11	1.44	62.85
Min	2.19	17.93	1.09	27.81	Min	5.5	29.53	0.42	37.97
Mean	4.92	41.6	32.02	44.7	Mean	9.45	42.8	0.76	46.99
Stdv	1.97	16.24	19.59	23.88	Stdv	3.66	9.24	0.41	11.32

Table A.6 Data analysis EDS of GSs.

Graphene		
		
Spectrum	C	O

**Table A.7** Data analysis EDS of GSs (cont).

1	98.52	1.48
2	100	
3	99.37	0.63
4	100	
5	99.3	0.7
Max	100	1.48
Min	98.52	0.63
Mean	99.44	0.94
Stdv	0.61	0.47

### A.3 Data BET

**Table A.8** Data analysis BET of TiO<sub>2</sub>/SiO<sub>2</sub>/GSs

Sample	Specific surface area (m <sup>2</sup> /g)	Mean pore D (nm)	Vm (cm <sup>3</sup> /g)	Total pore volume (cm <sup>3</sup> /g)
G0T450	1.28E+02	8.5563	29.464	0.274
G0.04T450	1.38E+02	7.5975	31.767	0.263
G0.07T400	1.28E+02	8.3557	23.251	0.280
G0.07T450	1.39E+02	8.4441	32.012	0.294
G0.07T500	1.26E+02	8.1570	23.052	0.269
G0.14T450	1.46E+02	9.0459	33.629	0.297

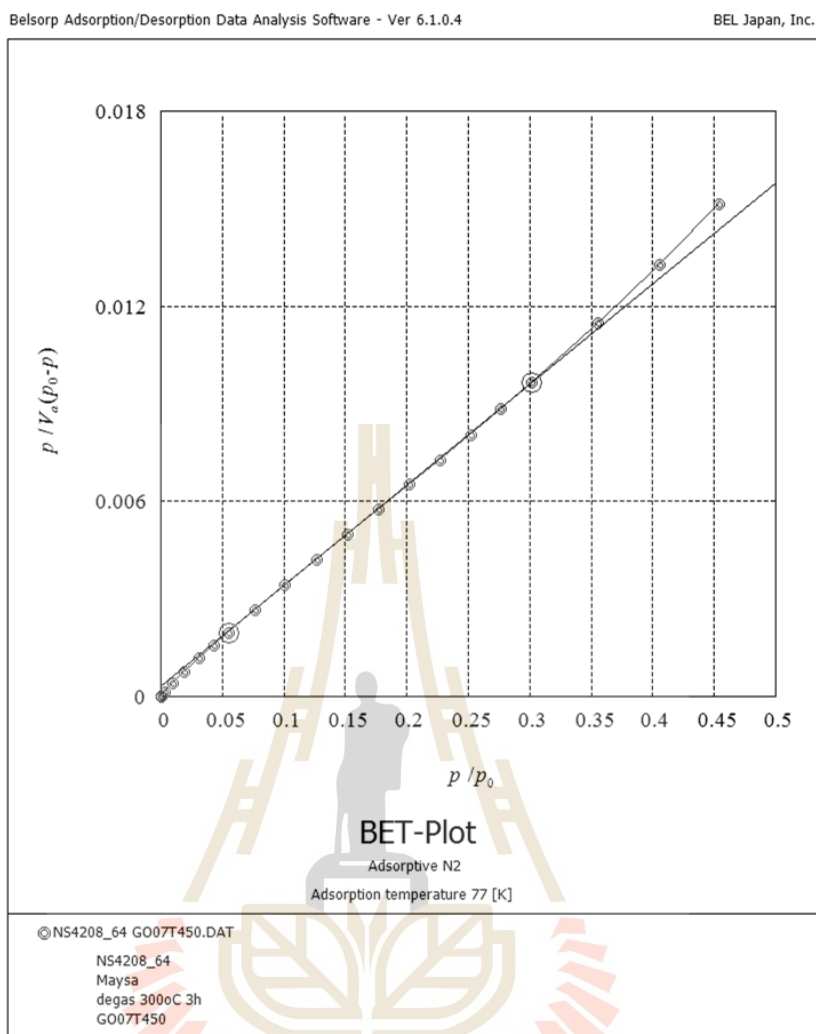


Figure A.1 BET plot of  $\text{TiO}_2/\text{SiO}_2/\text{GSs}$

#### A.4 Data MB degradation

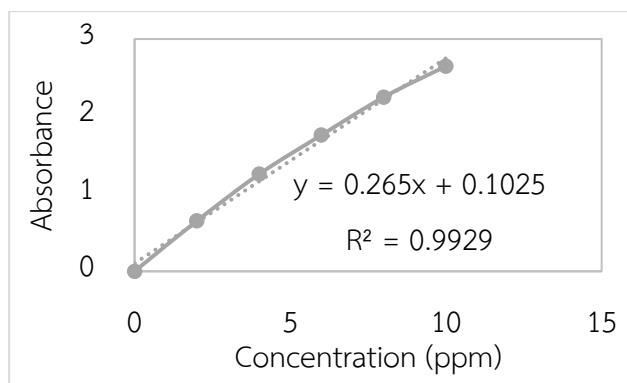


Figure A.2 Calibration standard curve of Methylene Blue.

#### A.4.1 Initial Condition

Table A.9 Data absorbance of MB for the initial condition.

		Sun						
Weight (g)		0	30	60	90	120	150	180
2 ppm of MB	0.05	0.726	0.269	0.246	0.239	0.267	0.218	0.217
	0.1	0.726	0.213	0.159	0.146	0.123	0.115	0.116
	0.15	0.726	0.207	0.204	0.142	0.176	0.144	0.161
Concentration (ppm)								
1 g of MB	1	0.377	0.145	0.12	0.107	0.104	0.102	0.103
	2	0.726	0.213	0.159	0.146	0.123	0.115	0.116
	4	1.226	0.605	0.532	0.589	0.642	0.601	0.638

Equation (A.3) is used for calculating the concentration of MB

$$C = \frac{(A-b)}{x}$$

(A.3)



A is absorbance,  $x=0.265$ , and  $b=0.1025$

**Table A.10** Concentration of MB for each time frame.

Weight (g)		Concentration (ppm)						
		0	30	60	90	120	150	180
2 ppm of MB	0.05	2.352	0.628	0.541	0.515	0.620	0.435	0.432
	0.1	2.352	0.417	0.213	0.164	0.077	0.047	0.050
	0.15	2.352	0.394	0.383	0.149	0.277	0.156	0.220
		Concentration (ppm)						
1 g of MB	1	1.036	0.160	0.066	0.017	0.005	0.000	0.001
	2	2.352	0.4170	0.2132	0.1642	0.0774	0.0472	0.0509
	4	4.240	1.8962	1.6208	1.8358	2.0358	1.8811	2.0208

Equation (A.4) is used for calculating  $\eta$  degradation (%).

$$\eta = \frac{C_0 - C}{C_0} \times 100\% \quad (\text{A.4})$$

$C_0$  is the initial concentration (at  $t=0$ ) and  $C$  is the concentration at  $t$  time.

**Table A.11**  $\eta$  degradation (%) of MB

Weight (g)		$\eta$ degradation (%)						
		0	30	60	90	120	150	180
2 ppm of MB	0.05	0	73.30	76.98	78.11	73.62	81.48	81.64
	0.1	0	82.28	90.94	93.02	96.71	98.00	97.83
	0.15	0	83.24	83.72	93.66	88.21	93.34	90.62

Table A.12  $\eta$  degradation (%) of MB (cont).

Concentration (ppm)								
1 g of MB	1	0	84.52	93.62	98.36	99.45	99.99	99.82
	2	0	82.28	90.94	93.02	96.71	98.00	97.83
	4	0	55.27	61.77	56.70	51.98	55.63	52.34

Equations (A.3) and (A.4) later be used for degradation MB.

#### A.4.2 Degradation of MB

Table A.13 Data of degradation of MB in dark condition

		Absorbance						
G	Tcal	0	30	60	90	120	150	180
0	450	0.726	0.542	0.515	0.38	0.278	0.28	0.277
0.04	450	0.726	0.545	0.41	0.362	0.267	0.264	0.229
	400	0.726	0.513	0.486	0.4	0.307	0.192	0.181
0.07	450	0.726	0.555	0.29	0.247	0.201	0.18	0.189
	500	0.726	0.637	0.524	0.525	0.432	0.424	0.421
0.14	450	0.726	0.664	0.544	0.507	0.502	0.462	0.455

		Concentration						
G	Tcal	0	30	60	90	120	150	180
0	450	2.3528	1.6585	1.5566	1.0472	0.6623	0.6698	0.6585
0.04	450	2.3528	1.6698	1.1604	0.9792	0.6208	0.6094	0.4774
	400	2.3528	1.5491	1.4472	1.1226	0.7717	0.3377	0.2962
0.07	450	2.3528	1.7075	0.7075	0.5453	0.3717	0.2925	0.3264
	500	2.3528	2.017	1.5906	1.5943	1.2434	1.2132	1.2019

**Table A.14** Data of degradation of MB in dark condition (cont).

η decolorization								
G	Tcal	0	30	60	90	120	150	180
0.14	450	2.3528	2.1189	1.666	1.5264	1.5075	1.3566	1.3302
0	450	0	29.51	33.84	55.49	71.85	71.53	72.01
0.04	450	0	29.03	50.68	58.38	73.62	74.1	79.71
	400	0	34.16	38.49	52.29	67.2	85.65	87.41
0.07	450	0	27.43	69.93	76.82	84.2	87.57	86.13
	500	0	14.27	32.4	32.24	47.15	48.44	48.92
0.14	450	0	9.94	29.19	35.12	35.93	42.34	43.46

**Table A.15** Data of degradation of MB under sunlight

Absorbance								
G	Tcal	0	30	60	90	120	150	180
0	450	0.726	0.324	0.247	0.247	0.19	0.17	0.174
0.04	450	0.726	0.308	0.19	0.193	0.19	0.171	0.182
	400	0.726	0.346	0.322	0.266	0.198	0.189	0.131
0.07	450	0.726	0.213	0.159	0.146	0.123	0.115	0.116
	500	0.726	0.404	0.207	0.187	0.177	0.149	0.141
0.14	450	0.726	0.42	0.424	0.293	0.261	0.218	0.224
Concentration								
G	Tcal	0	30	60	90	120	150	180
0	450	2.3528	0.8358	0.5453	0.5453	0.3302	0.2547	0.2698
0.04	450	2.3528	0.7755	0.3302	0.3415	0.3302	0.2585	0.3
	400	2.3528	0.9189	0.8283	0.617	0.3604	0.3264	0.1075
0.07	450	2.3528	0.417	0.2132	0.1642	0.0774	0.0472	0.0509

**Table A.16** Data of degradation of MB under sunlight (cont).

	500	2.3528	1.1377	0.3943	0.3189	0.2811	0.1755	0.1453
	450	2.3528	1.1981	1.2132	0.7189	0.5981	0.4358	0.4585
<b><math>\eta</math> decolorization</b>								
<b>G</b>	<b>Tcal</b>	<b>0</b>	<b>30</b>	<b>60</b>	<b>90</b>	<b>120</b>	<b>150</b>	<b>180</b>
0	450	0	64.47	76.82	76.82	85.97	89.17	88.53
0.04	450	0	67.04	85.97	85.49	85.97	89.01	87.25
	400	0	60.95	64.8	73.78	84.68	86.13	95.43
0.07	450	0	82.28	90.94	93.02	96.71	98	97.83
	500	0	51.64	83.24	86.45	88.05	92.54	93.83
0.14	450	0	49.08	48.44	69.45	74.58	81.48	80.51

**Table A.17** Data of  $\ln C_0/C$  of MB.

<b>G</b>	<b>Tcal</b>	<b><math>\ln(C_0/C)</math></b>						
		<b>0</b>	<b>30</b>	<b>60</b>	<b>90</b>	<b>120</b>	<b>150</b>	<b>180</b>
0	450	0	1.0349	1.4621	1.4621	1.9637	2.2232	2.1657
0.04	450	0	1.1099	1.9637	1.93	1.9637	2.2085	2.0596
	400	0	0.9402	1.044	1.3385	1.8762	1.9752	3.0854
0.07	450	0	1.7303	2.4011	2.6626	3.4149	3.9096	3.8327
	500	0	0.7266	1.7862	1.9986	2.1245	2.5959	2.7847
0.14	450	0	0.6749	0.6624	1.1857	1.3696	1.6861	1.6354

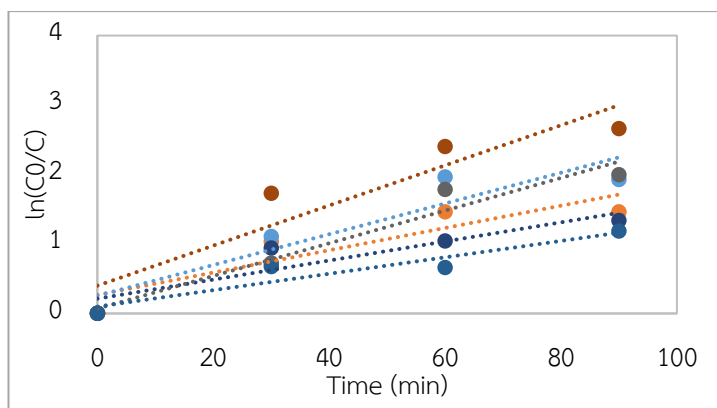


Figure A.3 Graph of  $\ln C_0/C$  versus time (min)

From graph above, linear equation is got,  $y = mx + b$  where  $\ln(C_0/C) = kt + b$

Table A.18 Rate constant of  $\text{TiO}_2/\text{SiO}_2/\text{GSs}$  powder.

G	Tcal	k (min <sup>-1</sup> )	B
0	450	0.016	0.2678
0.04	450	0.0221	0.2543
	400	0.0137	0.2128
0.07	450	0.0289	0.3997
	500	0.0235	0.0695
0.14	450	0.0118	0.099

Table A.19 Model of  $\eta$  degradation of  $\text{TiO}_2/\text{SiO}_2/\text{GSs}$  powder.

G	Tcal	$\eta$ degradation (model)						
		0	30	60	90	120	150	180
0	450	0	1.0349	1.4621	1.4621	1.9637	2.2232	2.1657
0.04	450	0	1.1099	1.9637	1.9300	1.9637	2.2085	2.0596
	400	0	0.9402	1.0440	1.3385	1.8762	1.9752	3.0854
0.07	450	0	1.7303	2.4011	2.6626	3.4149	3.9096	3.8327

**Table A.20** Model of  $\eta$  degradation of TiO<sub>2</sub>/SiO<sub>2</sub>/GSs powder (cont).

	500	0	0.7266	1.7862	1.9986	2.1245	2.5959	2.7847
	400	0	0.9736	1.4348	1.8453	1.9300	2.1797	2.3836
<b>0.14</b>	450	0	0.6749	0.6624	1.1857	1.3696	1.6861	1.6354
	500	0	1.1446	1.6354	1.8453	1.8252	2.4190	2.4190

**Table A.21** Data of degradation of MB under LED

		Absorbance						
G	Tcal	0	30	60	90	120	150	180
0	450	0.726	0.35	0.296	0.35	0.333	0.295	0.256
0.04	450	0.726	0.421	0.391	0.369	0.273	0.272	0.222
	400	0.726	0.442	0.427	0.329	0.24	0.245	0.207
0.07	450	0.726	0.437	0.371	0.307	0.233	0.224	0.207
	500	0.726	0.437	0.352	0.352	0.349	0.285	0.271
0.14	450	0.726	0.626	0.439	0.43	0.402	0.412	0.409
		Concentration						
G	Tcal	0	30	60	90	120	150	180
0	450	2.3528	0.9340	0.7302	0.9340	0.8698	0.7264	0.5792
0.04	450	2.3528	1.2019	1.0887	1.0057	0.6434	0.6396	0.4509
	400	2.3528	1.2811	1.2245	0.8547	0.5189	0.5377	0.3943
0.07	450	2.3528	1.2623	1.0132	0.7717	0.4925	0.4585	0.3943
	500	2.3528	1.2623	0.9415	0.9415	0.9302	0.6887	0.6358
0.14	450	2.3528	1.9755	1.2698	1.2358	1.1302	1.1679	1.1566
		$\eta$ decolorization						
G	Tcal	0	30	60	90	120	150	180
0	450	0	60.30	68.97	60.30	63.03	69.13	75.38
0.04	450	0	48.92	53.73	57.26	72.65	72.81	80.83

**Table A.22** Data of degradation of MB under LED (cont).

	400	0	45.55	47.96	63.67	77.95	77.15	83.24
0.07	450	0	46.35	56.94	67.20	79.07	80.51	83.24
	500	0	46.35	59.98	59.98	60.47	70.73	72.98
0.14	450	0		16.04	46.03	47.47	51.96	50.36

**Table A.23** Data of degradation of MB under UV light

		Absorbance						
		0	30	60	90	120	150	180
<b>G0.07T450</b>		0.94	0.58	0.578	0.571	0.567	0.538	0.534
		0.94	0.592	0.591	0.574	0.564	0.539	0.534
		Concentration with standard						
		0	30	60	90	120	150	180
<b>G0.07T450</b>		3.1604	1.8019	1.7943	1.768	1.7528	1.6434	1.6283
		3.1604	1.8472	1.8434	1.779	1.7415	1.6472	1.6283
		Concentration						
		0	30	60	90	120	150	180
<b>G0.07T450</b>		3.1604	0.4434	0.4283	0.3755	0.3453	0.1264	0.0962
		3.1604	0.5340	0.5264	0.3981	0.3226	0.1340	0.0962
		$\eta$ degradation						
		0	30	60	90	120	150	180
<b>G0.07T450</b>		0	85.97	86.45	88.12	89.07	96.00	96.96
		0	83.10	83.34	87.40	89.79	95.76	96.96

Note. For UV light, because it is the initial work range of TiO<sub>2</sub>, to avoid the error of fast degradation of MB, the analysis is using the method of standard addition into a sample. To calculate the exact concentration of the sample, Equation

$$C = \frac{(C \times 10) - (C_{\text{std}} \times 5)}{5}$$

is used.



Table A.24 Data of repetition of G0.07T450

		Absorbance						
		0	30	60	90	120	150	180
Dark	I	0.726	0.555	0.29	0.247	0.201	0.18	0.189
	II	0.726	0.587	0.335	0.303	0.28	0.224	0.246
	III	0.94	0.709	0.236	0.262	0.242	0.264	
	IV	0.726	0.58	0.407	0.341	0.286	0.241	0.15
Sun	I	0.726	0.213	0.159	0.146	0.123	0.115	0.116
	II	0.94	0.302	0.266	0.268	0.182	0.166	0.16
	III	0.726	0.32	0.275	0.25	0.215	0.18	0.15
	IV	0.726	0.295	0.283	0.275	0.257	0.247	0.18
		Concentration						
		0	30	60	90	120	150	180
Dark	I	2.3528	1.7075	0.7075	0.5453	0.3717	0.2925	0.3264
	II	2.3528	1.8283	0.8774	0.7566	0.6698	0.4585	0.5415
	III	3.1604	2.2887	0.5038	0.6019	0.5264	0.6094	-0.387
	IV	2.3528	1.8019	1.1491	0.9000	0.6925	0.5226	0.1792
Sun	I	2.3528	0.4170	0.2132	0.1642	0.0774	0.0472	0.0509
	II	3.1604	0.7528	0.6170	0.6245	0.3000	0.2396	0.2170
	III	2.3528	0.8208	0.6509	0.5566	0.4245	0.2925	0.1792
	IV	2.3528	0.7264	0.6811	0.6509	0.5830	0.5453	0.2925
		$\eta$ degradation						
		0	30	60	90	120	150	180
Dark	I	0	27.43	69.93	76.82	84.20	87.57	86.13
	II	0	22.29	62.71	67.84	71.53	80.51	76.98
	III	0	27.58	84.06	80.96	83.34	80.72	112.24
	IV	0	23.42	51.16	61.75	70.57	77.79	92.38
Sun	I	0	82.28	90.94	93.02	96.71	98.00	97.83
	II	0	76.18	80.48	80.24	90.51	92.42	93.13
	III	0	65.12	72.33	76.34	81.96	87.57	92.38
	IV	0	69.13	71.05	72.33	75.22	76.82	87.57

## APPENDIX B

### RAW DATA OF ANALYSIS OF TiO<sub>2</sub>/SiO<sub>2</sub>/GSs COMPACT

#### B.1 Data MB degradation

Equation (A.3) and (A.4) is used for degradation MB by G0.07T450 compact.

**Table B.1** Data of degradation of MB in dark condition.

		Absorbance						
Thickness (cm)		0	30	60	90	120	150	180
	0.3	0.94	0.544	0.39	0.298	0.272	0.225	0.2
<b>G0.07</b>	0.5	0.94	0.492	0.34	0.324	0.25	0.192	0.194
<b>T450</b>	0.8	0.94	0.413	0.313	0.26	0.3	0.254	0.216
	1	0.94	0.478	0.218	0.209	0.211	0.204	0.209
		Concentration						
Thickness (cm)		0	30	60	90	120	150	180
	0.3	3.1604	1.6660	1.0849	0.7377	0.6396	0.4623	0.3679
<b>G0.07</b>	0.5	3.1604	1.4698	0.8962	0.8358	0.5566	0.3377	0.3453
<b>T450</b>	0.8	3.1604	1.1717	0.7943	0.5943	0.7453	0.5717	0.4283
	1	3.1604	1.4170	0.4358	0.4019	0.4094	0.3830	0.4019
		η degradation						
Thickness (cm)		0	30	60	90	120	150	180
	0.3	0	47.28	65.67	76.66	79.76	85.37	88.36
<b>G0.07</b>	0.5	0	53.49	71.64	73.55	82.39	89.31	89.07
<b>T450</b>	0.8	0	62.93	74.87	81.19	76.42	81.91	86.45
	1	0	55.16	86.21	87.28	87.04	87.88	87.28

Table B.2 Data of degradation of MB under sunlight.

		Absorbance						
Thickness (cm)		0	30	60	90	120	150	180
	0.3	0.94	0.596	0.562	0.562	0.56	0.53	0.524
<b>G0.07</b>	0.5	0.94	0.592	0.59	0.582	0.56	0.552	0.536
<b>T450</b>	0.8	0.94	0.594	0.592	0.546	0.544	0.524	0.526
	1	0.94	0.568	0.542	0.548	0.542	0.54	0.544
		Concentration with standard						
Thickness (cm)		0	30	60	90	120	150	180
	0.3	3.1604	1.8623	1.7340	1.7340	1.7264	1.6132	1.5906
<b>G0.07</b>	0.5	3.1604	1.8472	1.8396	1.8094	1.7264	1.6962	1.6358
<b>T450</b>	0.8	3.1604	1.8547	1.8472	1.6736	1.6660	1.5906	1.5981
	1	3.1604	1.7566	1.6585	1.6811	1.6585	1.6509	1.6660
		Concentration						
Thickness (cm)		0	30	60	90	120	150	180
	0.3	3.1604	0.5642	0.3075	0.3075	0.2925	0.0660	0.0208
<b>G0.07</b>	0.5	3.1604	0.5340	0.5189	0.4585	0.2925	0.2321	0.1113
<b>T450</b>	0.8	3.1604	0.5491	0.5340	0.1868	0.1717	0.0208	0.0358
	1	3.1604	0.3528	0.1566	0.2019	0.1566	0.1415	0.1717
		$\eta$ degradation						
Thickness (cm)		0	30	60	90	120	150	180
	0.3	0	82.15	90.27	90.27	90.75	97.91	99.34
<b>G0.07</b>	0.5	0	83.10	83.58	85.49	90.75	92.66	96.48
<b>T450</b>	0.8	0	82.63	83.10	94.09	94.57	99.34	98.87
	1	0	88.84	95.04	93.61	95.04	95.52	94.57

Note. Because degradation has happened fast under sunlight, the analysis is using the method of standard addition into a sample. To calculate the exact concentration of

the sample, Equation  $C = \frac{(C \times 10) - (C_{std} \times 5)}{5}$  is used.

Table B.3 Data of degradation of MB under LED.

		Absorbance						
Thickness (cm)		0	30	60	90	120	150	180
	0.3	0.94	0	0	0	0	0	0
<b>G0.07</b>	0.5	0.94	0.5	0.372	0.258	0.16	0.162	0.16
<b>T450</b>	0.8	0.94	0.282	0.208	0.2	0.184	0.188	0.169
	1	0.94	0.18	0.182	0.152	0.154	0.156	0.196
		Concentration						
Thickness (cm)		0	30	60	90	120	150	180
	0.3	3.1604						
<b>G0.07</b>	0.5	3.1604	1.5000	1.0170	0.5868	0.2170	0.2245	0.2170
<b>T450</b>	0.8	3.1604	0.6774	0.3981	0.3679	0.3075	0.3226	0.2509
	1	3.1604	0.2925	0.3000	0.1868	0.1943	0.2019	0.3528
		$\eta$ degradation						
Thickness (cm)		0	30	60	90	120	150	180
	0.3	0	100.00	100.00	100.00	100.00	100.00	100.00
<b>G0.07</b>	0.5	0	52.54	67.82	81.43	93.13	92.90	93.13
<b>T450</b>	0.8	0	78.57	87.40	88.36	90.27	89.79	92.06
	1	0	90.75	90.51	94.09	93.85	93.61	88.84

Table B.4 Data of degradation of MB under UV light.

		Absorbance						
Thickness (cm)		0	30	60	90	120	150	180
	0.3	0.94	0.56	0.562	0.546	0.536	0.53	0.524
<b>G0.07</b>	0.5	0.94	0.552	0.549	0.532	0.529	0.526	0.526
<b>T450</b>	<b>0.8</b>	0.94	0.554	0.549	0.544	0.534	0.524	0.526
	1	0.94	0.548	0.542	0.538	0.524	0.522	0.523
		Concentration with standard						
Thickness (cm)		0	30	60	90	120	150	180
<b>G0.07</b>	0.3	3.1604	1.7264	1.7340	1.6736	1.6358	1.6132	1.5906

Table B.5 Data of degradation of MB under UV light (cont).

	0.5	3.1604	1.6962	1.6849	1.6208	1.6094	1.5981	1.5981
<b>T450</b>	0.8	3.1604	1.7038	1.6849	1.6660	1.6283	1.5906	1.5981
	1	3.1604	1.6811	1.6585	1.6434	1.5906	1.5830	1.5868
<b>Concentration</b>								
<b>Thickness (cm)</b>	<b>0</b>	<b>30</b>	<b>60</b>	<b>90</b>	<b>120</b>	<b>150</b>	<b>180</b>	
	0.3	3.1604	0.2925	0.3075	0.1868	0.1113	0.0660	0.0208
<b>G0.07</b>	0.5	3.1604	0.2321	0.2094	0.0811	0.0585	0.0358	0.0358
<b>T450</b>	0.8	3.1604	0.2472	0.2094	0.1717	0.0962	0.0208	0.0358
	1	3.1604	0.2019	0.1566	0.1264	0.0208	0.0057	0.0132
<b>η degradation</b>								
<b>Thickness (cm)</b>	<b>0</b>	<b>30</b>	<b>60</b>	<b>90</b>	<b>120</b>	<b>150</b>	<b>180</b>	
	0.3	0	90.75	90.27	94.09	96.48	97.91	99.34
<b>G0.07</b>	0.5	0	92.66	93.37	97.43	98.15	98.87	98.87
<b>T450</b>	0.8	0	92.18	93.37	94.57	96.96	99.34	98.87
	1	0	93.61	95.04	96.00	99.34	99.82	99.58

Note. Because degradation has happened fast under UV light, the analysis is using the method of standard addition into a sample. To calculate the exact concentration of the sample, Equation  $C = \frac{(C \times 10) - (C_{std} \times 5)}{5}$  is used.

Table B.6 Data of repetition of G0.07T450

		<b>Absorbance</b>						
<b>Thickness (cm)</b>		<b>0</b>	<b>30</b>	<b>60</b>	<b>90</b>	<b>120</b>	<b>150</b>	<b>180</b>
<b>I</b>	0.3	0.94	0.146	0.132	0.105	0.116	0.106	0.104
	0.5	0.94	0.222	0.16	0.112	0.12	0.109	0.109
	0.8	0.94	0.184	0.122	0.108	0.104	0.104	0.105
	1	0.94	0.11	0.107	0.107	0.103	0.107	0.107
<b>II</b>	0.3	0.94	0.344	0.204	0.12	0.162	0.15	0.152

Table B.7 Data of repetition of G0.07T450 (cont).

	0.5	0.94	0.376	0.28	0.178	0.144	0.112	0.116
	0.8	0.94	0.346	0.208	0.116	0.18	0.238	0.182
	1	0.94	0.126	0.092	0.112	0.22	0.192	0.114
III	0.3	0.94	0.294	0.214	0.116	0.176	0.258	0.156
	0.5	0.94	0.354	0.146	0.11	0.105	0.109	0.104
	0.8	0.94	0.128	0.166	0.156	0.152	0.122	0.132
	1	0.94	0.184	0.109	0.109	0.108	0.146	0.104
<b>Concentration</b>								
<b>Thickness (cm)</b>	<b>0</b>	<b>30</b>	<b>60</b>	<b>90</b>	<b>120</b>	<b>150</b>	<b>180</b>	
I	0.3	3.1604	0.1642	0.1113	0.0094	0.0509	0.0132	0.0057
	0.5	3.1604	0.4509	0.2170	0.0358	0.0660	0.0245	0.0245
	0.8	3.1604	0.3075	0.0736	0.0208	0.0057	0.0057	0.0094
	1	3.1604	0.0283	0.0170	0.0170	0.0019	0.0170	0.0170
II	0.3	3.1604	0.9113	0.3830	0.0660	0.2245	0.1792	0.1868
	0.5	3.1604	1.0321	0.6698	0.2849	0.1566	0.0358	0.0509
	0.8	3.1604	0.9189	0.3981	0.0509	0.2925	0.5113	0.3000
	1	3.1604	0.0887	-0.039	0.0358	0.4434	0.3377	0.0434
III	0.3	3.1604	0.7226	0.4208	0.0509	0.2774	0.5868	0.2019
	0.5	3.1604	0.9491	0.1642	0.0283	0.0094	0.0245	0.0057
	0.8	3.1604	0.0962	0.2396	0.2019	0.1868	0.0736	0.1113
	1	3.1604	0.3075	0.0245	0.0245	0.0208	0.1642	0.0057
<b><math>\eta</math> degradation</b>								
<b>Thickness (cm)</b>	<b>0</b>	<b>30</b>	<b>60</b>	<b>90</b>	<b>120</b>	<b>150</b>	<b>180</b>	
I	0.3	0	94.81	96.48	99.70	98.39	99.58	99.82
	0.5	0	85.73	93.13	98.87	97.91	99.22	99.22
	0.8	0	90.27	97.67	99.34	99.82	99.82	99.70
	1	0	99.10	99.46	99.46	99.94	99.46	99.46
II	0.3	0	71.16	87.88	97.91	92.90	94.33	94.09
	0.5	0	67.34	78.81	90.99	95.04	98.87	98.39
	0.8	0	70.93	87.40	98.39	90.75	83.82	90.51

Table B.8 Data of repetition of G0.07T450 (cont).

III	1	0	97.19	101.25	98.87	85.97	89.31	98.63
	0.3	0	77.13	86.69	98.39	91.22	81.43	93.61
	0.5	0	69.97	94.81	99.10	99.70	99.22	99.82
	0.8	0	96.96	92.42	93.61	94.09	97.67	96.48
	1	0	90.27	99.22	99.22	99.34	94.81	99.82

## B.2 Experimental procedure of NDEA degradation



Figure B.1 Prepared standard solutions.



Figure B.2 250 mL sample of NDEA (3 samples) and put 2 pieces  $\text{TiO}_2/\text{SiO}_2/\text{GSs}$  sample (t0.5) into the NDEA solution.





**Figure B.3** Take  $\pm 25$  mL of each NDEA sample every 0 minutes, 15 minutes, 30 minutes, 60 minutes, 90 minutes, 120 minutes, 180 minutes, and 300 minutes and put it into a dark bottle. Analyze by GC-MS.

### B.3 Data NDEA degradation

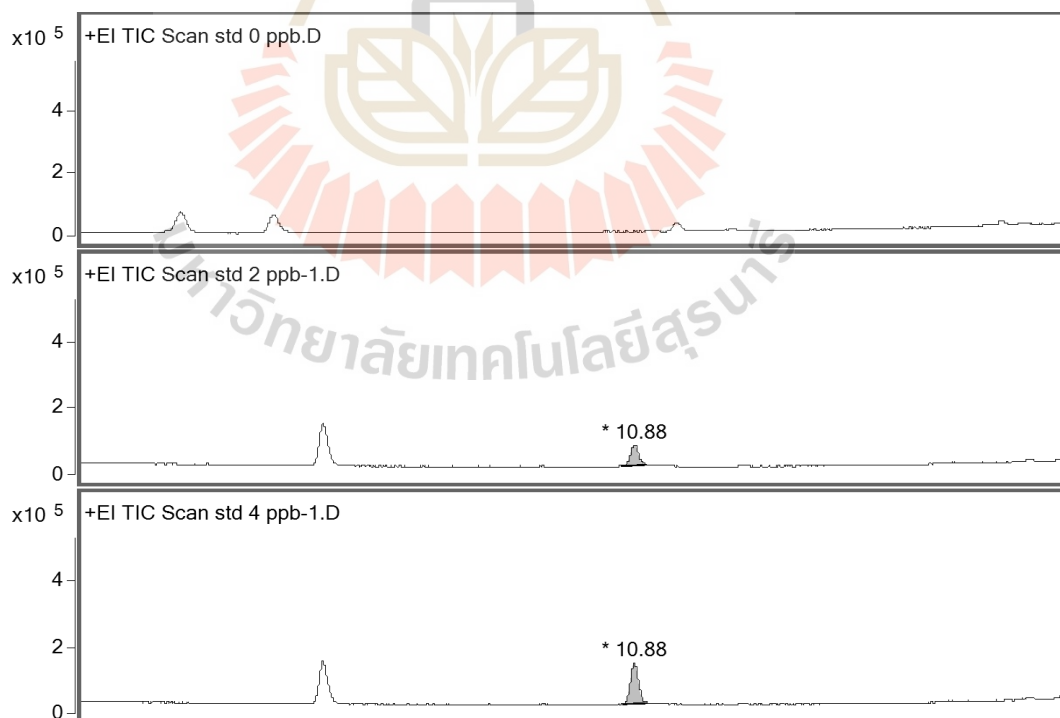


**Figure B.4** GC-MS result of NDEA standard

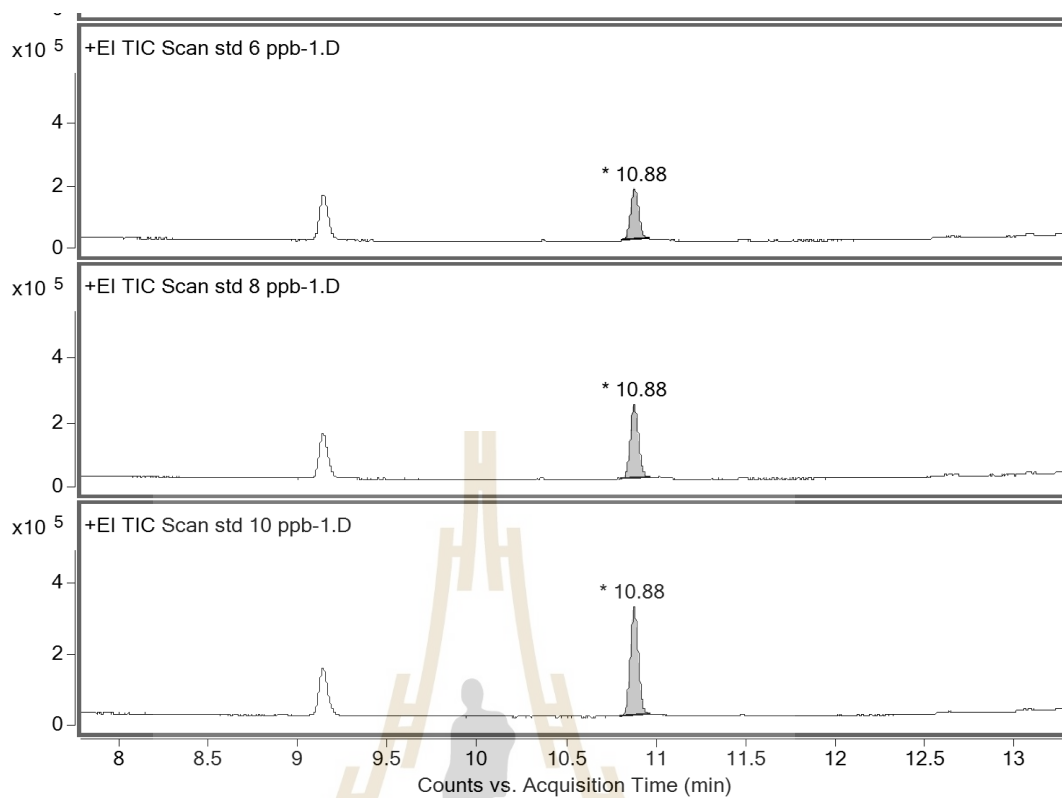


Figure B.5 GC-MS result of NDEA standard (cont).

Table B.9 Calibration standard data of NDEA

Standard concentration (ppb)	Area
0	0
2	190684
4	382898
6	565508
8	749653
10	945576

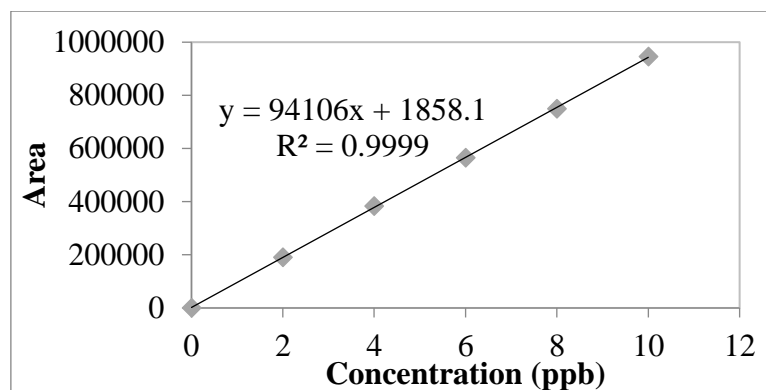


Figure B.6 Calibration standard data of NDEA

Equation (B.1) is used for calculating the concentration of NDEA

$$C = \frac{(A-b)}{x}$$

(B.1)

A is Area, x=94106, and b=1858.1

Table B.10 Data analysis of NDEA sample.

Sample	Area	Concentration (ppb)	Concentration (ppm)	Avg concentration (ppm)
T0-1	933697	9.9020	0.99	1.0006
	953205	10.1093	1.01	
T0-2	959683	10.1781	1.02	1.0153
	954982	10.1282	1.01	
T0-3	953493	10.1124	1.01	1.0102
	951583	10.0921	1.01	
T15-1	819243	8.6858	0.87	0.8724
	826353	8.7613	0.88	

**Table B.11** Data analysis of NDEA sample (cont).

T15-2	838142	8.8866	0.89	0.8925
	845407	8.9638	0.90	
T15-3	831380	8.8148	0.88	0.8837
	835659	8.8602	0.89	
T30-1	760686	8.0635	0.81	0.8022
	752783	7.9796	0.80	
T30-2	738444	7.8272	0.78	0.7801
	733577	7.7755	0.78	
T30-3	709540	7.5201	0.75	0.7559
	716921	7.5985	0.76	
T60-1	464417	4.9153	0.49	0.4945
	469991	4.9745	0.50	
T60-2	478325	5.0631	0.51	0.5078
	481054	5.0921	0.51	
T60-3	491877	5.2071	0.52	0.5175
	485814	5.1427	0.51	
T90-1	280845	2.9646	0.30	0.2940
	276187	2.9151	0.29	
T90-2	282060	2.9775	0.30	0.2970
	280601	2.9620	0.30	
T90-3	292268	3.0860	0.31	0.3081
	291351	3.0762	0.31	
T120-1	147661	1.5493	0.15	0.1550
	147877	1.5516	0.16	
T120-2	148682	1.5602	0.16	0.1560
	148704	1.5604	0.16	
T120-3	148219	1.5553	0.16	0.1558
	148656	1.5599	0.16	
T180-1	59263	0.6100	0.06	0.0606
	58497	0.6019	0.06	

**Table B.12** Data analysis of NDEA sample (cont).

T180-2	47283	0.4827	0.05	0.0481
	47057	0.4803	0.05	
T180-3	76930	0.7977	0.08	0.0794
	76254	0.7906	0.08	
T300-1	40019	0.4055	0.04	0.0405
	39947	0.4047	0.04	
T300-2	41863	0.4251	0.04	0.0424
	41573	0.4220	0.04	
T300-3	48031	0.4906	0.05	0.0493
	48386	0.4944	0.05	

**Table B.13** Data of degradation of NDEA under sunlight.

t0.5		Concentration						
rep	0	15	30	60	90	120	180	300
I	1.0006	0.8724	0.8022	0.4945	0.2940	0.1506	0.0624	0.04229
II	1.0153	0.8925	0.7801	0.5078	0.2970	0.1515	0.0499	0.044134
III	1.0102	0.8837	0.7559	0.5175	0.3081	0.1558	0.0794	0.049253
		$\eta$ degradation						
rep	0	15	30	60	90	120	180	300
I	0	12.81	19.83	50.58	70.62	84.95	93.77	95.77
II	0	12.09	23.16	49.99	70.75	85.07	95.08	95.65
III	0	12.52	25.17	48.77	69.50	84.58	92.14	95.12
		$\ln(C_0/C)$						
rep	0	15	30	60	90	120	180	300
I	0	0.1371	0.2210	0.7048	1.2248	1.8939	2.7752	3.1638
II	0	0.1289	0.2635	0.6930	1.2293	1.9021	3.0124	3.1357
III	0	0.1338	0.2900	0.6689	1.1875	1.8696	2.5432	3.0209

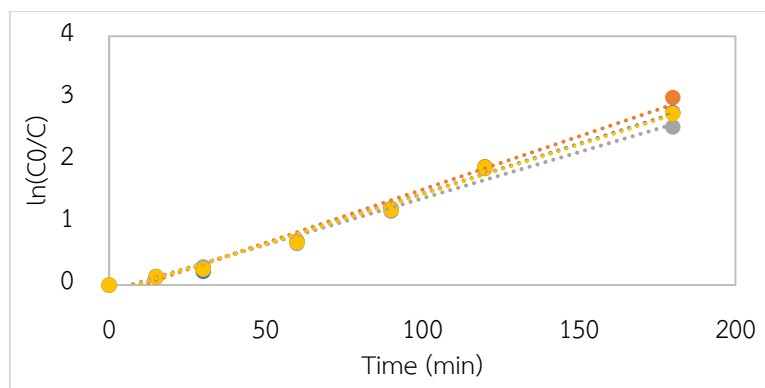


Figure B.7 Graph of  $\ln C_0/C$  versus time (min)

From the graph above, a linear equation is got,  $y = mx + b$  where  $\ln(C_0/C) = kt + b$

Table B.14 Rate constant of  $\text{TiO}_2/\text{SiO}_2/\text{GSs}$  t(0.5).

	Rep	k (min <sup>-1</sup> )	b
t0.5	I	0.0161	-0.1437
	II	0.0171	-0.1774
	III	0.0149	-0.0966
	Avg	0.0159	-0.1363

Table B.15 Model of  $\eta$  degradation of  $\text{TiO}_2/\text{SiO}_2/\text{GSs}$  t(0.5).

t0.5	$\eta$ degradation (model)							
	rep	0	15	30	60	90	120	180
I	0	28.77	56.06	72.89	83.28	89.68	93.63	99.08
II	0	28.51	57.20	74.37	84.66	90.82	94.50	99.29
III	0	29.56	54.95	71.19	81.57	88.22	92.46	98.74
Avg	0	28.87	55.86	72.60	83.00	89.45	93.45	99.03

## APPENDIX C

### LIST OF PUBLICATIONS

#### C.1 List of Publications

Ayuningtyas, M. L., Watcharamaisakul, S., & Junpirom, S. (2021). Effective Solar Light Photocatalysis by Graphene Sheets (GSs) Addition on the Composite  $\text{TiO}_2/\text{SiO}_2$ . *Engineering Journal*, 25(6), 1-13. <https://doi.org/10.4186/ej.2021.25.6.1>.

Ayuningtyas, M. L., Watcharamaisakul, S., & Junpirom, S. (2021). Immobilization of  $\text{TiO}_2/\text{SiO}_2/\text{GSs}$  Photocatalyst onto Supporting Materials by Dipping Method and Effectiveness on Photocatalytic Activity . *Suranaree Journal of Science of Technology*, In Press.





## VITAE

Mia Lestari Ayuningtyas was born in Manado, Sulawesi, Indonesia in 1992. She received the B.S. degree in Nuclear Chemical Engineering from Polytechnic Institute of Nuclear Technology, Indonesia, in 2014. She is a Ph.D. candidate in Material Engineering, Suranaree University of Technology, Thailand. Her previous research focused on nanomaterial M41S for radiopharmaceuticals purposes. Her research interest now is including nanomaterials and photocatalysts. Ms. Mia Lestari Ayuningtyas was a recipient of the SUT-Ph.D. scholarship for ASEAN at Suranaree University of Technology in 2015.

